DESIGN AND ANALYSIS OF BEAM STEERING ANTENNAS FOR NEXT-GENERATION WIRELESS COMMUNICATION

by

Shafaq Kausar

A dissertation

submitted in partial fulfillment

of the requirements for the degree of

Doctor of Philosophy in Electrical and Computer Engineering

Boise State University

May 2022

BOISE STATE UNIVERSITY GRADUATE COLLEGE

DEFENSE COMMITTEE AND FINAL READING APPROVALS

of the dissertation submitted by

Shafaq Kausar

Dissertation Title: Design and Analysis of Beam Steering Antennas for Next-Generation Wireless Communication

Date of Final Oral Examination: 10 May 2022

The following individuals read and discussed the dissertation submitted by student Shafaq Kausar, and they evaluated her presentation and response to questions during the final oral examination. They found that the student passed the final oral examination.

Hani Mehrpouyan, Ph.D.	Chair, Supervisory Committee
Nader Rafla, Ph.D.	Member, Supervisory Committee
Hao Chen, Ph.D.	Member, Supervisory Committee

The final reading approval of the dissertation was granted by Dr. Hani Mehrpouyan, Ph.D., Chair, Supervisory Committee. The dissertation was approved by the Graduate College.

DEDICATION

Dedicated to my lovely family, you all made this journey smooth and beautiful for me.

ACKNOWLEDGMENT

I wish to express my sincere gratitude to my advisor, Dr. Hani Mehrpouyan for his consistent mentoring throughout this journey. He provided me with the excellent platform to realize unique research methodologies and to think 'out of the box'. His insighful thoughts and valuable feedback helped me to refine the ideas. Dr. Hani has always been there to support his students above and beyond which has been a driving force to achieve high goals. Without his support and sheer knowledge, the goal of this project would have never been realized.

I would also like to thank my committee members, Dr. Hao Chen and Dr. Nadar Rafla for their valuable feedback and insightful comments on my work. Their feedback has been extremely valuable and helped me to refine the research ideas. I am grateful to Dr. Tyler Brown for serving as a Graduate Faculty Representative.

I would also like to thank Dr. Hao Chen and Dr. Kurtis Cantley for the mentorship during my course work. The way you taught the courses was extremely beneficial and made the lectures fun and interesting.

I am grateful to my teammates Hossein Mehri, Mojtaba Almasi, Mahfuza Khatun, Saeideh Shad, and Roohollah Amiri for the productive discussions and companionship.

I am grateful to the staff of the ECE department and department manager Jenn Ambrose for her support and guidance throughout these years.

Lastly, I would like to express my sincere gratitude to my family for your love, sheer support and absolute backing. Your love and support kept me motivated throughout these years.

ABSTRACT

Reconfigurable antennas have gained immense interest since the last few decades. Reconfigurable a ntennas c an s teer b eams d ynamically i n r esponse t o t he s ignal environment, they can also support multiple simultaneous beams. This research work aims to make considerable advancements in the design and analysis of low cost and low power beam steerable antennas. It focuses on the design and demonstration of several prototypes with advanced functionalities, such as passive (broadband, multi-beam, shapable beams) and active (electronically reconfigurable) antennas. The first p art o f t his d issertation c overs t he d esign a nd d evelopment o f passive metamaterial based multibeam antenna at 30 GHz. Designed antenna is capable of independently steering multiple beams in the azimuth and elevation plane by the two dimensional displacement of feed radiators placed in front of the passive meta-surface. The meta-surface acts as an electromagnetic lens. The unit cell of the meta-surface consists of three layers of Rogers 5880 substrate and four layers of etched copper. The unit cell is designed such that the phase of unit cell transmission coefficient is varied from 0 to 360 degrees by changing the length of the etched copper pattern. As a proof of concept, a multi-layered meta-surface is designed by using conventional uni-focal phase distribution. Multi-beam steering of 0 to 360 degrees in azimuth plane and +/- 40 degrees in elevation plane has been achieved. Antenna peak gain is 34.5 dBi at 30 GHz, the 3 dB bandwidth is from 28.5 to 32.2 GHz. In the next stage scan loss was optimized by synthesizing the meta-surface with bi-focal phase distribution. The scan range of antenna was further extended by designing the multi-facet transmitarray,

which increased the scan range to +/-80 degrees. The designed antenna supports multiple-input and multiple-output (MIMO), this introduces diversity and provides an additional degree of freedom to overcome losses at mm-Wave frequencies. This is a mission enabling technology as the antenna supports seamless hand-off between multiple users by forming high gain independently steerable beams. Comparable antennas to the date are low gain, bulky, have limited number of beams and a narrow field of view. Due to absence of active components the designed antenna is low cost and robust. Moreover, the substrate is selected such that the antenna can withstand harsh deep space environmental conditions and it can be folded for easy deployment. Due to potentially low fabrication cost and ability to support MIMO, the designed antenna is a good candidate for next generation satellite communication and mm-Wave 5G systems. The second part of the work covers the design of a novel reconfigurable metasurface antenna to achieve low power and low-cost electronic beam steering. Initially, the unit-cell loaded with varactor diode for dynamic phase control was designed and experimentally validated. The unit cell consists of unique single layered geometry, phase agility of 360 degree has been achieved by tuning varactor diode. The unit-cell was then used to design the reconfigurable reflectarray antenna comprising 14 x 14 unit cells and 196 varactor diodes. A prototype was realized and characterized. Designed antenna has a maximum gain of 19 dBi with beam steering of +/-60 degrees in elevation plane and 360 degrees in azimuth plane.

TABLE OF CONTENTS

ABSTRACT iv

LIST OF TABLES x

LIST OF FIGURES xi

LIST OF ABBREVIATIONS xvi

1 Introduction 1

1.1 Background 4

1.1.1 Mechanical Beam Steering 5

1.1.2 Analog Beam-forming 5

1.1.3 Digital Beamforming 6

1.1.4 Switched Beam Antennas 7

1.1.5 Passive Electrically Steerable Antenna 9

1.1.6 Reconfigurable Reflectarray and Transmitarray Antennas 12

1.1.7 Research Motivation and Goals 13

1.1.8 Prior Art and our Proposed Solutions 15

1.1.9 Organization of Literature 22

2 Basic Definitions and Terminologies 24

2.1 Reconfigurable Antenna 24

2.2 Antenna Gain 24

2.3 Antenna Efficiency 25
2.4 Main Beam and Side Lobes 26
2.5 Basic Terminologies for Reflectarray/Transmitarray Antenna Configurations 26
2.5.1 Metasurface 26
2.5.2 Unit cell 27
2.5.3 Substrate 27
2.5.4 Phase Range of Unit Cell 27
2.5.5 Single layered/Multi layered Unit cell 28
2.5.6 Gain Scan Loss 29

3 Theoretical Analysis of Transmitarray/Reflectarray 30
3.1 Mathematical Reasoning 30
3.2 Approaches to Design the Phasing Elements 39
3.2.1 Phase Tuning using Variable Transmission Line (delay line) 40
3.2.2 Phase Tuning using Variable Length Elements 41
3.2.3 Elements with Variable Rotation Angle 42
3.2.4 Phase Tuning using Tunable Substrates 42
3.2.5 Phase Tuning by Integrating Phasing Elements with Dynamic Components 44
3.3 Reflectarray\transmitarray Design Issues 44
3.3.1 Errors due to limited unit cell phase range 44
3.3.2 Element loss: 45
3.3.3 Quantization errors 45
3.3.4 Infinite array approximation error 46

3.3.5 Limited Bandwidth 46

4 Design of Metamaterial based Antenna for Multi-beam Wide-angle Scanning 47

4.1 Unit Cell Design and Analysis for Multi-beam Transmitarray Antenna . 48

4.2 Beam Scanning using Designed Metasurface 56

4.3 Fabricated Prototype and Measured Results 64

4.4 Phase Synthesis for Scan Loss Reduction 71

4.5 Folded Transmitarray for Deep Space Missions 73

4.6 Multi-facet Transmitarray for Ultrawide Scan Angle 75

4.7 Conclusion 77

5 Reflect-array Surface Design and Analysis 78

5.1 Radiating Structure (Unit cell) Design 78

5.2 Phase Shifting Mechanism 81

5.3 Aperture Phase Distribution 83

5.4 Fabricated Prototype 87

5.5 Reflectarray Surface Design Using the Novel Unit Cell 88

5.6 Reflect-array design using passive unit cell 91

5.6.1 Beam Steering Configuration 94

6 Conclusion and Applications 97

6.1 5G Millimetric Wave (mm-Wave) Communication 97

6.2 Satellite Communication (LEO & MEO) 98

6.3 SATCOM On-the-move (Communication with GEO Satellite) 100

6.4 Enabling the High Throughput with Spot Beams and Polarization Diversity 102

REFERENCES 103

LIST OF TABLES

5.1 Beam steering mechanism. 96

LIST OF FIGURES

1.1 Illustration of directional beam steering. 4

1.2 Analog beamforming. 6

1.3 Digital beamforming. 7

1.4 Schematics of switched beam antenna. 8

1.5 Coverage pattern for switch beam antennas. 8

1.6 Interference rejection comparison. 9

1.7 Example of electronically steerable parasitic antenna array (a) Simulated antenna (b) Fabricated antenna. 11

1.8 The model of Yagi antenna. 11

1.9 Reflect-array antenna basic configuration 13

1.10 Reflectarray Antenna 15

1.11 Transmitarray Antenna 15

1.12 Electronically tunable reflectarray system 17

1.13 Designed electronically tunable reflectarray antenna. 18

1.14 Beam focusing using phase shifting elements. 20

1.15 Beam steering configuration with feed displacement. 21

1.16 Multibeam configuration using passive metasurface. 22

1.17 Outline 23

2.1 3-D gain plot. 25

2.2 Antenna propagation pattern. 26

2.3 Unit cell. 27
2.4 Multilayered and single layered reflectarray. 28
2.5 Gain vs scan loss. 29

3.1 4-Element array. 31
3.2 Geometry of planar array. 35
3.3 Reflectarray schematics. 36
3.4 Phase compensation in antenna arrays. 39
3.5 Unit cells with variable length delay lines. 41
3.6 Unit cell with variable dimensions. 41
3.7 Unit cells with variable rotation angle. 42
3.8 Liquid crystal based element. 43

4.1 Designed unit cell at 30 GHz. 49
4.2 Unit cell transmission coefficient S_{21}phase. 50
4.3 Unit cell transmission coefficient S_{21}magnitude. 50
4.4 Process flow for metasurface design. 52
4.5 Designed metasurfaces (a) 80.5 x 80.5 mm. (b) 103 x 103 mm, and (c) 222 mm 222 mm. 52
4.6 Feed image on metasurface to realize the edge taper. 53
4.7 Emitted pencil beam from metasurface. 54
4.8 Radiation pattern of designed antenna (a) 3D Radiation Pattern (b) 2D Radiation Pattern. 54
4.9 Transmit-array integrated with pyramidal feed horn for linear polarization. 55
4.10 Transmit-array integrated with conical feed horn for circular polarization. 55

4.11 Axial ratio plots of metasurface integrated with linearly and circularly polarized feed horns. 56
4.12 Phase distribution on transmitarray aperture (a) boresight, (b) 5°, (c) 10°, (d) 20° , (e) 25°, (f) 30°, and (g) 40° 58
4.13 Comparison of phase distribution for beam steering using aperture tuning and feed displacement. 59
4.14 Working mechanism. 60
4.15 2D radiation pattern. 60
4.16 Comparison of 2x2 MIMO using traditional and proposed antenna. . . . 61
4.17 Two independently steerable beams. 62
4.18 Three independently steerable beams. 62
4.19 Five independently steerable beams. 63
4.20 3D radiation pattern for multiple simultaneous beams with peak gain of 35.5 dB. (a) single beam (b) dual beam (c) three independent beams, (d) four independent beams, and (e) five independent beams. 64
4.21 Fabricated transmitarray. 65
4.22 Measurement setup. 66
4.23 Measured bore-sight radiation patterns from 27 to 32 GHz. 66
4.24 Bore-sight gain vs frequency plot. 67
4.25 Total efficiency of antenna (boresight). 67
4.26 Measured radiation pattern from 27 to 32 GHz with the feed displacement of 30 mm from origin, beam steered at 13° 68
4.27 Antenna gain vs frequency plot for feed displacement of 30 mm. 69
4.28 Peak gain vs frequency plot for 30 mm feed displacement 69

4.29 Measured radiation pattern from 27 GHz to 32 GHz with the feed displacement of 60 mm from origin, beam steered at 28 degrees. 70
4.30 Peak gain vs frequency plot for 60 mm feed displacement. 70
4.31 Beam steered at 40° at center frequency of 30 GHz (feed displacement of 78 mm from origin). 71
4.32 Beam scanning after scan loss optimization. 72
4.33 Simulated folded lens with hinges. 74
4.34 Depiction of folded transmitarray on spacecraft. 74
4.35 3-Facet metasurface. 76
4.36 Radiation pattern of multifacet transmitarray. 76

5.1 Designed reflectarray phasing element (unit cell). 80
5.2 3-D view of simulated unit cell. 80
5.3 Floquet port analysis. 81
5.4 Unit cell with master slave boundaries. 81
5.5 Schematics of varactor loaded unit cell. 83
5.6 Phase range of unit cell. 85
5.7 Reflection loss. 85
5.8 Fabricated unit cell (front view). 87
5.9 Fabricated unit cell (back plane). 87
5.10 Unit cell placed at the end of waveguide (W75S001-3). 88
5.11 Array of unit cells (back plane). 89
5.12 Radiation pattern of designed 14x14 element reflectarray. (a) Boresight pattern (b) steered at 10°(c) steered at 20° (d) steered at 30° (e) steered at 40° (f) steered at 50°, and (g) steered at 60°. 90

5.13 Fabricated reflectarray. 90
5.14 Reflectarray mounted on turn-table in test chamber. 91
5.15 Unit cell geometries (a) Circular Ring (b) Double square (c) Circular ring and double square elements 92
5.16 Phase range for different geometries. 93
5.17 Reflection loss. 93
5.18 Reflect-array surface and beam steering configuration. 94
5.19 3D radiation pattern showing beam steering: (a) - 20, (b) 0, (c) +20; (d) -40; (e) +40. 95
5.20 Far-field radiation pattern in the H-plane. Peaks at -40, -20, 0, +20 and +40. 96

6.1 Back-haul networks using high gain antennas. 98
6.2 Satellite communication. 99
6.3 Satellite communication. 100
6.4 Satellite Communication-on-the-Move (SOTM). 101
6.5 Multi-Satellite Connectivity. 101
6.6 Example of four-color multi spot coverage. 102

LIST OF ABBREVIATIONS

– RA Reflectarray

– EIRP Effective Isotropic Radiated Power

– EM Electromagnetic

– MEM Microelectromechanical

– UC Unit cell

– LC Liquid Crystal

– mmWave Millimetric Waves

– DSP Digital Signal Processing

– CMA Circular Monopole Array

– LEO Low Earth Orbit

– MEO Middle Earth Orbit

– 5G Fifth Generation

– LHCP Left Hand Circular Polarization

– RHCP Right Hand Circular Polarization

– FCC Federal Communications Commission

– RF Radio Frequency

– SATCOM Satellite Communication

– SATCOM-on-the-move Satellite communication on the move

– TA Transmitarray

CHAPTER 1

INTRODUCTION

The need for improved spectral efficiency is increasing day by day. Due to technological advancements the demand of increased bandwidth will keep growing [1, 2, 3, 4]. To cater for the increasing demand of high data rates, increased channel capacity, and improved spectral efficiency high gain reconfigurable antennas have become a topic of great interest. They can dynamically change their radiation pattern in response to the signal environment. Reconfigurable antennas employ spatial diversity instead of spectrum division. They improve system quality, capacity and also allow the use of higher modulation schemes hence, reconfigurable antennas will play a key role in the next generation of wireless communication.

Beam reconfigurability is critically important in many applications [5]. For example, in radar applications, high gain beams need to be scanned to detect the target maneuvers. Antenna reconfigurability is also required in satellite communication where satellites revolve around Earth and beam scanning is required to maintain the communication link with non-stationary satellites. Similarly, to communicate with geostationary satellites beam steering antennas are required when a user is in motion. In millimetric wave (mmWave) wireless systems directive antennas provide high signal strength to overcome the path losses which consequently improves the quality of service. The effective isotropic radiated power (EIRP) can be expressed as:

$$EIRP = G_{tx}P_{tx} \tag{1.1}$$

$$EIRP(dB) = P_{tx} + G_{tx} \tag{1.2}$$

where, P_{tx} is the transmitter power, and G_{tx} is the antenna gain.

The use of high gain antenna increases the antenna gain (G_{tx}) which increases the EIPR, thus improving the overall network performance. Therefore, compared to omnidirectional antennas, smart antennas can dramatically improve the performance (such as power consumption, diversity, SNR, capacity, etc) of a wireless system. Smart antennas are backbone of wireless communication and will play a vital role in next generation communication networks [6, 7].

Communication at high frequency bands (mm-Wave frequency) is emerging as a good solution to fulfill the demand of increased bandwidth and higher data rates [1, 8]. However, path loss becomes considerably high at mmWave frequencies which effects the quality of communication link. The free space path loss equation is given below [9].

$$P_L = 92.4 + 20log(f_c) + 20log(d_x) \tag{1.3}$$

Where P_L is path loss in dB, f_c is frequency of operation and d_x is the distance between antennas (transmit and receiver antennas). Link budget is severely impacted by path loss which deteriorates the quality of wireless link [10, 11]. The solution to such problems is reducing the transmission distances and employing highly directional antennas [12].

Antennas capable of beam steering can provide high gain and can suppress noise and interference by avoiding communication towards the undesired direction [13]. As explained in Fig. 1.1, the antenna is getting signals from node 1, node 2 and node 3, however only node 2 is sending the desired signal. Hence, signals from node 1 and node 3 are creating interference and lowering the quality of service. If beam steering antennas are used here, the antenna can reconfigure its beam towards the desired direction (node 2) and suppress the unwanted signals from other directions. Similarly, the use of multi-beam reconfigurable antennas enable transmitting/receiving nodes to communicate with multiple users simultaneously thus increasing the spectral efficiency and throughput to multi folds as compared to the systems where a single fixed beam is employed. To incorporate the smart antennas in next generation wireless communication we need to design efficient, low cost and low profile antennas. Uniqueness of proposed antennas in this work are the design simplicity, low cost and multi-beam steering capability.

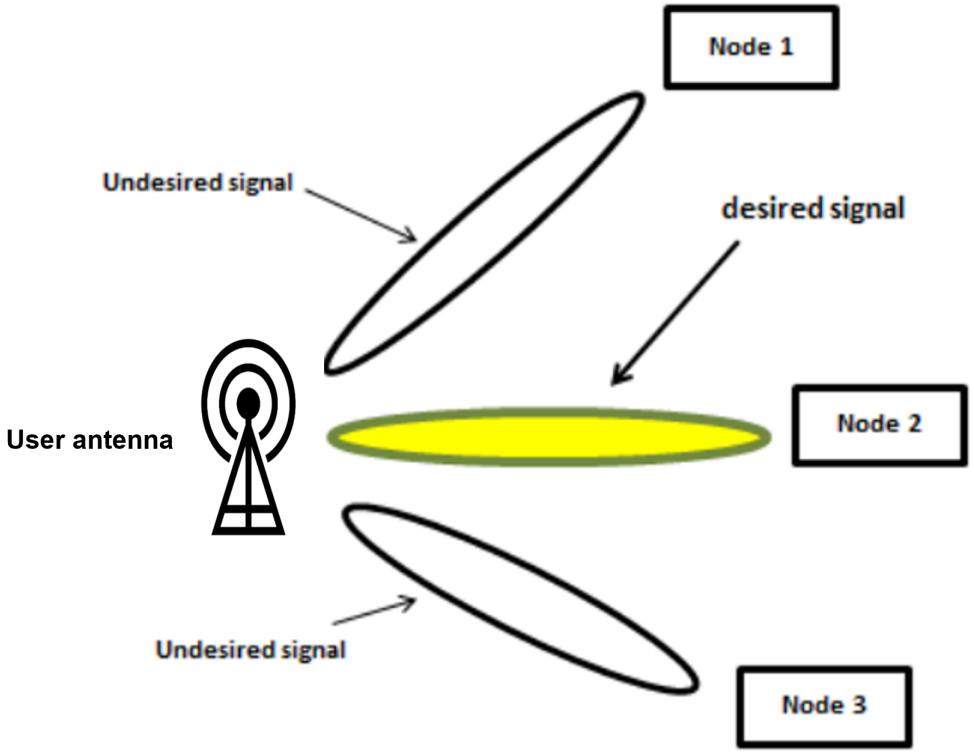

Figure 1.1: Illustration of directional beam steering.

1.1 Background

Smart or reconfigurable antennas have the ability to adopt their radiation pattern according to the environment. They are capable of modifying their radiation pattern dynamically in the controlled manner. Beam steering can be done mechanically, electronically or via a hybrid of electronic and mechanical steering. Various types of beam steering techniques will be covered in this section. We shall also investigate the merits and demerits of different beam steering techniques. Analysis of various beam steering techniques is given below.

1.1.1 Mechanical Beam Steering

Mechanically steered antennas involve mechanically moving the antenna assembly towards the intended direction using electric motors. They can provide low losses, high gain, and steering flexibility.

The conventional mechanically steered parabolic dishes do have some drawbacks, which include slow steering, physically large aperture, and having only a single independently steerable beam. As a result, alternative methods to improve these features and adding new functionalities is highly desirable.

1.1.2 Analog Beam-forming

Analog beam forming can be used to steer the antenna radiation pattern electronically without moving the antenna assembly. In analog beam forming, signal magnitude as well as phase can be changed which helps in beam steering as well as beam shaping. Fig. 1.2 depicts an example of analog beamforming based on a phase array module. As shown, signals goes through the transmit chain where the signal amplitude (A_k) as well as phase (θ_k) can be controlled to generate an antenna beam in the desired direction. Analog beam-forming is typically used in phased array antennas. It provides a lot of flexibility to reconfigure the radiation pattern electronically. However, this technique has some drawbacks. Each array element in phased array has a phase shifter and associated feed distribution network. Feed distribution network and required electronics increase the overall cost and complexity of design. Moreover, at high frequencies the feed network can add parasitic radiations which can severely impact the RF efficiency.

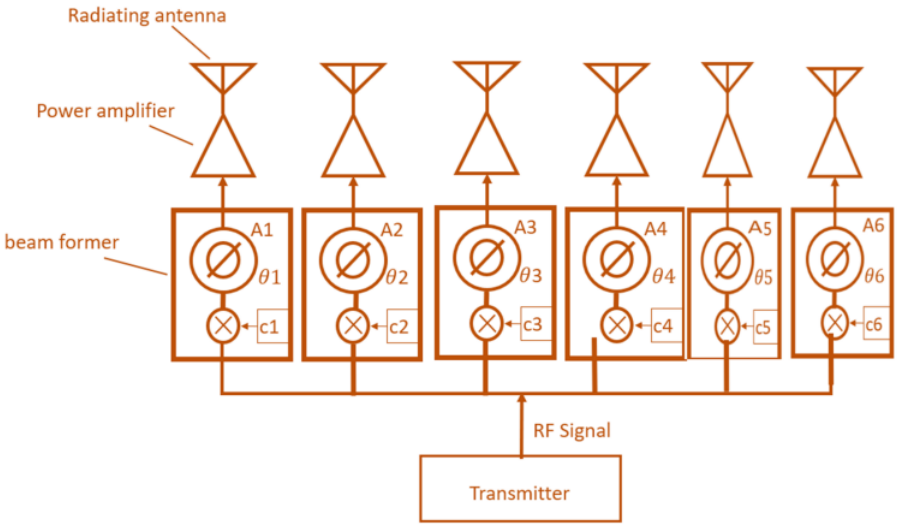

Figure 1.2: Analog beamforming.

1.1.3 Digital Beamforming

In digital beamforming amplitude/phase adjustment and their sum is carried out in the digital domain, Fig. 1.3 depicts a digital beam-forming module. Digital beam-forming consists of frequency converters, digital down converters (DDCs), analog to digital converters (A/D converter), complex weight multiplication and summing modules. Radio frequency (RF) signal is converted to intermediate signal (IF). A local oscillator signal is fed to a mixer in order to perform RF to IF conversion. After filtering, the signal then goes through the A/D converter and the digitized signal is then fed to the beam forming modules. This technique has bandwidth flexibility, it allows a user to generate multiple beams and also offers good control over beam shaping and steering. However, due to individual RF chains and complicated beam-forming modules such systems are subject to high power consumption and high cost.

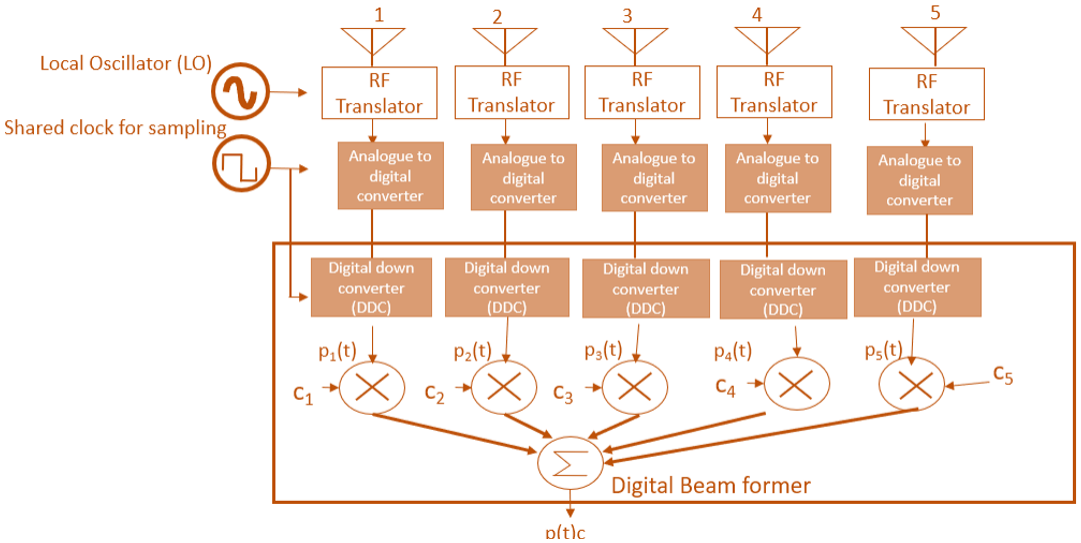

Figure 1.3: Digital beamforming.

1.1.4 Switched Beam Antennas

In this type of antenna, elements are arranged such that they cover a specific range of interest. Elements are usually arranged in a semicircular arrangement. Elements are activated when there is a need to communicate in a particular direction of interest [14, 15]. Fig. 1.4 shows the schematics of a switched beams antenna, eight antennas are arranged in a semi circular geometry and each antenna covers a specific range. Switched beam antenna can be single beam or multi beam. Multi beam antenna can accommodate multiple users at a same time as shown in Fig. 1.5, the antenna communicates with user 1, user 2 and user 3 simultaneously.

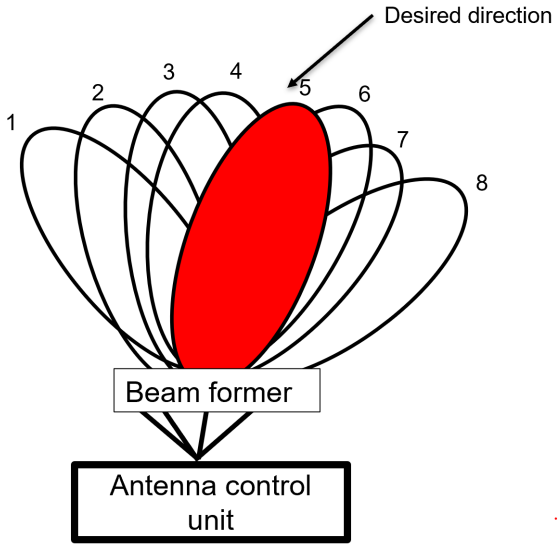

Figure 1.4: Schematics of switched beam antenna.

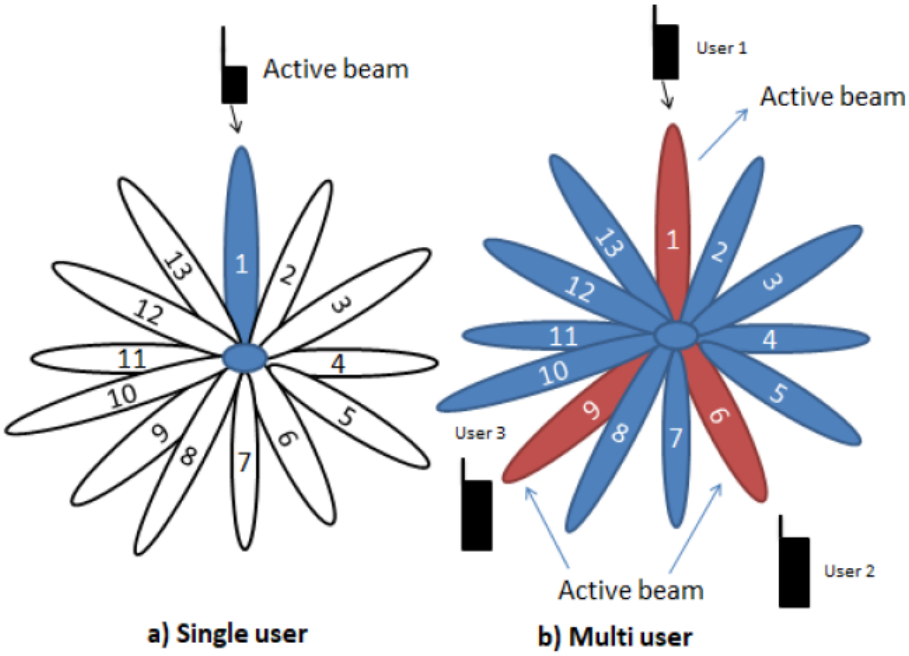

Figure 1.5: Coverage pattern for switch beam antennas.

In switch beam antennas, the overall goal is to increase the gain in desired direction. However beams are fixed /predefined and the intended user may not be

in the center of the beam. Shortcomings of these antennas are increased size and redundancy, interference and mutual coupling can occur between antennas which can affect the network efficiency. This technique is complicated to use for areas where interference is high. Fig. 1.6 compares the interference rejection comparison of a switched beam antenna and adoptive antenna. We can observe that the switch beam antenna can catch the interference and may lower the quality of reception for areas where interference is considerably high. Moreover, they are not capable of nulling the interference and have less coverage as compared to adoptive antennas. Despite all the disadvantages, this technique is less complicated as compared to completely adaptive systems and also increases the network range.

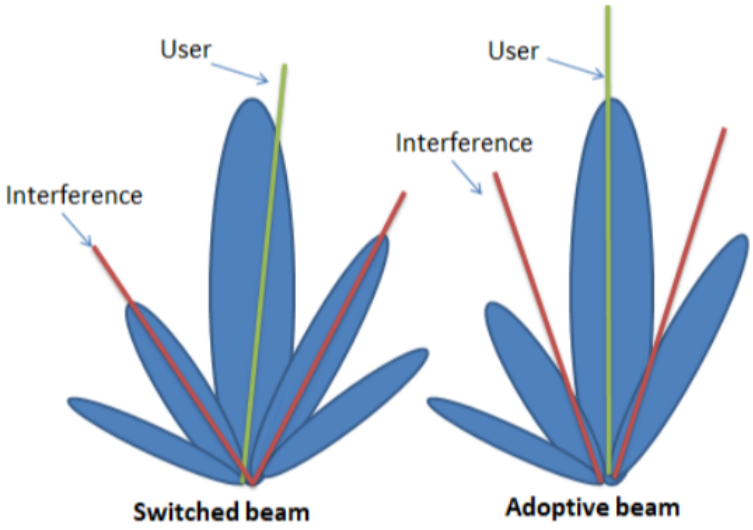

Figure 1.6: Interference rejection comparison.

1.1.5 Passive Electrically Steerable Antenna

Parasitic or passive electrically steerable antennas have usually one active element and multiple parasitic elements. Excitation is applied to the active element only and

parasitic elements are excited through mutual coupling between driven element (active element) and parasitic elements. The term parasitic is used for the element which gets energy through mutual coupling from the active element. A Yagi Udha antenna is considered as a basic and simplest parasitic steerable antenna. An example of a Yagi antenna is shown in Fig. 1.8. It consists of directors, reflectors and a driven element made up of half wave dipoles. Directors absorb the radiations from driven elements and redirect them with a different phase. Waves from multiple elements superpose to enhance the radiation pattern. In this manner, antenna gain increases substantially as compared to the gain of a simple dipole. This type of configuration can radiate in a specific direction. This design has been transformed into different configurations to achieve steerable patterns. Circular monopole array (CMA) is another configuration of parasitic steerable antennas [16, 17, 18, 19]. In such antennas, a driven element is placed at the center and parasitic elements surround the driven element [20, 21] . Parasitic elements are energized from driven central element via mutual coupling. An Electronically Steerable Parasitic Array Radiator Antenna (ESPAR) is an example of parasitic circular monopole array. It consists of a central monopole surrounded by six parasitic monopoles as shown in Fig. 1.7. An ESPAR antenna is simple and cheap to construct and can be used for directional communication.

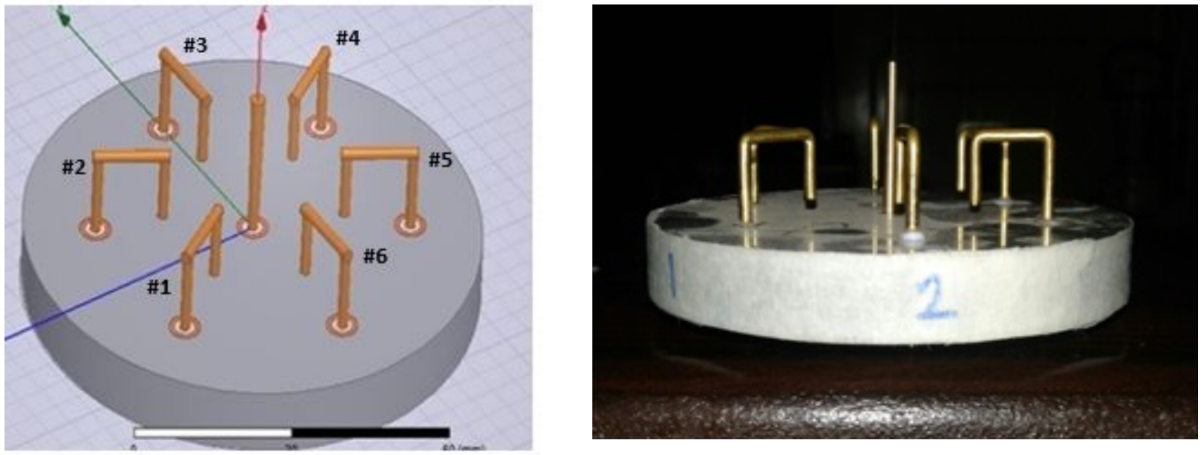

(a) (b)

Figure 1.7: Example of electronically steerable parasitic antenna array (a) Simulated antenna (b) Fabricated antenna.

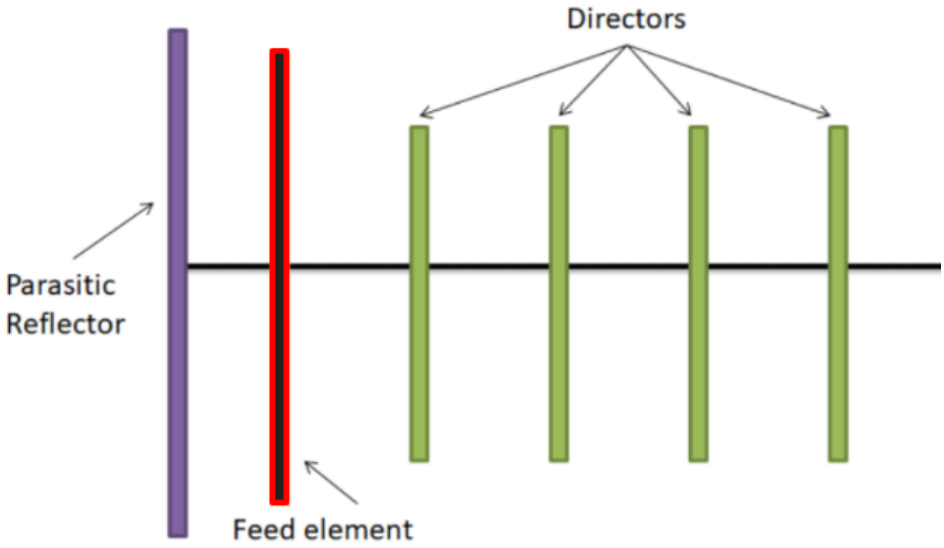

Figure 1.8: The model of Yagi antenna.

Beam steering in ESPAR antenna can be controlled by loading the array elements with varactors or phase shifters. Varactors provide variable reactance dependent on the applied voltage and control the overall radiation pattern formed by elements.

Parasitic antenna are easy to fabricate and are extremely low cost. Mutual coupling reduces power consumption of antenna systems and saves cost. However, major drawbacks of such antennas are limited gain and bandwidth. Hence, these antenna can not be used in high end devices.

1.1.6 Reconfigurable Reflectarray and Transmitarray Antennas

Steerable reflectarray antennas combine the advantages of parabolic reflectors and planar arrays. Reflectarray is made up of a combination of array elements (acting as a reflector) and a feed antenna [22, 23, 24]. In conventional reflector antenna, feed antenna is placed at the focal point of the reflector. The reflector reflects the EM waves towards the intended direction. In reflectarray antennas several elements are mounted to form an array structure as shown in Fig. 1.9. The array elements can be parasitic or driven depending upon the particular geometry of antenna. To generate the beam towards the desired direction each element needs to provide predefined phase compensation [25]. To achieve the required phase delay several configurations have been proposed. Array elements can be made with patches having variable length dimensions. By varying the dimensions of radiating patches, a desired phase range from 0° to 360° can be achieved [23]. Such antenna configurations combine the advantages of parabolic reflectors and the planar structure of antenna arrays. Due to flat and compact form, reflectarray enables an inexpensive fabrication procedure. To avoid the feed blockage in reflectarray, transmitarray can be used. Transmitarray capitalizes on the advantages of lens and phased arrays. Unlike reflectarray, transmitarray does not have ground plane so the incident signals pass through the aperture and hence feed blockage can be avoided. Reflectarray/transmitarray elements with dynamic phase tuning can provide continuous beam steering. Transmitarray can

steer the beam passively by integrating it with feed array. Elements of feed array are located at the focal plane of transmitarray and by turning on individual elements beam can be scanned. Multi-layered unit cell and multiple resonating elements can be employed to increase the bandwidth of reflectarray/transmitarray antennas. High gain, easy fabrication, compact form and dynamic beam scanning capabilities make them a potential candidate for telecommunications, spacecrafts, radars and wireless applications.

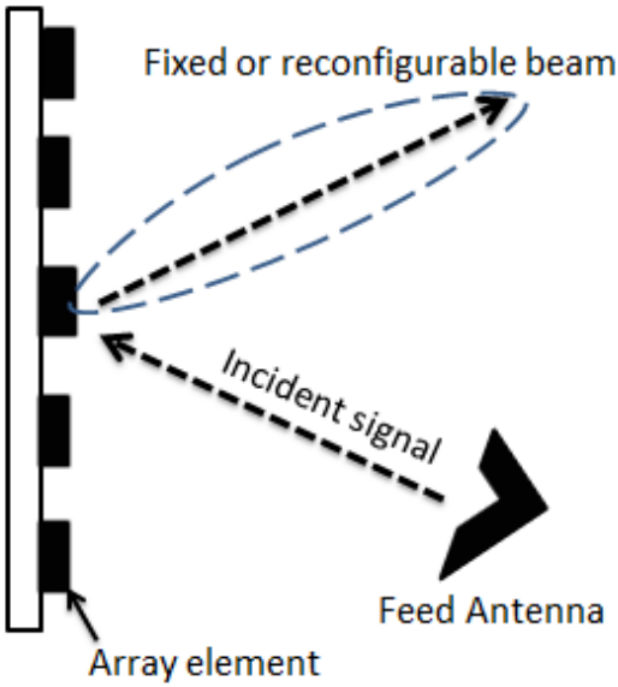

Figure 1.9: Reflect-array antenna basic configuration

1.1.7 Research Motivation and Goals

To incorporate the reconfigurable antennas in next generation wireless communication we need to design efficient, low cost, low power, and low profile antennas. Most of the current beam steering solutions are based on phased arrays. Phased

arrays are costly, have complex feed network, and suffer from parasitic radiations of feed network. Similarly, other antenna types including switched beam antennas and analog/digital beam forming antennas have their own shortcomings in terms of cost, complexity and power consumption. To avoid the complex feed network we considered spatial feeding for exciting the radiating aperture. Prominent examples of spatial feeding are reflectarray and transmitarray antennas discussed in the previous section (reference figure 1.10 and 1.11 respectively). A reflectarray/transmitarray can be tuned electronically by varying the electrical properties of individual elements. Unlike conventional parabolic reflectors and lenses, transmitarrays and reflectarrays are planar and tunable. They can be easily integrated with mounting surfaces. The phase distribution on reflectarray/transmitarray aperture can be easily tuned for dynamic beam control. Another prominent advantage of reflectarray/transmitarray is the possibility of applying phase synthesis to improve antenna characteristics, for instance using transmitarray we can generate dual or quad beams using only a single feed antenna, that is possible by applying the phase optimization which can support multiple beams. Similarly we can apply phase synthesis (like bifocal, quad focal, multi-focal phase distribution) to overcome gain scan loss or phase synthesis to control the side lobe level (like Particle Swam Optimization). In this work we propose the reconfigurable reflectarray and transmitarray antennas for next generation wireless networks. This work aims to address and resolve antenna design challenges in wireless communication with focus on multi beam solution, reconfigurability, polarization diversity, high gain, and low cost.

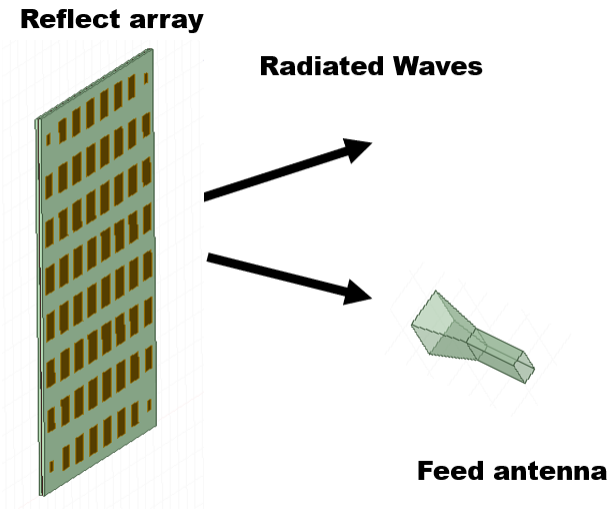

Figure 1.10: Reflectarray Antenna

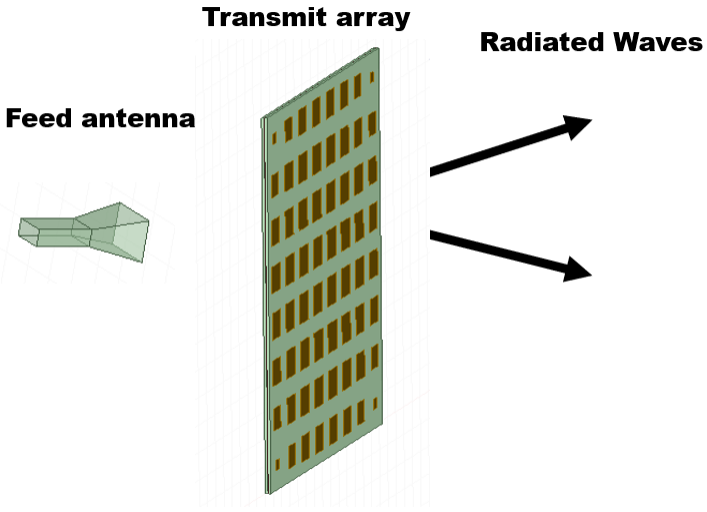

Figure 1.11: Transmitarray Antenna

1.1.8 Prior Art and our Proposed Solutions

At present, the most commonly used beam steering method is phased array. However, as we have discussed earlier phased arrays have multiple disadvantages

such as: high cost due to phase shifters, complicated beam forming architecture, high losses and high power consumption.

As a counterpart of phased arrays we propose a varactor controlled reflectarray antenna. The proposed design methodology combines the best features of two well-know high gain antennas which are; reflector antennas and microstrip arrays. Reflect-array combines the simplicity of the reflector antenna with performance versatility of phased arrays. Unlike the conventional parabolic reflector, reflect-array is a flat surface, and consists of a structure as simple as a single-layer grounded dielectric substrate on which the arrays are printed. Unlike the printed planar arrays/phased arrays, reflect-arrays do not have a complicated and costly beam forming network. As far as features are concerned, the best alternative to microstrip arrays and parabolic reflectors are microstrip reflectarray antennas [25]. Some of the attributes of reflectarray antennas are low profile, low cost, low power consumption, low mechanical complexity, compactness, conformity to mounting surface, beam scanning ability, and simplicity in implementation. These attributes make reflectarray antennas desirable as compared to phased arrays and parabolic reflectors. Reflect-arrays use spatial feeding which eliminates the need of a complex feeding network. It also eliminates the losses and parasitic radiations of feed network. Instead of using the phase shifter, beam steering in proposed reflectarray can be accomplished by using varactor diodes. This makes the design cost effective and simple to implement. Uniqueness of proposed reflectarray antenna is its design simplicity, low cost and effective beam steering capability. Fig. 1.12 shows the conceptual interpretation of our designed antenna. Our proposed design has the capability to provide high gain and low cost beam steering. The designed antenna has novel unit cell architecture that provides a large degree of phase tunability. The designed antenna has excellent beam steering capabilities with

good figure of merit. It is noteworthy that our proposed antenna achieves all these attributes with single layered architecture which makes our designed antenna low profile and cost effective. The proposed design reduces the cost and complexity of architecture while maintaining the continuous phase variation. Hence the proposed antenna is well suited for high end applications.

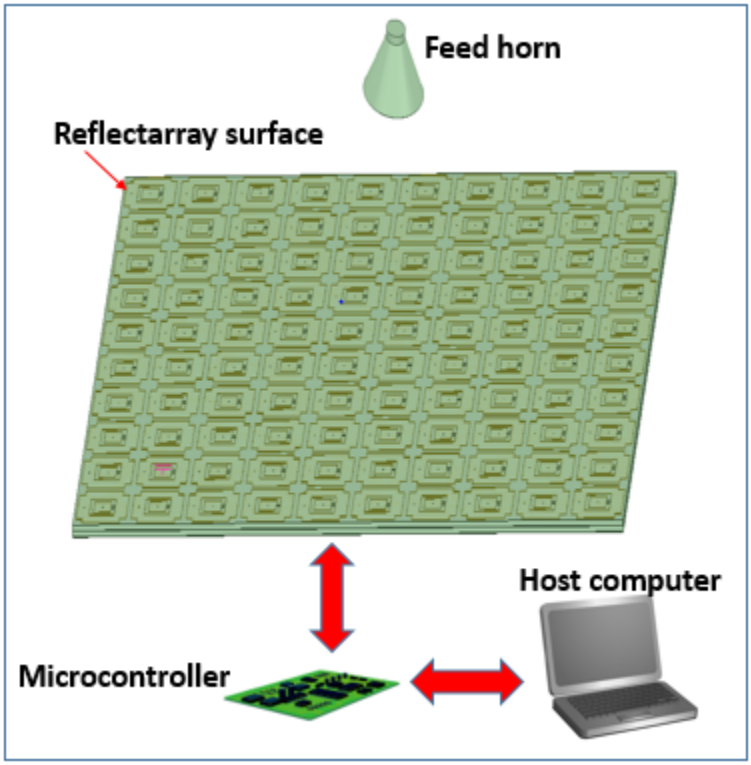

Figure 1.12: Electronically tunable reflectarray system

One untapped capability of reflectarray antennas is dynamic beam forming using the reconfigurable elements (unit cells). Unit cells are tuned to achieve the wide phase agility of 360^o. Reflectarray based on such unit cells provides an excellent platform to design a reconfigurable antenna that overcomes the limitations of traditional phased array antennas. Reflectarray do not involve complex feed distribution network and

individual RF chains are not required to feed each phasing element. Hence this approach provides many advantages as compared to traditional beam forming antennas including reduced hardware per element and increased efficiencies (due to spatial feeding). In the proposed design, the phasing elements are controlled by using varactor diodes. To keep the design low profile and simple, we have designed single layered phasing elements. Despite a single layer, phasing elements show excellent results in terms of scan range, figure of merit, bandwidth and reflection losses. The proposed design reduces the cost and complexity of the architecture and provides the continuous phase variation. Novelty of proposed design is its unique element design and low profile architecture. Instead of using the typical geometry for unit cells (phasing elements) like square patches, rings, crosses, dipoles and so forth we have designed a unique single layered phasing element. Fig. 1.13 shows the designed prototype.

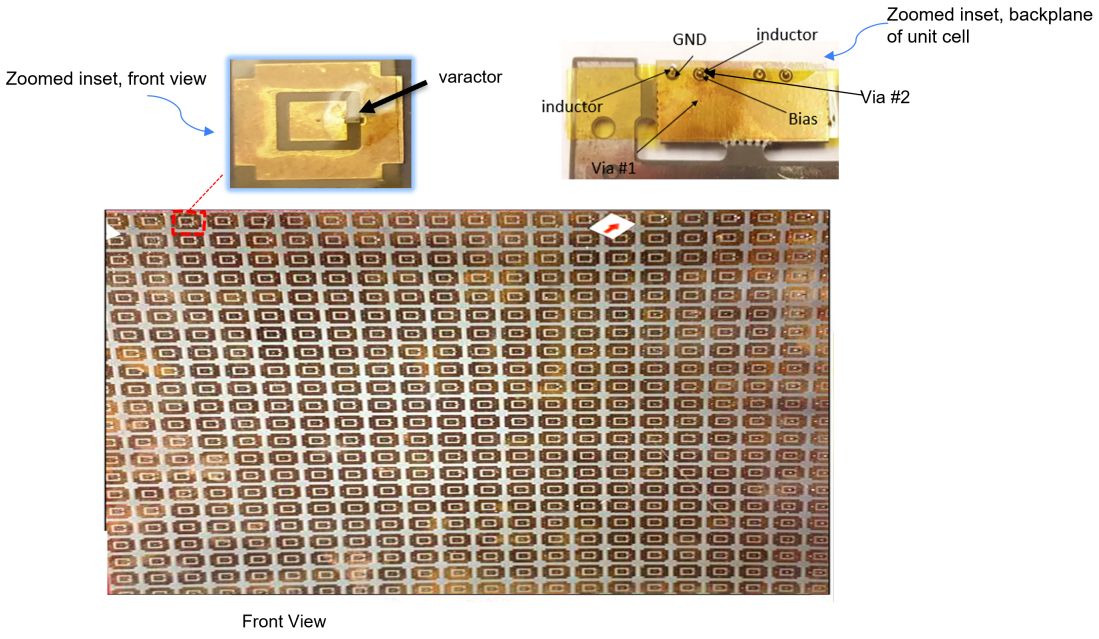

Figure 1.13: Designed electronically tunable reflectarray antenna.

The solution mentioned above provides reconfigurability while maintaining the low cost and simplicity, after successfully validating the above mentioned solution for beam agility we focused our attention towards generating the multiple high gain beams simultaneously, for this purpose we switched to transmit-array. A multi beam solution involves multiple feeds and feed blockage can be avoided with transmissive aperture. Multiple simultaneous beams enable MIMO implementation by creating a communication channel with multiple users/nodes simultaneously which increases the data rates and boosts overall system performance. Conventional multi beam solutions involve dense beam forming modules which are complex, power hungry and expensive. Our proposed solution involves the integration of transmitarray (lens) and multiple feed horns, where multiple reconfigurable beams are formed using transformation optics. Beam-steering is achieved by the 2D displacement of the feed horns above stationary passive aperture, Fig.1.15 and Fig.1.16 show the working mechanism. Transmitarray consists of a multi-layered unit cell, the required phase shift to collimate the beam towards the intended direction is achieved by using variable sized elements. Each cells acts like a phase shifter and adjusts the phase of incident signals so that the output waves coherently combine to make a directed beam as shown in Fig. 1.14. The proposed antenna involves 2D movement of feed horn(s) to realize wide angle beam steering in elevation plane and azimuth plane. Multiple feed horns are placed over the radiating aperture and robotic arms are employed to move the feed horns independently. This method enables creating multiple beams simultaneously as opposed to conventional mechanically steered antennas. The proposed approach does not involve active components hence does not suffer from; non-linearity issues, losses by RF components and thermal heating issues faced by conventional electronically

scanned antennas. As compared to conventional phased arrays the power consumption in the proposed antenna is low by multiple folds. Furthermore, the designed radiating element has been fabricated on printed circuit board which makes the the design simple and light. The proposed antenna features great advantages in terms of cost and complexity, yet achieves 2D steering and better scanning performance than other mechanical beam-scanning solutions demonstrated to date. The proposed solution can be easily realized since only feed displacement is required which simplifies the antenna assembly and also allows multi-beam solution (which is not possible with main stream mechanically steered antennas available in market).

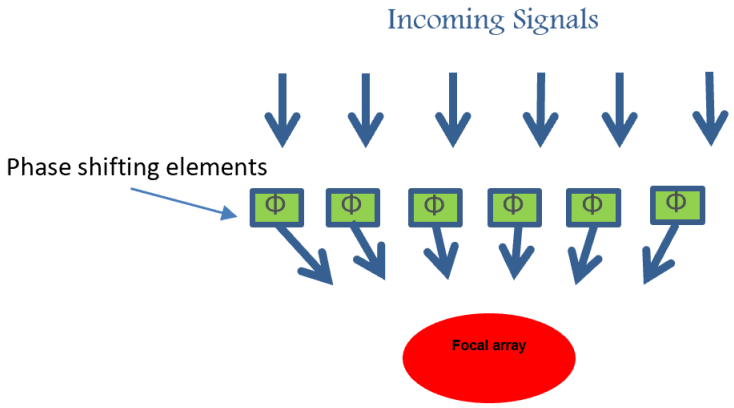

Figure 1.14: Beam focusing using phase shifting elements.

Inherently, the flat antennas suffer from scan loss which limits the beam scan range, our designed approach has minimized the scan loss and consequently increased the scan range by applying the optimum phase synthesis on transmitarray aperture. All practical constraints have been considered including antenna cost, selection of robust and certified materials to withstand harsh environmental conditions, and creating the fold-able version for easy deployment. Phase synthesis has been done to reduce the scan loss. Comparable antennas to date are bulky, have low gain, limited

scan range, limited number of beams or suffer from beam resolution issues. Furthermore, as opposed to complex digital beam forming, we can easily make multiple beams without complex hardware as we are using transformation optics. All of these features make it a mission enabling technology. As a proof of concept we present a design example which is composed of multilayered transmitarray. Beam steering of 360 degrees in azimuth plane and -40° to +40° in elevation plane has been achieved using this approach which was later increased to -80^o to $+80^o$ using multi-facet approach. We also demonstrated the capability of multi-beam steering using the proposed approach. The proposed approach can be implemented both mechanically and electronically. The mechanical implementation involves the feed displacement in x-y plane above stationery transmitarray and the electronic implementation involves switching between multiple feeds instead of displacement. Prominent attributes of our designed antenna are; increased efficiency, wide scan range, multi-beam capability, polarization diversity, high gain, and foldable assembly.

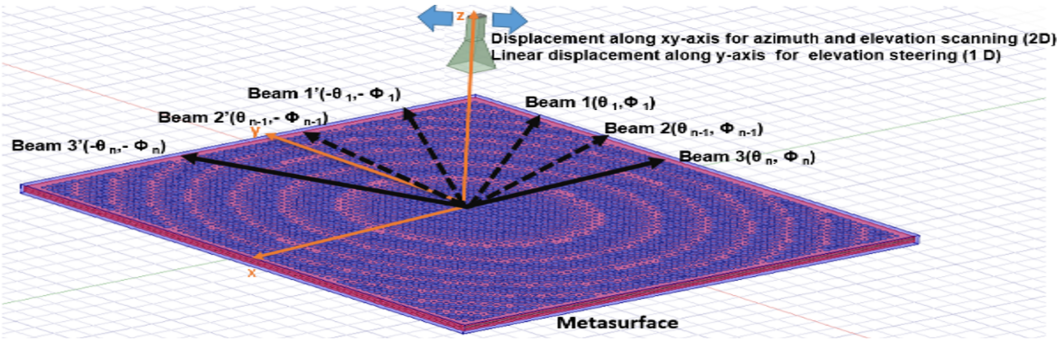

Figure 1.15: Beam steering configuration with feed displacement.

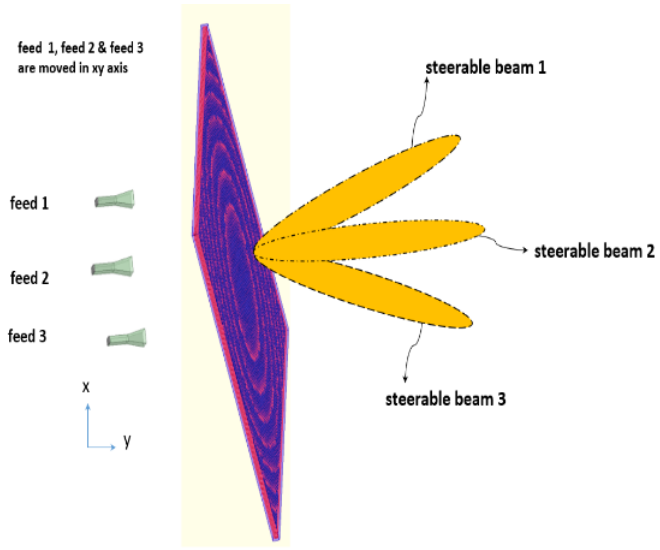

Figure 1.16: Multibeam configuration using passive metasurface.

1.1.9 Organization of Literature

In this chapter we have discussed the challenges, comparative analysis, cost and limitations of various beam-steering techniques. Currently, design cost and complexity of beam-steering antennas is high and there is a need to drive the cost down, there is also a need to develop cost effective and low powered solutions for multi-beam steering. Our proposed multi-beam transmit-array provides the capability of generating multiple simultaneous beams both electronically as well as mechanically. Similarly, our proposed varactor based reflectarray approach offers enormous cost saving and reduced complexity compared to conventional phased array. In the following chapters, we shall cover the mathematical modeling of reflectarray/transmitarray antennas, design and analysis of varactor based reflectarray (11 GHz) and passive multi beam transmitarray antenna at 30 GHz. In the end we will present the potential applications of designed antennas for practical applications like 5G mmWave system and satellite

communication (Satcom). Outline of literature is shown in Fig. 1.17.

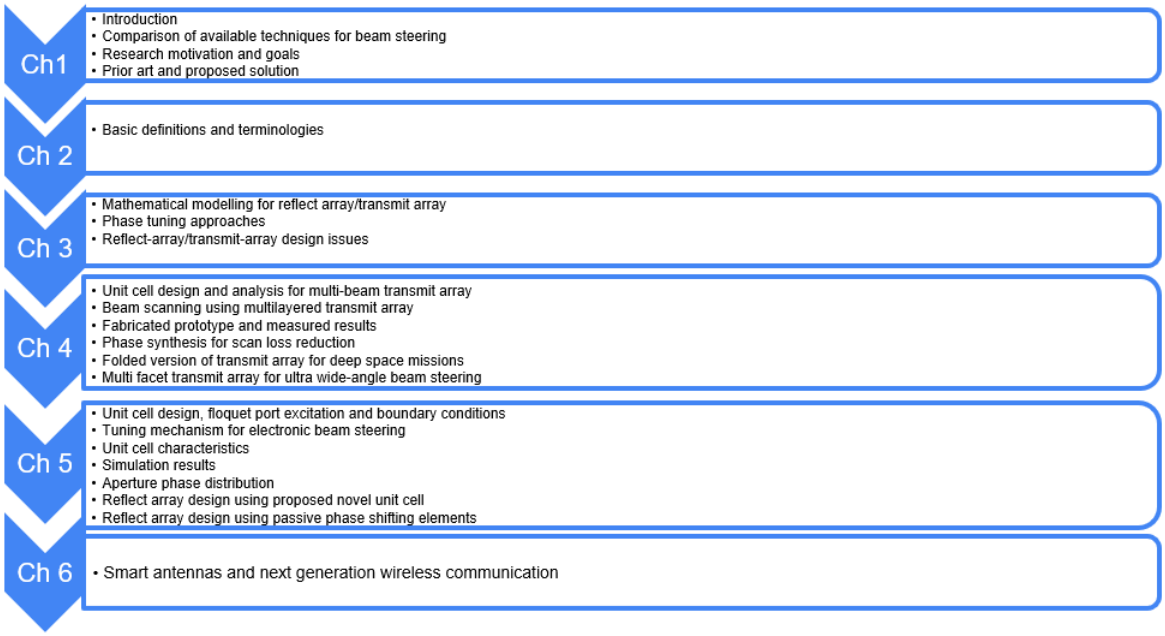

Figure 1.17: Outline

CHAPTER 2

BASIC DEFINITIONS AND TERMINOLOGIES

2.1 Reconfigurable Antenna

A reconfigurable antenna is an antenna which is capable of altering its radiation properties dynamically according to the environment. A Smart antenna has capability of tracking the signal and can transmit/receive multiple signals at once.

2.2 Antenna Gain

Antenna gain specifies how strong signal an antenna is receiving or transmitting from a particular direction. The higher the antenna gain, the higher is the signal strength transmitted or received from a particular direction. Fig. 2.1 shows an example of 3D gain plot. Antenna gain can be related to directivity and efficiency as:

$$G = D * e_{ff} \tag{2.1}$$

where, D is antenna directivity and e_{ff} is efficiency of antenna.

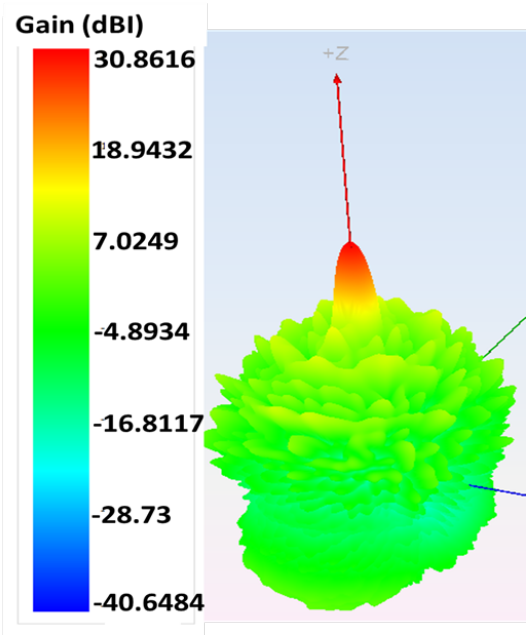

Figure 2.1: 3-D gain plot.

2.3 Antenna Efficiency

Efficiency of an antenna shows the ratio of power radiated to the incident power. If efficiency of antenna is high that means most of the power available at antenna's feed point has been radiated in space. Low efficiency shows that most of the power delivered to antenna has been reflected back or absorbed within antenna. Low efficiency can be because of following factors.

- Impedance mismatch
- Conduction losses
- Dielectric losses

Mathematically efficiency can be expressed as:

$$E_R = \frac{P_r}{P_{in}} \tag{2.2}$$

Where P_r is the radiated power by antenna and P_{in} is the input power.

2.4 Main Beam and Side Lobes

The main lobe or main beam of an antenna shows the region of maximum field strength. The main lobe exhibits higher power intensity. The side lobe on the other hand shows lower field strength as compared to the main lobe. Fig. 2.2 shows the radiation pattern of an antenna containing main lobe and side lobes.

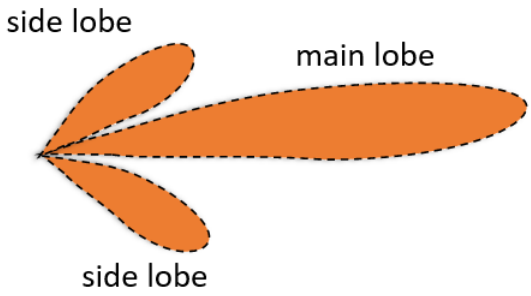

Figure 2.2: Antenna propagation pattern.

2.5 Basic Terminologies for Reflectarray/Transmitarray Antenna Configurations

2.5.1 Metasurface

A metasurface is an artificial sub-wavelength micro-structured interface that manipulates electromagnetic waves by spatially arranged cells.

2.5.2 Unit cell

Unit cells are the building block of metasurface. Each unit cell acts as a phase shifter. Entire surface can be built up by the repetition of unit cell in three dimensions. Fig. 2.3 shows an example of metasurface made by repetitions of unit cell.

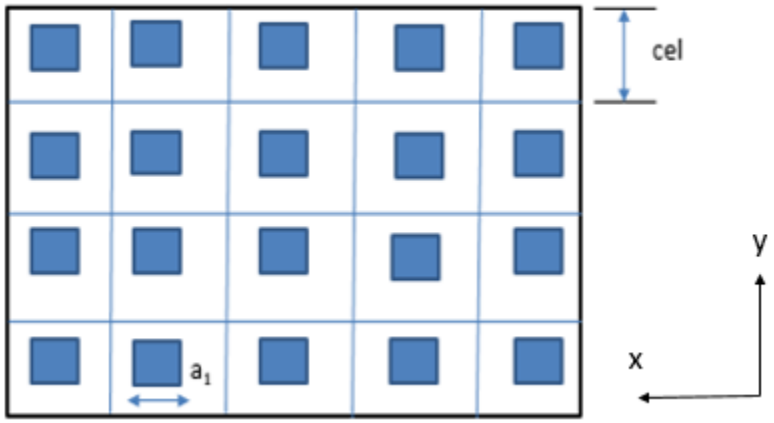

Figure 2.3: Unit cell.

2.5.3 Substrate

Printed antennas are made by etching the element pattern on substrate. Substrate provides a medium for etching the element patterns. Hence, substrate plays a vital role in antenna designing. Variation in substrate properties and thickness can greatly affect the antenna properties.

2.5.4 Phase Range of Unit Cell

Phase range of unit cell defines its beam steering capability, it defines the amount of phase shift a unit cell adds to the incident wave. Scattering properties of incident

wave greatly depends on unit cell geometry/properties. In reflect-array/transmit-array antennas, the goal is to design a unit cell which has phase range of 360°.

2.5.5 Single layered/Multi layered Unit cell

Metasurface unit cells can be single or multi-layered.

- Single layered cells are light weight, easy to fabricate, and provide a very sharp resonant curve. However, it is difficult to achieve the full phase range of 360 degrees using the single layer resonant cells.

- Multi layered cells extend the phase range even beyond a full 360° cycle and provide a flatter resonance at the cost of increased fabrication complexity and weight.

Fig. 2.4 shows configuration of single and multilayered metasurface.

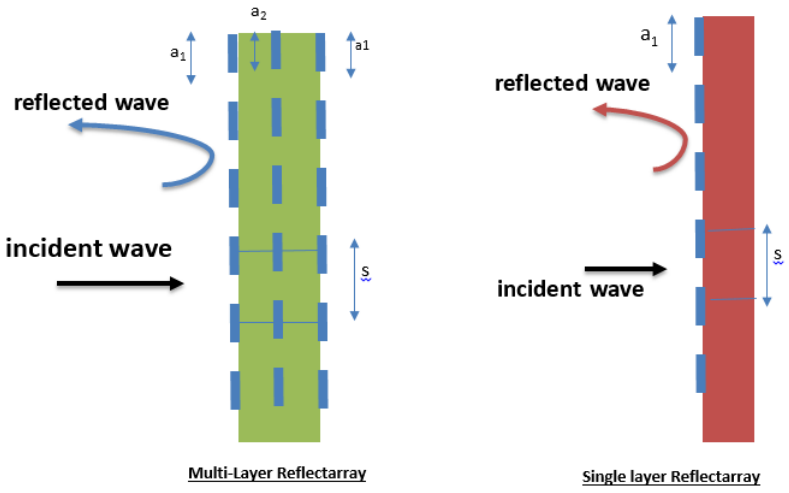

Figure 2.4: Multilayered and single layered reflectarray.

2.5.6 Gain Scan Loss

Gain scan loss depicts the loss in antenna gain as the beam is steered off broadside. Fig. 2.5 plots scan loss vs. scan angle. We can observe that at boresight the scan loss is zero and as we move away from boresight antenna gain drops. At 60^o we observe the scan loss of 4 dB in this particular example. Gain scan loss is an important antenna parameter and it needs to be reasonably lower to achieve the optimal performance of an antenna.

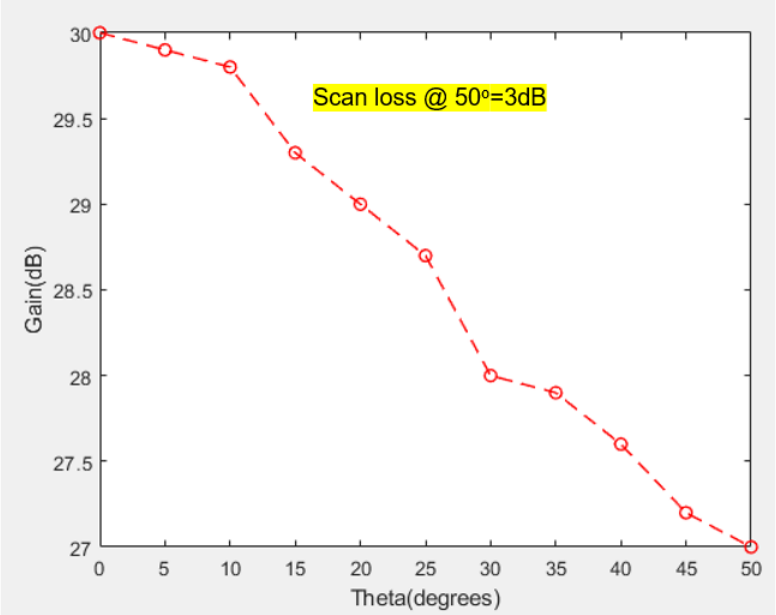

Figure 2.5: Gain vs scan loss.

CHAPTER 3

THEORETICAL ANALYSIS OF TRANSMITARRAY/REFLECTARRAY

As discussed in chapter 1, reflectarray/transmitarray (also know as metasurface) antenna consists of planar or conformal surface and illuminating feed antenna. Principally, transmitarrays and reflectarrays work in similar fashion. Their design involves design and characterization of phasing elements (unit cell), feed radiator design and aperture phase distribution. We developed the MATLAB algorithm to automate the aperture phase distribution to effectively design the reflectarray/transmitarray aperture. We shall discuss all of these procedures in detail in the following chapters. In this chapter we will study basics of synthesizing the phase distribution on the reflectarray and transmitarray aperture. We shall also discuss different phase tuning approaches to see how individual elements are designed to produce the shaped or collimated beam in the desired direction.

3.1 Mathematical Reasoning

Far-field radiation pattern of a space-fed array antenna, e.g., reflectarray and transmitarray, can be computed using the array theory. Consider the array of antenna elements as shown in Fig. 3.1.

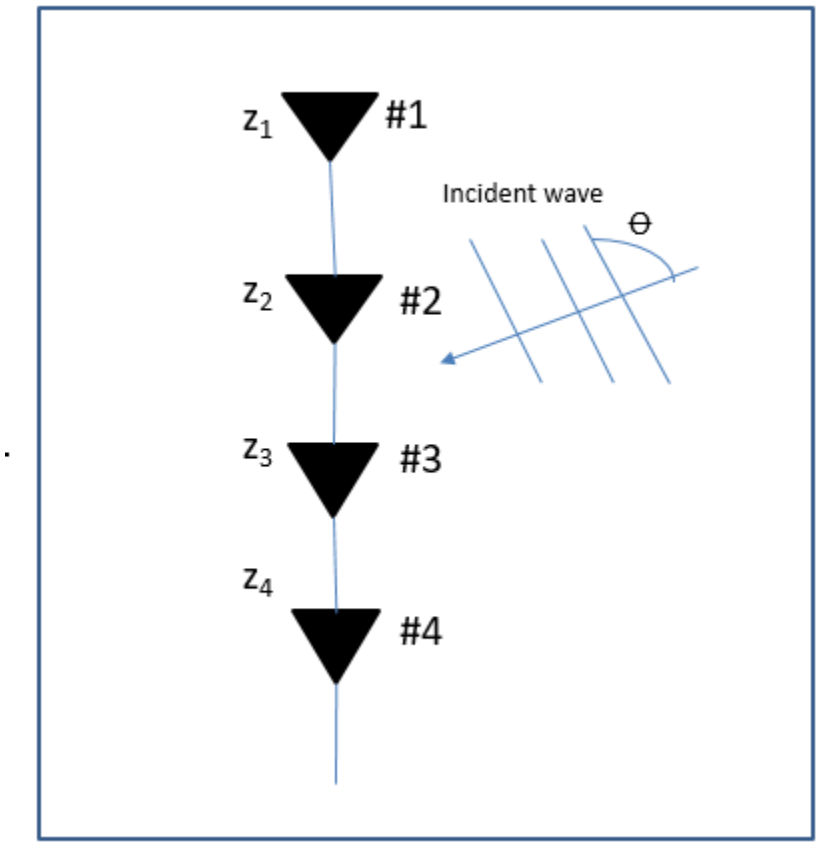

Figure 3.1: 4-Element array.

Radiation pattern of each element is given as:

$$P(\theta, \phi)$$

Assume element 1 to be located at:

$$P_{1=}(x_1, y_1, z_1)$$

Similarly i_{th} element will be located at:

$$P_{i=}(x_i, y_i, z_i)$$

For element 1, the output will be

$$Y_1 = P(\theta, \phi) I_1 e^{-jk_0.\vec{r_1}} \tag{3.1}$$

Where I_1 is the excitation coefficient.

Similarly for element 2 the output will be:

$$Y_2 = P(\theta, \phi) I_2 e^{-jk_0.\vec{r_2}} \tag{3.2}$$

Similarly for n_{th} element the output will be:

$$Y_N = P(\theta, \phi) I_N e^{-jk_0.\vec{r_N}} \tag{3.3}$$

The output of all the elements summed together will be given as:

$$Y = P(\theta, \phi) I_1 e^{-jk_0.\vec{r_1}} + P(\theta, \phi) I_2 e^{-jk_0.\vec{r_2}} + P(\theta, \phi) I_3 e^{-jk_0.\vec{r_3}} + ... + P(\theta, \phi) I_N e^{-jk_0.\vec{r_N}} \tag{3.4}$$

The above equation can be simplified as:

$$Y = P(\theta, \phi) \sum_{i=0}^{N-1} I_i e^{-jk_o.\vec{r}_i} \tag{3.5}$$

$$Y = P(\theta, \phi) * ArrayFactor$$

$$ArrayFactor = \sum_{i=0}^{N-1} I_i e^{-jk_o.\vec{r_i}}$$

The product of element pattern and array factor determine the radiation pattern of array. The general form of the array factor is defined as [26]:

$$AF = \sum_{i=0}^{N-1} J_i e^{-jk_o \hat{\boldsymbol{r}}.\vec{r'}} \tag{3.6}$$

Where $\boldsymbol{J_i}$ is the excitation of i_{th} element.

$\hat{\boldsymbol{r}}$ is unit vector of observation point, and

$\vec{\boldsymbol{r'}}$ is the position vector of i_{th} element with respect to a reference element on array.

Lets consider the linear uniformly spaced array along z-axis.

$$\hat{r} = sin\theta cos\phi\hat{x} + sin\theta sin\phi\hat{y} + cos\theta\hat{z}$$

$$\vec{r_i} = z_i'\hat{z}$$

$$\hat{r}.\vec{r_i} = (sin\theta cos\phi\hat{x} + sin\theta sin\phi\hat{y} + cos\theta\hat{z}).z_i\vec{z} \tag{3.7}$$

$$\hat{r}.\vec{r_i} = cos\theta z_i'$$

Hence array factor becomes:

$$AF = \sum_{i=0}^{N-1} J_i e^{jk_o z_i' cos\theta} \tag{3.8}$$

Similarly the array factor for evenly spaced arrays along x-axis can be expressed as:

$$\vec{r_i} = x_i' \hat{x}$$

$$\hat{r}.\vec{r_i} = (sin\theta cos\phi \hat{x} + sin\theta sin\phi \hat{y} + cos\theta \hat{z}).x_i' \hat{x} \tag{3.9}$$

$$\hat{r}.\vec{r_i} = x_i' sin\theta cos\phi$$

$$AF = \sum_{i=0}^{N-1} J_i e^{jk_o x_i' sin\theta cos\phi} \tag{3.10}$$

In similar manner we can express the array factor for planar arrays oriented in x-y directions as shown in Fig. 3.2.

$$\hat{r} = sin\theta cos\phi \hat{x} + sin\theta sin\phi \hat{y} + cos\theta \hat{z}$$

$$\vec{r_i} = x_i' \hat{x} + y_i' \hat{y}$$

$$\hat{r}.\vec{r_{mn}} = (sin\theta cos\phi \hat{x} + sin\theta sin\phi \hat{y} + cos\theta \hat{z}).(x_{mn}' \hat{x} + y_{mn} \hat{y}) \tag{3.11}$$

$$\hat{r}.\vec{r_{mn}} = sin\theta cos\phi x'_{mn} + sin\theta sin\phi y'_{mn} \tag{3.12}$$

Hence the array factor for planar arrays can be expressed as:

$$AF = \sum_{m=0}^{N-1}\sum_{n=0}^{N-1} J_i e^{jk_o(sin\theta cos\phi x'_{mn} + sin\theta sin\phi y'_{mn})} \tag{3.13}$$

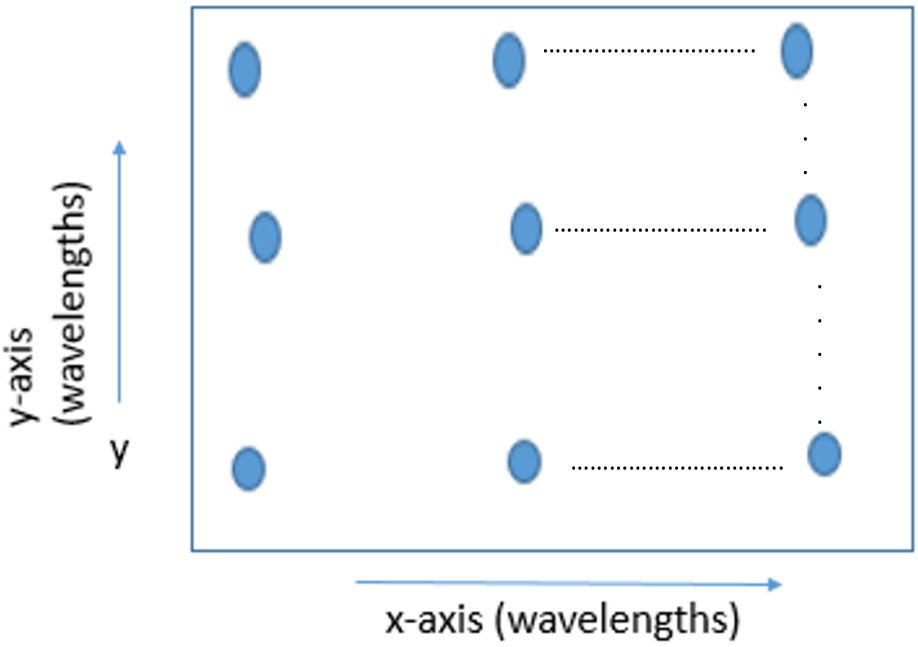

Figure 3.2: Geometry of planar array.

In planar antenna arrays, progressive phase distribution is applied to individual array elements to focus the beam towards the desired direction. Reflectarrays/transmitarray have the similar operating principle; however, feed antenna position needs to be taken into account. To explain the operating mechanism of reflectarray, consider an imaginary plane say X‘ (shown by dotted line in Fig. 3.3). In order to produce a directive beam in the direction (θ_o, ϕ_o) the transmitted fields (by the feed radiator) and emitted beams (by each element of the array) must cover the same electrical

distance to the plane so that uniform phase distribution is achieved across the plane. Mathematically this can be expressed as [25, 27]:

$$-k_o d_i + \varphi_{Ri} = \beta_i \tag{3.14}$$

$$i = 1, 2, 3, 4....N$$

Where, k_o is the wave number.

d_i is the distance between feed antenna and i_{th} element.

β_i shows the progressive phase distribution at i_{th} element.

φ_{Ri} is the phase shift required at i_{th} element.

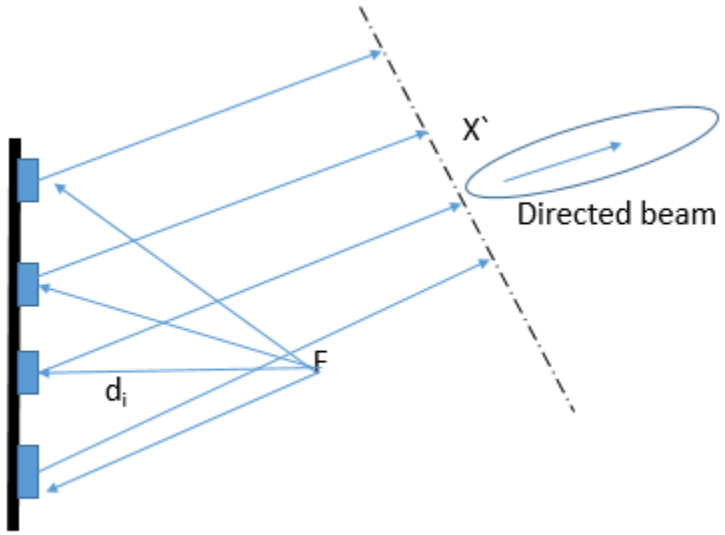

Figure 3.3: Reflectarray schematics.

Using the array factor for N element planar array we derived previously:

$$AF = \sum_{i=0}^{N-1} J_i e^{jk_o \hat{\boldsymbol{r}}.\vec{r'}} \tag{3.15}$$

$$J_i = J_i e^{j\beta_i} \tag{3.16}$$

$$AF = \sum_{i=0}^{N-1} J_i e^{j(\beta_i + k_o[x'_i sin\theta cos\phi + y'_i sin\theta sin\phi]} \tag{3.17}$$

$$\beta_i = -k_o[x'_i sin\theta cos\phi + y'_i sin\theta sin\phi] \tag{3.18}$$

Therefore, to form beam in a direction (θ_o,ϕ_o) the phase shift required by each element is given as:

$$\varphi_R(x_i, y_i) = k_o(d_i - x_i sin\theta_o cos\phi_o - y_i sin\theta_o sin\phi_o) \tag{3.19}$$

$$\varphi_R(x_i, y_i) = k_o[d_i - x_i sin\theta_o cos\phi_o - y_i sin\theta_o sin\phi_o] \tag{3.20}$$

$$d_i = \sqrt{(x_i - x_f)^2 + (y_i - y_f)^2 + (z_f)^2} \tag{3.21}$$

Where, (x_i,y_i) are coordinates of reflectarray i_{th} unit cell, and

(x_f, y_f, z_f) are coordinates of feed phase center.

Thus Equation (3.22) is used to calculate the phase shifts that have to be programmed into the individual array elements to form beam in the direction (θ_o, ϕ_o). Reflectarray/transmitarray metasurfaces can produce fixed or reconfigurable beam. For fixed beam reflectarray/transmitarray the radiation pattern is fixed in particular

direction and beam steering can not be achieved. For reconfigurable reflectarray, beam steering can be achieved by tuning the phasing elements of metasurface. Reconfigurable metasurfaces are desirable since they can adopt the radiation pattern according to the environment.

The phase compensation in antenna arrays can be explained by assuming the N elements array shown in Fig. 3.4. To form a directional beam, waves must reach the observation point p at the same time. However the element 1 is closer to the observation point and element 2 is relatively apart from observation point. To make sure the rays reach the observation point at the same time we need to compensate for this path length and this compensation is indicated by red line in Fig. 3.4, using trigonometry the path length y can be defined as:

$$y = dsin(\theta)$$

where d is inter element spacing and θ is the angle of desired beam.

$$\frac{\lambda}{y} = \frac{2\pi}{\varphi}$$

$$\varphi = y(2\pi\lambda)$$

$$\varphi = \frac{2\pi(dsin(\theta))}{\lambda}$$

$$\varphi = k_o(dsin\theta)$$

Where k_o is free space propagation constant. Therefore to make a directed beam towards θ, the progressive phase shift of $k_o dsin\theta$ has to be applied on each element.

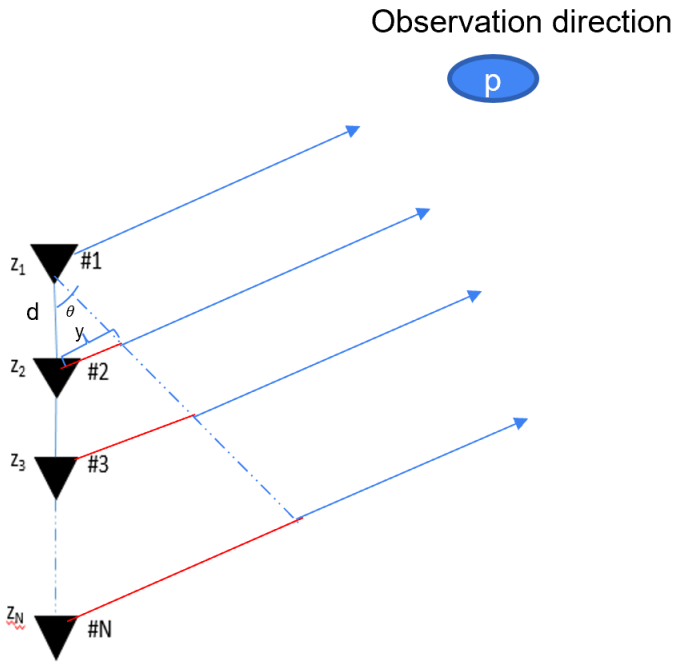

Figure 3.4: Phase compensation in antenna arrays.

3.2 Approaches to Design the Phasing Elements

Different approaches are available for phase tuning of metasurface. Selecting a phase tuning methodology is a critical step in designing the radiating aperture. Some phase tuning approaches yield fixed beam metasurfaces and on the other hand a lot of phase tuning approaches are available for designing reconfigurable metasurface antennas. Phase tuning approaches can be categorized as:

1. Phase tuning using phase/time-delay lines.

2. Phase tuning using tunable substrate.

3. Phase tuning using elements with variable dimensions.

4. Phase tuning using variable rotation angles.

5. Phase tuning by loading elements with dynamic components (varactor diodes, PIN diodes etc.)

In phase tuning approach using the phase/time delay, the incident EM wave received by the element is phase shifted using the delay lines. In tuning approach, using the variable size elements, the phase is controlled by changing the dimensions of metasurface unit cells. Unlike the former two approaches, phase tuning using electronic components (e.g PIN diodes, varactors etc.) and tunable substrate offers reconfigurability. In these approaches we can tune the elements to direct radiated beam in multiple directions. Phase tuning using variable rotation angles is mainly used for circularly polarized designs. We shall discuss the detailed overview of all these phase tuning approaches in this section.

3.2.1 Phase Tuning using Variable Transmission Line (delay line)

In this approach, metasurface unit cells have variable length delay lines, typically microstrip transmission lines. Phase shift added by each element depends on the length of transmission line. Fig. 3.5 shows a schematic model of this approach. Variable sized delay lines add variable path delay to the incident signals which can be used to provide the phase compensation to produce the collimated beam towards the desired direction.

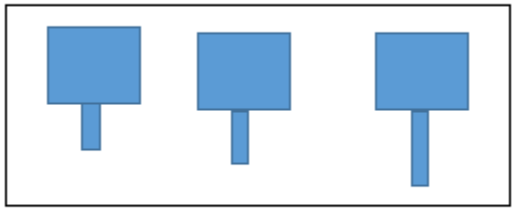

Figure 3.5: Unit cells with variable length delay lines.

3.2.2 Phase Tuning using Variable Length Elements

Reconfigurability can be achieved by using variable sized radiating elements. Phase of reflected wave changes as dimensions of elements are varied using this fact phase variation can be produced by varying the dimensions of reflectarray elements [25]. Fig. 3.6 shows an example of such array. The similar working mechanism holds for transmitarray where phase of transmitted wave can be changed by using variable sized passive scatters (unit cells). This method is discussed in detail in chapter 4 and 5.

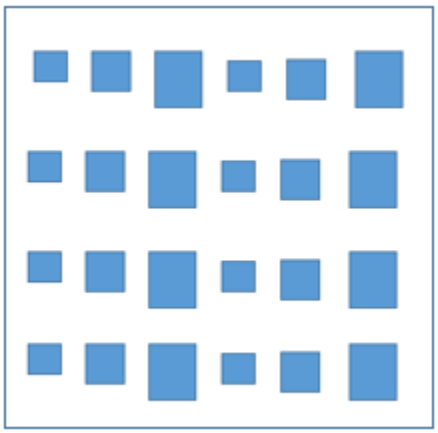

Figure 3.6: Unit cell with variable dimensions.

3.2.3 Elements with Variable Rotation Angle

This approach is used in circularly polarized antennas. Rotating a circularly polarized antenna about its origin changes the radiated phase by the same amount [28]. Fig. 3.7 shows an example of such configuration. We can observe that all phasing elements have the same geometry but because of different rotation angles the phase induced by these elements would be different.

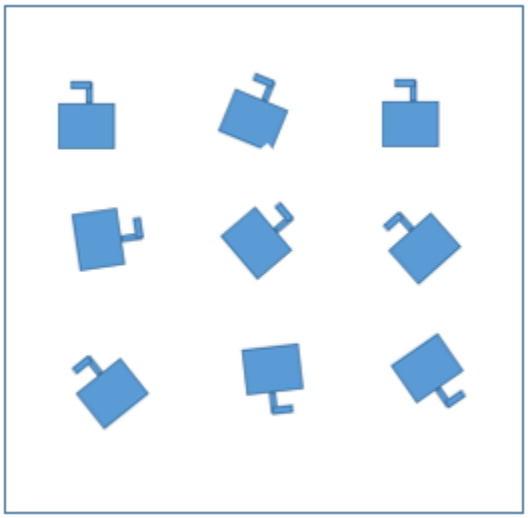

Figure 3.7: Unit cells with variable rotation angle.

3.2.4 Phase Tuning using Tunable Substrates

Electronic reconfigurability can be attained by using tunable substrates [29]. Characteristic impedance of unit cell can be changed by changing the dielectric constant of substrate which consequently induces the phase agility to tune the unit cell. In the last few years, lots of substrate tuning technologies have been introduced. Liquid crystal based tunable substrates are being widely explored for substrate tuning. Liquid crystals (LC) have unique optical properties. They are made up of elongated rod-like

molecules. They possesses properties of solid crystals and conventional liquids. For instance, LC may flow like liquids but its molecules may have been oriented like solid crystals. They possess different electrical characteristics dependent on external fields. The orientation of LC can be changed by applying an external electric field. Hence, effective permittivity can be changed by controlling bulk orientations. Varying the bias voltage changes the permittivity of material which changes the radiation characteristics of the phasing element. Fig. 3.8 shows an example of liquid crystal based unit cell where a layer of liquid crystal is added underneath the radiating patch. By applying variable voltage on patch, liquid crystal can be tuned to control the characteristic impedance of unit cell. Liquid crystals are temperature sensitive. Using tunable substrate it is relatively difficult to obtain a wide phase range of 360°. The fabrication process is complex and requires special facilities.

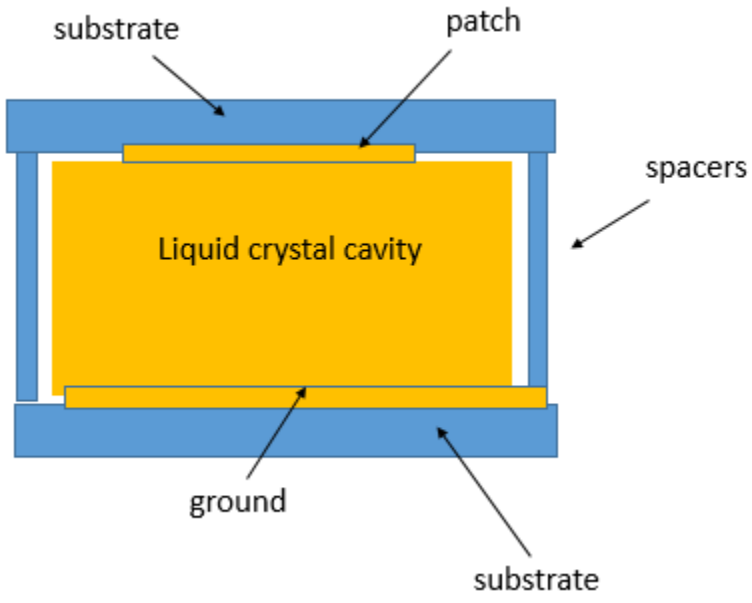

Figure 3.8: Liquid crystal based element.

3.2.5 Phase Tuning by Integrating Phasing Elements with Dynamic Components

Phase tuning of metasurface elements can be achieved by loading the phasing elements with a controllable phase shifter e.g. PIN diodes, varactors diodes and MEMs devices. This method provides an excellent beam steering solution since each element can be individually tuned. Resonance of elements can be directly controlled by using RF components. A varactor diode provides voltage dependent capacitance for element tuning and hence by varying the biasing voltage the varactor provides variable capacitance which in turn tunes the element. Our next chapter includes detailed discussion on varactor loaded elements for electronic beam steering.

3.3 Reflectarray\transmitarray Design Issues

The previous section outlined the different design approaches used to develop the reflectarray/transmitarray elements. When designing these elements, there are some design issues that designers need to cater in order to maximize the antenna performance. This section will highlight design issues that need to be accounted in order to make an optimum design.

3.3.1 Errors due to limited unit cell phase range

When metasurface is designed to produce the radiation pattern in direction of interest, each element/unit cell contributes to produce a specific phase shift. Ideally, unit cell should be able to produce the phase shift of 360^{o}. Unit cell phase range can be evaluated using a full wave electromagnetic (EM) simulator. If unit cells are not able to produce phase shift of 360°, some elements will have unattainable phase shift

which lowers the overall antenna gain and increases the side lobe level. In order to avoid phase errors metasurface elements should be capable of providing wide phase agility. Therefore to achieve the best design features, our aim is to keep the unit cell phase range of around 360 degrees for the metasurfaces designed in the chapter 4 and 5.

3.3.2 Element loss:

The unit cell losses include the conductor loss, reflection loss, and dielectric loss which degrade the transmission magnitude of transmitarray elements. Ideally unit cell should emit all the incident EM waves, however in actual due to losses within radiating structure a portion of incident wave is absorbed which deteriorates the overall performance of radiating structure. Unit cells with high transmission losses are inefficient and yield a poorly designed aperture. Antennas having poor reflection loss have poor figure of merit and hence a poor performance. Therefore while designing a phasing element, the element loss should be considered as an important design parameter and should be kept into consideration. Characteristics of unit cell can be modeled in EM simulator that includes transmission phase and magnitude response. Dielectric losses and conductor losses can be considered by selecting the practical materials in EM simulator which include the conductivity of conducting materials and loss tangent of dielectric materials.

3.3.3 Quantization errors

In the design process of metasurface, phase distribution is measured for desired angle and based on phase distribution phase shift on each element is calculated. To find the phase range of elements, tuning characteristics are varied depending on

control parameters (e.g. variation in dimensions or bias voltages etc). In this process the phase shift achieved are not continuous and practically we choose values which are closer to calculated quantized values of phase shifts. The difference between ideal phase shift and quantized phase produces quantization errors.

3.3.4 Infinite array approximation error

The basic step in reflectarray/transmitarray antenna designing is design and analysis of unit cell. For that purpose, an infinite array approach is used to realize the unit-cell characteristics. In this approach dimensions/characteristics of the adjacent elements are assumed to be almost identical. However in some cases this condition is violated that results in some errors. As an example in case of elements with variable dimensions during phase wrap elements dimensions jump from maximum dimension to minimum. Hence in that case this approximation may not be valid, which results in errors.

3.3.5 Limited Bandwidth

In practical designs, the bandwidth of the metasurface antenna is mainly effected by the narrow band limitation of the microstrip elements. Phase response of elements change with change in frequency therefore wideband elements need to be used which increases the overall bandwidth of the metasurface.

CHAPTER 4

DESIGN OF METAMATERIAL BASED ANTENNA FOR MULTI-BEAM WIDE-ANGLE SCANNING

This chapter covers the design of reconfigurable transmitarray antenna for various applications including 5G mmWave communication and satellite communication. As discussed in chapter 1, transmitarray is a flat lens which combines both optical and antenna array principles. Phase shift on transmitarray aperture can be implemented actively (by using tunable components like phase shifters, varactors, PIN diodes) or passively (by using variable sized elements). Unlike reflectarrays, transmitarrays do not suffer from feed blockage. They are lightweight, low cost and have a low profile. This chapter covers the design of transmitarray that can be used to produce multiple reconfigurable beams simultaneously to support applications such as wireless backhaul in 5G mobile networks and satellite communication (satcom) services. In frequency reuse schemes total network capacity is increased by re-using the allocated frequencies. However, sufficient isolation is required between signals to avoid the mutual interference. In satellite communication frequency reuse can be achieved by using orthogonal polarization to avoid the interference between adjacent beams, which requires satellite antennas to have polarization diversity. Our designed antenna supports both linear (vertical and horizontal polarization) and circular (RHCP/L-HCP) polarization without modifying the antenna geometry, the polarization diversity

enables frequency reuse and hence increases the network capacity. Phase synthesis has been applied to reduce the scan loss which consequently increases the scan range of antenna. The substrate is selected such that the antenna can withstand harsh deep space environment conditions and it can be folded for easy deployment. Section 4.1 presents the design, optimization and analysis of transmitarray unit-cells supporting both linear and circular polarization. The design and simulation of a multi beam steerable transmitarray based on designed unit cell is presented in section 4.2. Fabricated prototype and measured results are presented in section 4.3. Section 4.4 covers the scan loss optimization for designed transmitarray using bifocal phase distribution. Section 4.5 illustrates the design of folded version of designed lens/transmitarray for CubeSat. Section 4.6 covers the design of multi-facet transmitarray for wide-angle beam scanning.

4.1 Unit Cell Design and Analysis for Multi-beam Transmitarray Antenna

We have designed the polarization insensitive unit cell for transmitarray/lens antenna. The unit cell is designed based on printed circuit board technology which makes the designed surface planar, light weight, low profile, and fold-able (for space deployment). Master/slave boundary conditions and floquet port excitation have been used to model the unit cell. The unit cell consists of four-layered copper pattern etched on dielectric substrate. Multiple layers and variation in geometric shapes have been employed to add the diversity in design which enhances the phase range and bandwidth characteristics. To add polarization diversity in design, symmetrical geometry capable of supporting both linear and circular polarization was chosen. Top

and bottom layers of unit cell consist of circular patches while the middle two layers (layer 2 and layer 3) consist of square patches. The substrate used is Rogers Duroid 5880 (RT/duroid 5880). Rogers/duroid 5880 substrate has a low dielectric constant (Dk), low dielectric loss, and low outgassing, which makes it well suited for high frequency/broadband terrestrial and space applications. All three substrate layers are bonded together by bonding ply. Fig. 4.1 shows the designed unit cell.

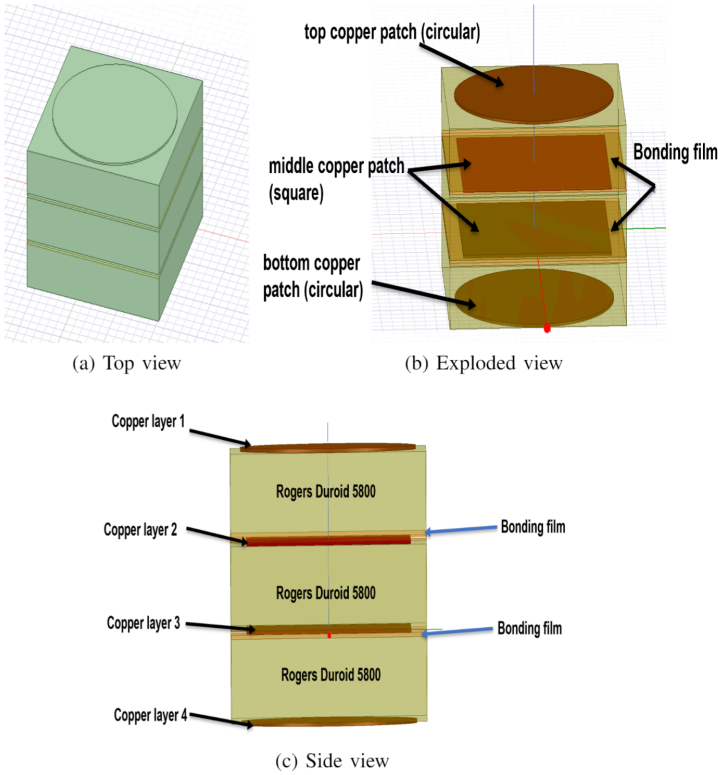

(a) Top view (b) Exploded view

(c) Side view

Figure 4.1: Designed unit cell at 30 GHz.

Beam focusing ideally requires the phase agility of 360°, the desired phase tunability is achieved by phase variation on variable sized elements/resonators. To obtain the required phase range, multiple structural parameters of unit cell were optimized, comprehensive parametric study of the unit cells was performed in order to achieve wide phase range and linear phase characteristics with low losses. Parametric study

was carried out varying the structural parameters (e.g patch length and width, radius of patch, spacing between respective layers) dimensions of unit cell pattern and their corresponding transmission coefficient values were stored in the database to generate the phase distribution for uni-focal transmitarray. Fig. 4.2 and Fig. 4.3 show the transmission coefficient phase and amplitude of the designed unit cell.

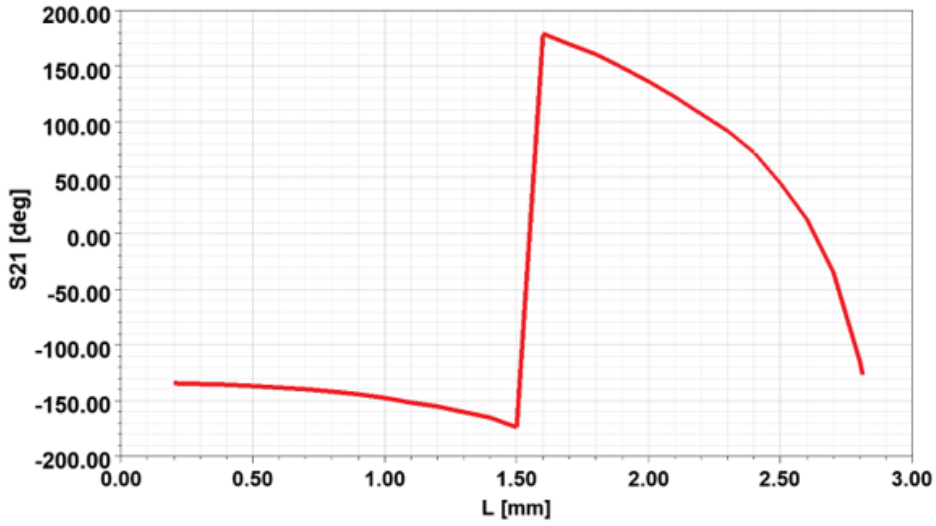

Figure 4.2: Unit cell transmission coefficient S_{21}phase.

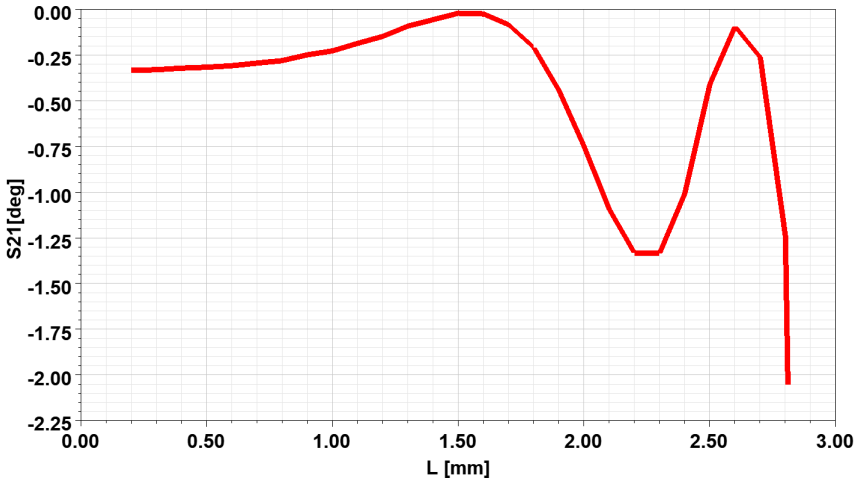

Figure 4.3: Unit cell transmission coefficient S_{21}magnitude.

Once the unit cell phase variation of around 360^o was obtained, phase distribution on metasurface aperture was defined taking into account the phase shift introduced by each element. As illustrated in chapter 3, to focus the beam in the desired direction each radiating element re-radiates the incident waves with a phase obtained as follows:

$$phi(x_i, y_i) = -k_o sin\theta_b cos\phi_b x_i - k_o sin\theta_b sin\phi_b y_i \tag{4.1}$$

where k_o is the free space propagation constant, (x_i, y_i) are coordinates of the i_{th} element, and ($\theta_{b,}\phi_b$) show the direction of desired beam.

Using 4.1 the phase shift introduced on each unit cell to steer the beam towards ($\theta_{b,}, \phi_b$) can be written as:

$$\phi_{Ri} = k_o(z_i - (x_i sin\theta_b cos\phi_b + y_i sin\phi_b sin\theta_b) \tag{4.2}$$

where z_i is the distance from the phase center of the feed to i_{th} element, described by the expression below.

$$z_i = \sqrt[2]{(x_i - x_f)^2 + (y_i - y_f)^2 + (z_i - z_f)^2}$$

where x_i, y_i and z_i are coordinates of i_{th} element and x_o, y_o, and z_o show the position of feed antenna.

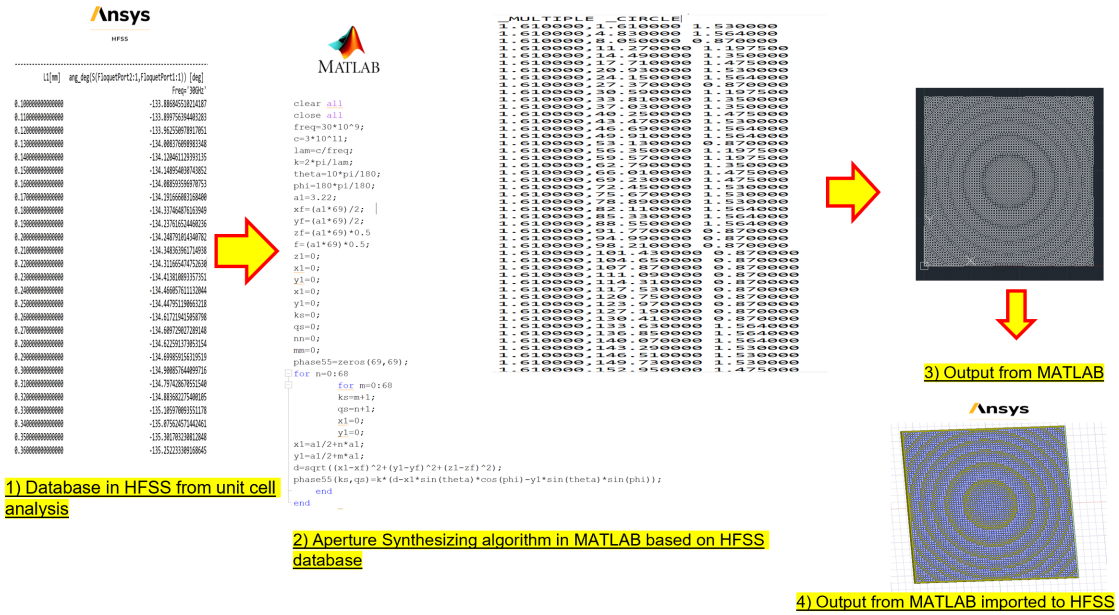

Figure 4.4: Process flow for metasurface design.

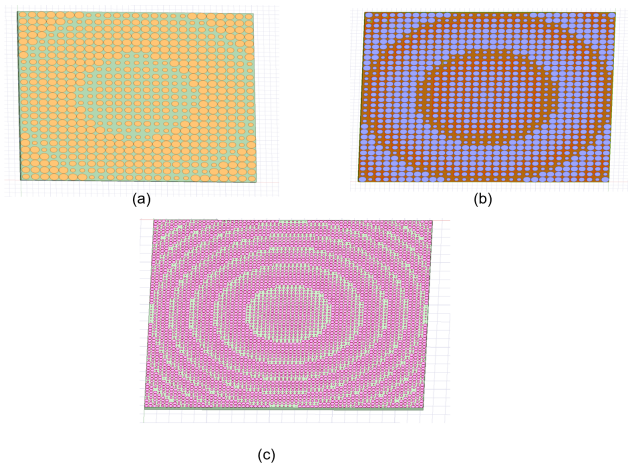

Figure 4.5: Designed metasurfaces (a) 80.5 x 80.5 mm. (b) 103 x 103 mm, and (c) 222 mm 222 mm.

MATLAB code has been developed that calculates the desired phase compensation at each array element based on 4.2 and generates the corresponding dxf files. The generated dxf files from MATLAB were imported to HFSS to create the multilayered

metasurface. Fig. 4.5 shows the process flow for metasurface design. We started with 80.5 mm x 80.5 mm and 103 x 103 mm element array as shown in the Fig. 4.5. After validating the design procedure, we scaled up the array size to approximately 222 mm x 222 mm. Feed radiator is placed at F/D of 0.5 with edge taper of around -14 dB, Fig. 4.6 shows the feed image on metasurface and Fig. 4.7 shows the emitted pencil beam from metasurface. Fig. 4.8 show the peak gain of designed metasurface. The designed surface can produce both linearly and circularly polarized beams. With linearly polarized feed (shown in Fig. 4.9), the emitted beams will have linear polarization. Likewise, with circularly polarized feed antenna (shown in Fig. 4.10) the designed surface produces circularly polarized beams. Hence the designed surface provides the flexibility to support both circular and linear polarization. Polarization of emitted beam will be same as polarization of incident wave. Fig. 4.11 shows the axial ratio plot for the case where transmit-array is integrated with linearly and circularly polarized feed. Axial ratio for bore-sight beam ($\theta = 0$, $\phi = 0$) is below 3 dB with circularly polarized feed and above 60 dB with linearly polarized feeds. Therefore, the designed surface is an excellent candidate for the applications where polarization diversity is required.

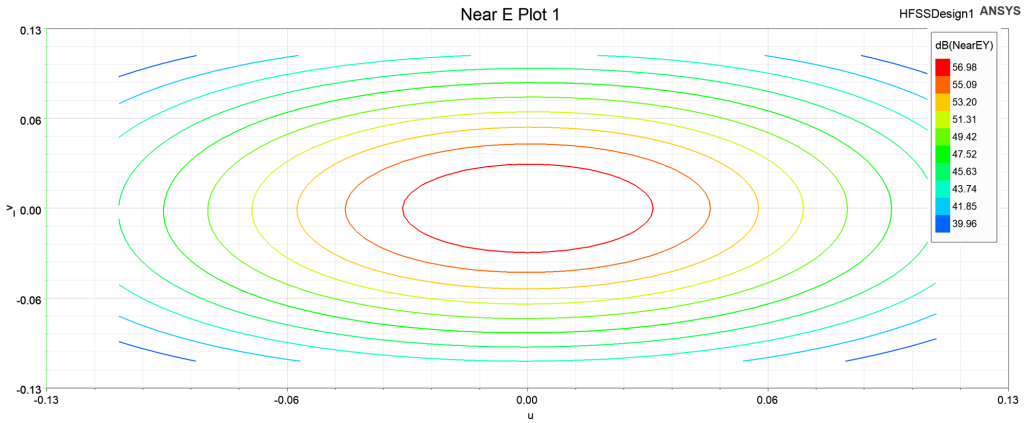

Figure 4.6: Feed image on metasurface to realize the edge taper.

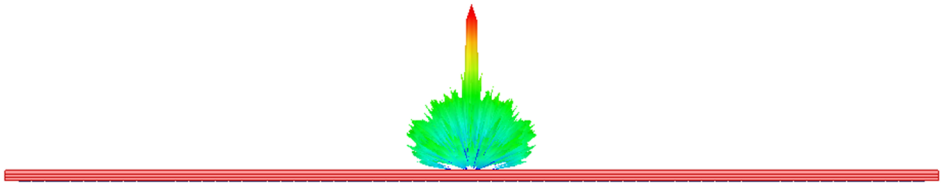

Figure 4.7: Emitted pencil beam from metasurface.

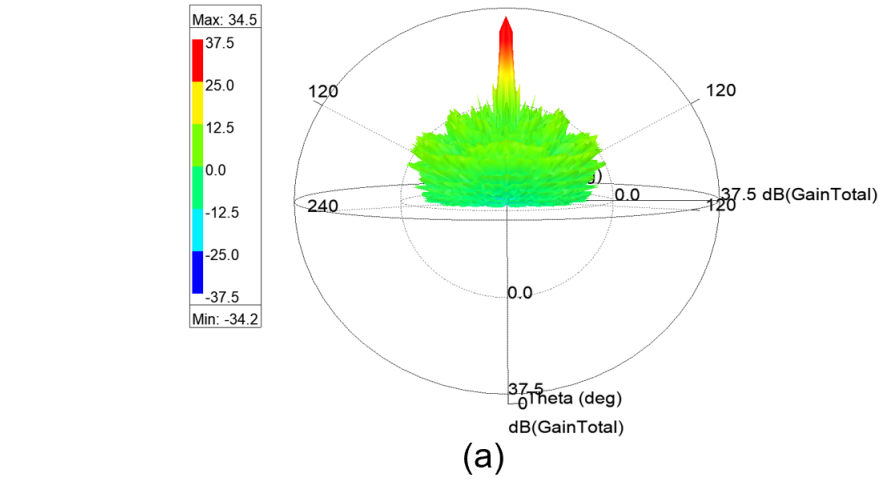

(a)

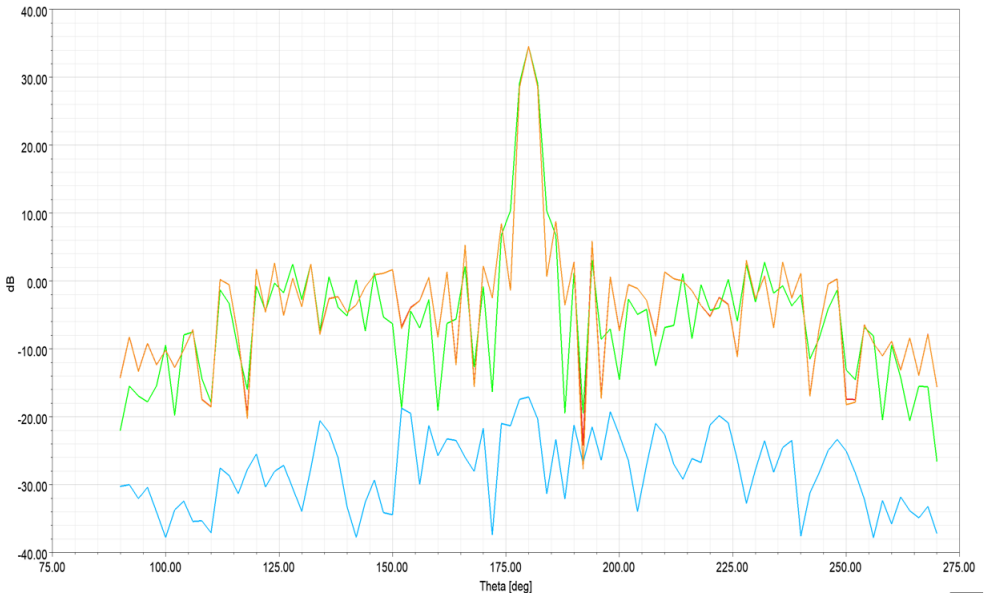

(b)

Figure 4.8: Radiation pattern of designed antenna (a) 3D Radiation Pattern (b) 2D Radiation Pattern.

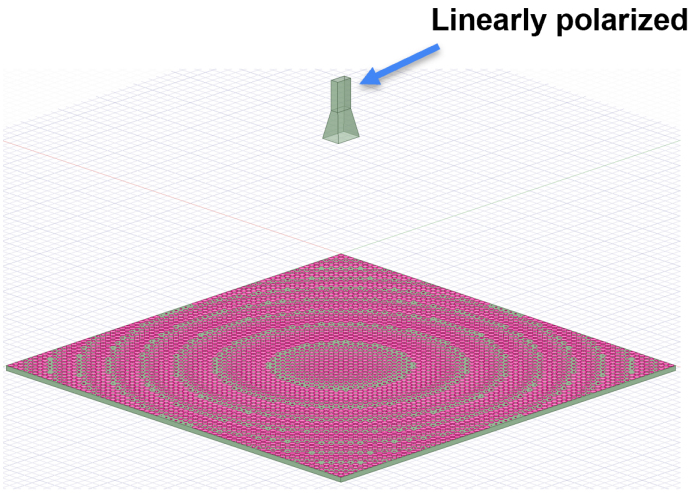

Figure 4.9: Transmit-array integrated with pyramidal feed horn for linear polarization.

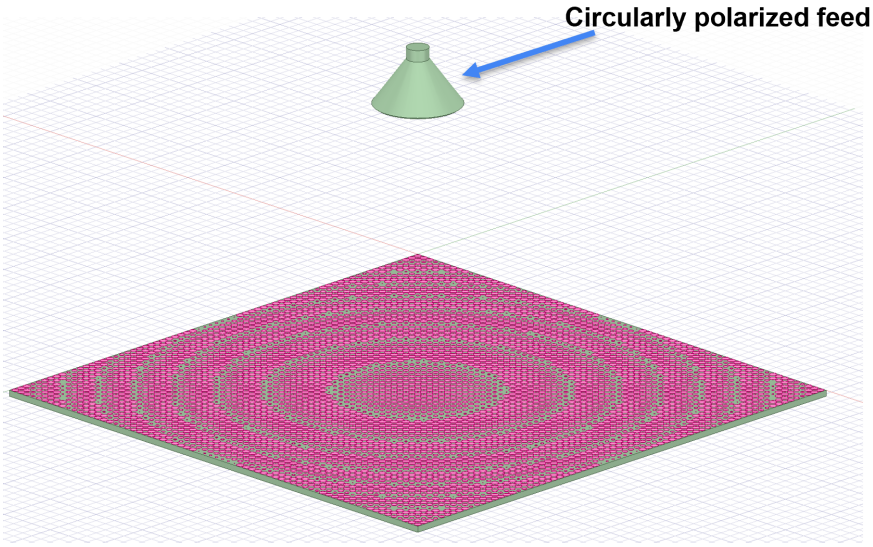

Figure 4.10: Transmit-array integrated with conical feed horn for circular polarization.

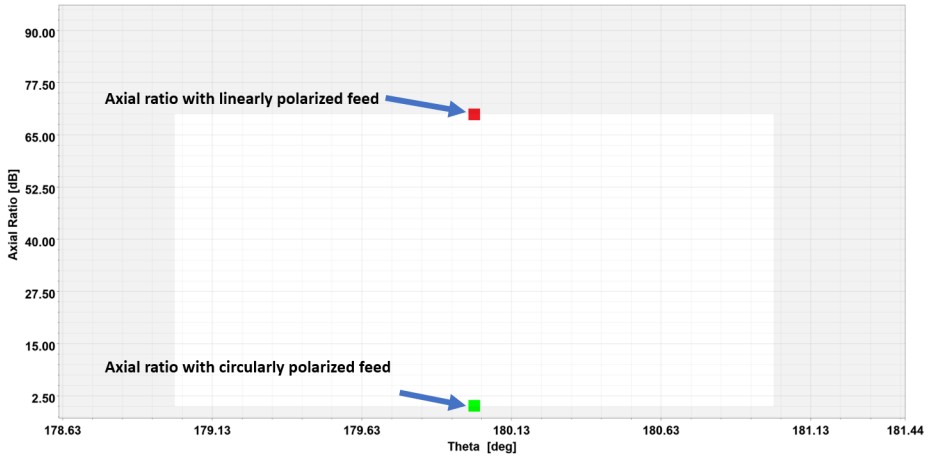

Figure 4.11: Axial ratio plots of metasurface integrated with linearly and circularly polarized feed horns.

4.2 Beam Scanning using Designed Metasurface

Fig. 4.14 shows the cross-sectional view of the beam-scanning mechanism adopted. In plane movement of feed horn scans the main beam in E/H plane, displacement of feed along x-y plane steers the main beam from -40 to +40 in elevation plane with full azimuth coverage. To steer the main beam, feed horn is displaced +/-78 mm from the origin along horizontal plane (x-axis). The radiation patterns computed at 30 GHz are plotted in Fig. 4.15 for beam directions varying between -40^o and 40^o. Peak simulated gain is 34.5 dB with aperture efficiency of 47.47%. The cross polarization level and side lobe levels are below 35 dB and 28 dB from peak gain respectively. The phase distribution of the designed transmit-array for beam scanning at bore-sight, 5^o, 10^o , 15^o, 20^o, 25^o, 30^o, 35^o, and 40^o has been depicted in Fig. 4.12. Fig. 4.13 shows the comparison of phase distribution for aperture tuning and feed displacement. We can observe that feed displacement mimics the distribution which we get by aperture tuning and hence feed displacement provides a very simple

and less complicated way to steer the beam without tuning thousands of individual array elements. This concept can be further extended to realize the multi-beam reconfigurable MIMO systems [30, 7, 31]. Whereby independently steerable beams can be realized by using multiple feed antennas placed in front of passive transmitarray surface. Fig. 4.17 shows the configuration for independently steerable beams, by movement of feed 1 and feed 2, independently steerable beams can be produced. Likewise, this configuration can be realized using three feed antennas which will result in three independently steerable beams depicted in Fig. 4.18, the same technique can be used to generate large number of simultaneous beams based on single beam per feed approach (Fig. 4.19 shows an example of five simultaneous beams and Fig. 4.20 shows the corresponding radiation pattern). Fig. 4.16 depicts the implementation of 2x2 MIMO using our designed antenna and traditional antennas respectively. It is noteworthy that this technique can be used electronically or mechanically. Electronic implementation requires switching between multiple feed elements while mechanical implementation involves displacement of feed horn.

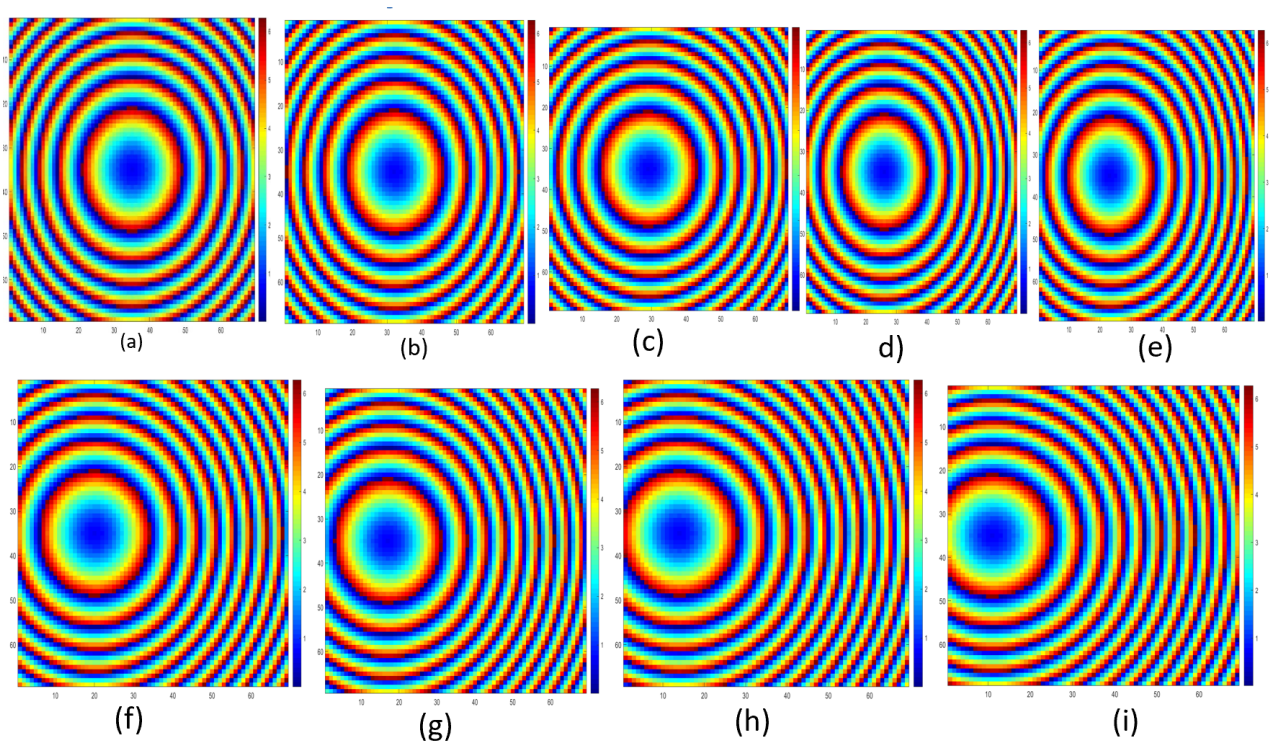

Figure 4.12: Phase distribution on transmitarray aperture (a) boresight, (b) 5°, (c) 10°, (d) 20° , (e) 25°, (f) 30°, and (g) 40°

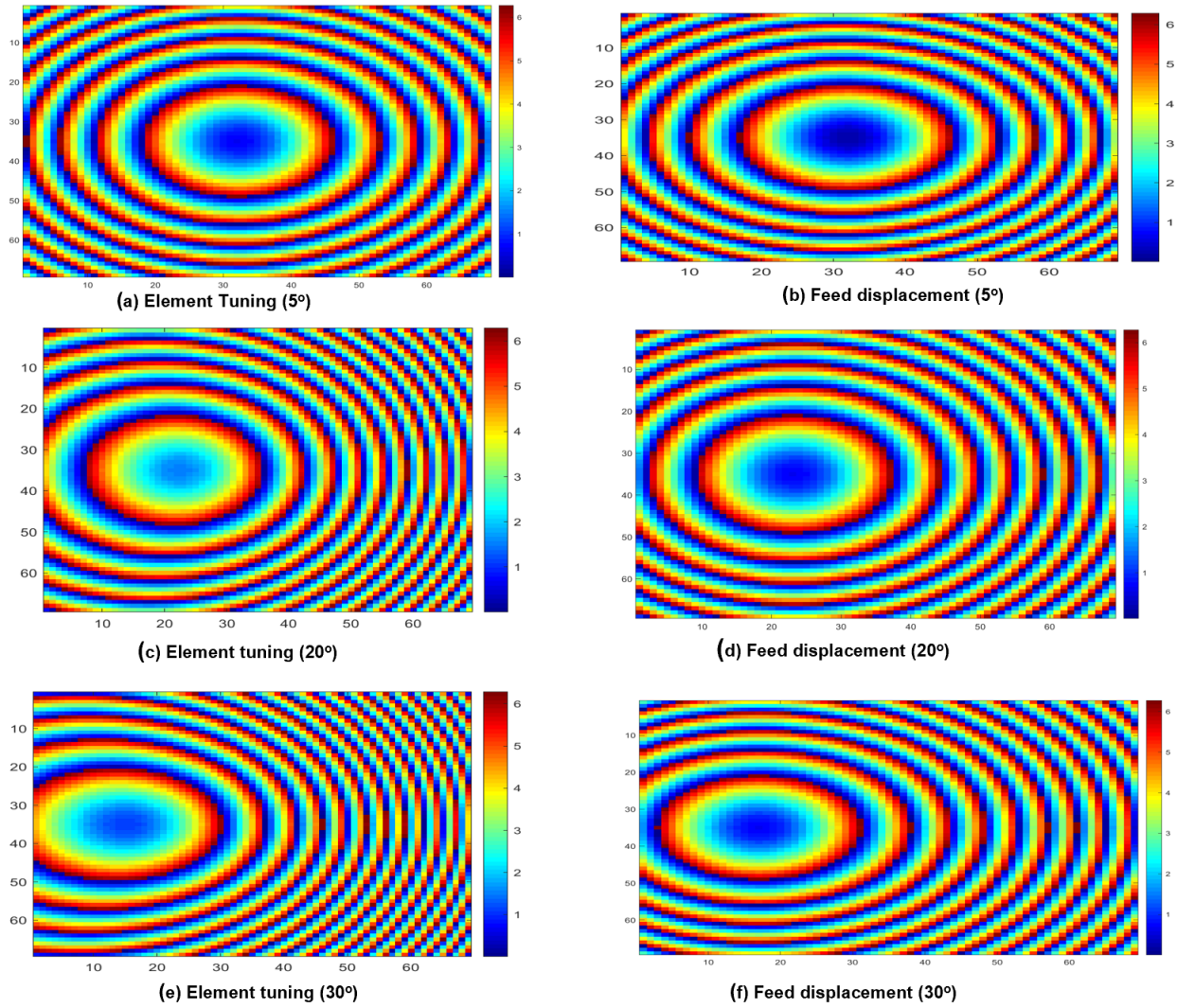

Figure 4.13: Comparison of phase distribution for beam steering using aperture tuning and feed displacement.

Fig. 4.20 shows the 3D radiation pattern of multiple beams generated by the designed metasurface. As evident from the radiation patterns, the proposed surface is an excellent fit for applications requiring single/multiple high gain beams.

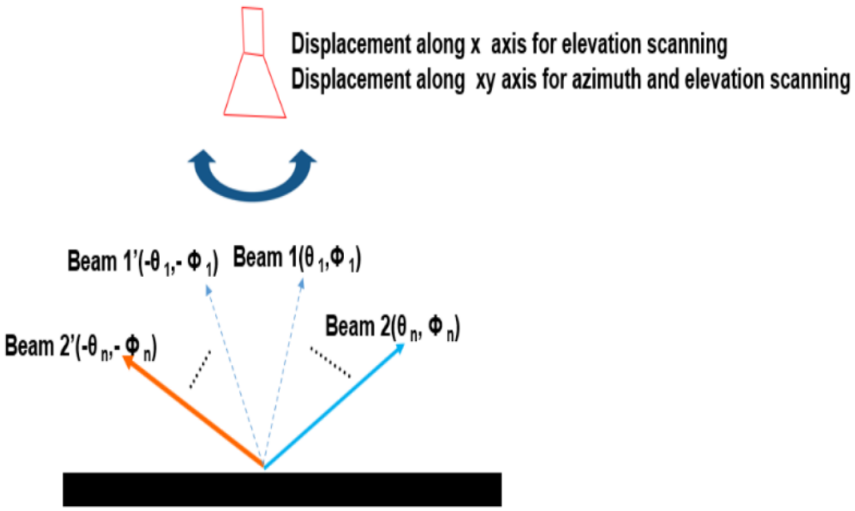

Figure 4.14: Working mechanism.

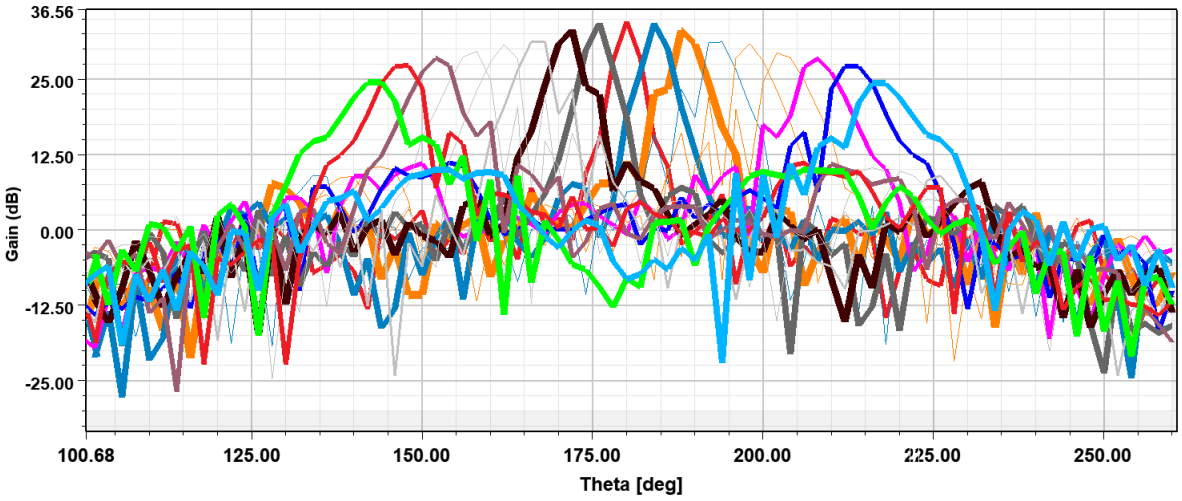

Figure 4.15: 2D radiation pattern.

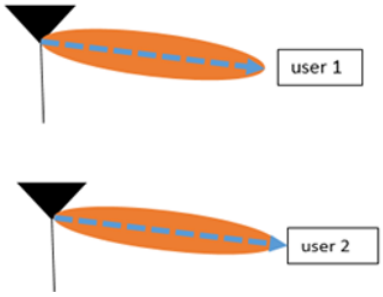

(a) 2x2 MIMO using proposed antenna, single antenna can communicate with multiple users

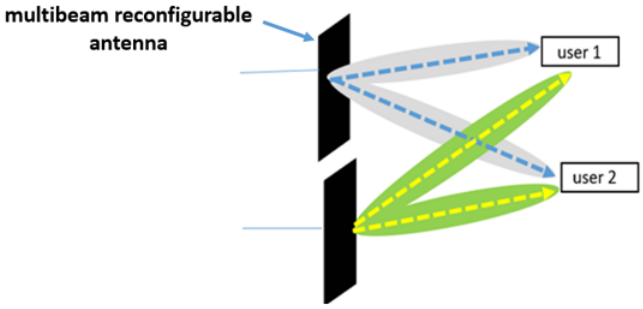

(b) MIMO with traditional antennas

Figure 4.16: Comparison of 2x2 MIMO using traditional and proposed antenna.

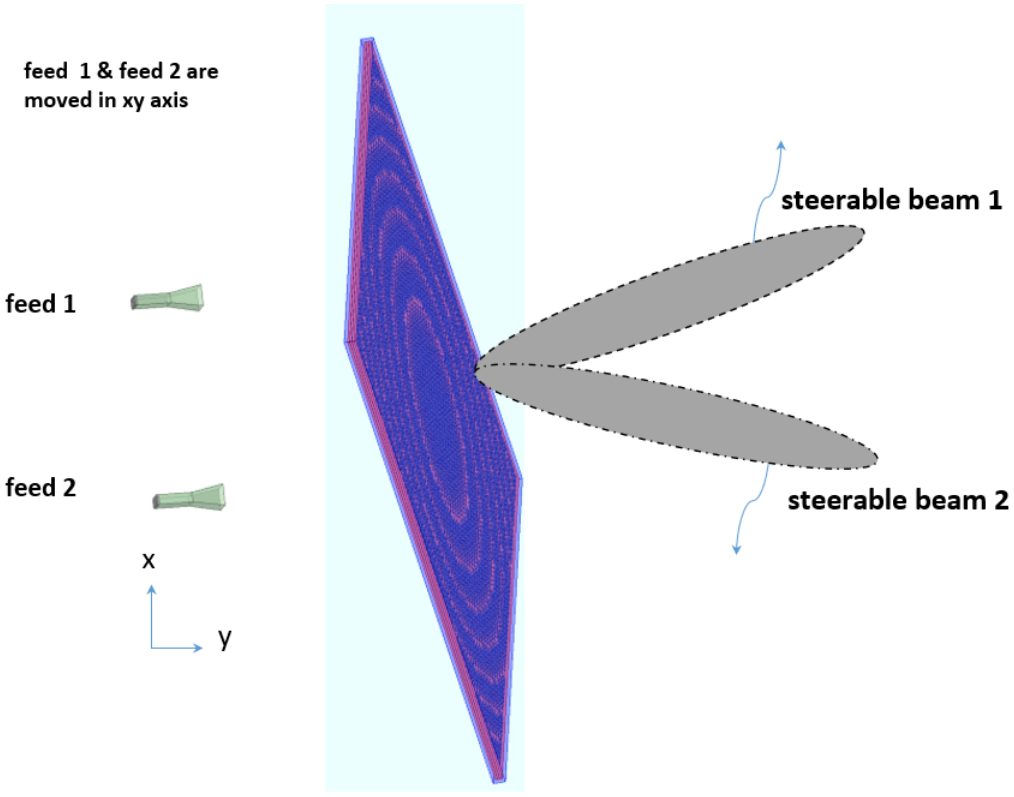

Figure 4.17: Two independently steerable beams.

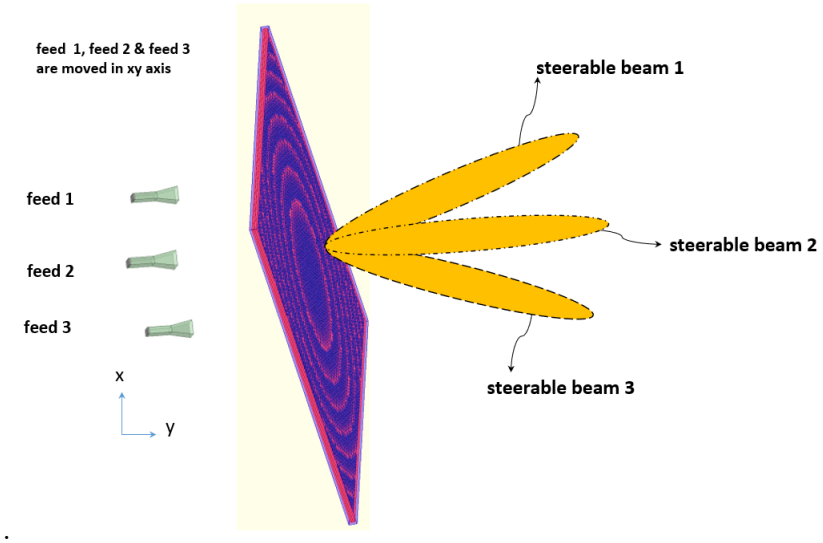

Figure 4.18: Three independently steerable beams.

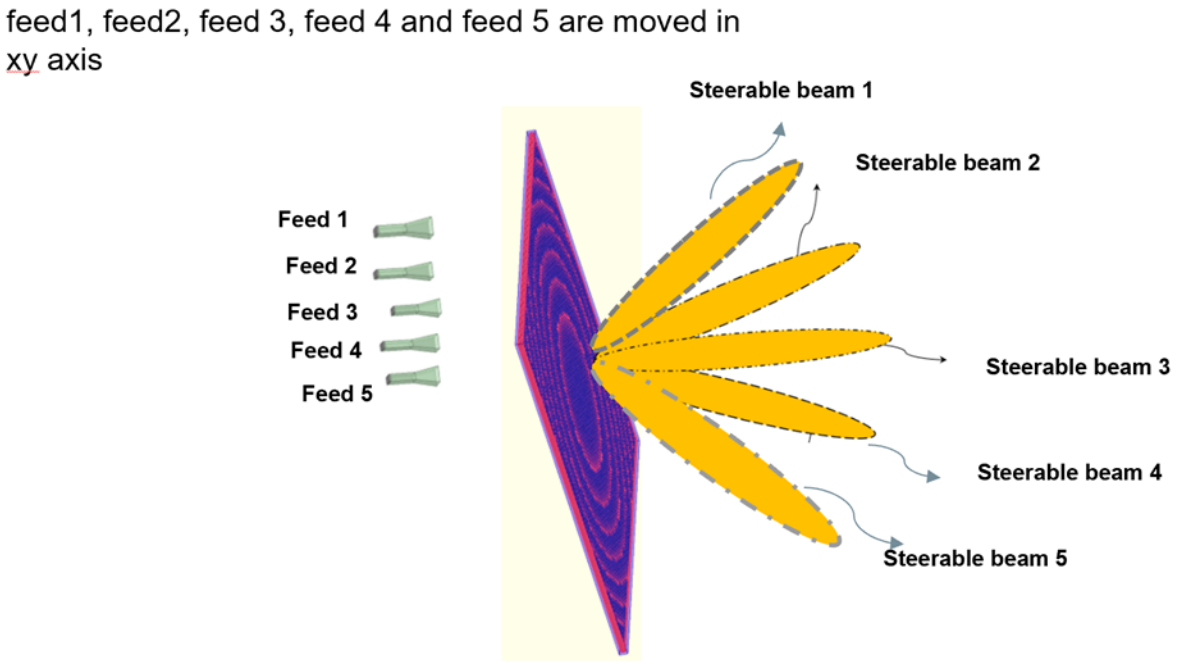

[30]

Figure 4.19: Five independently steerable beams.

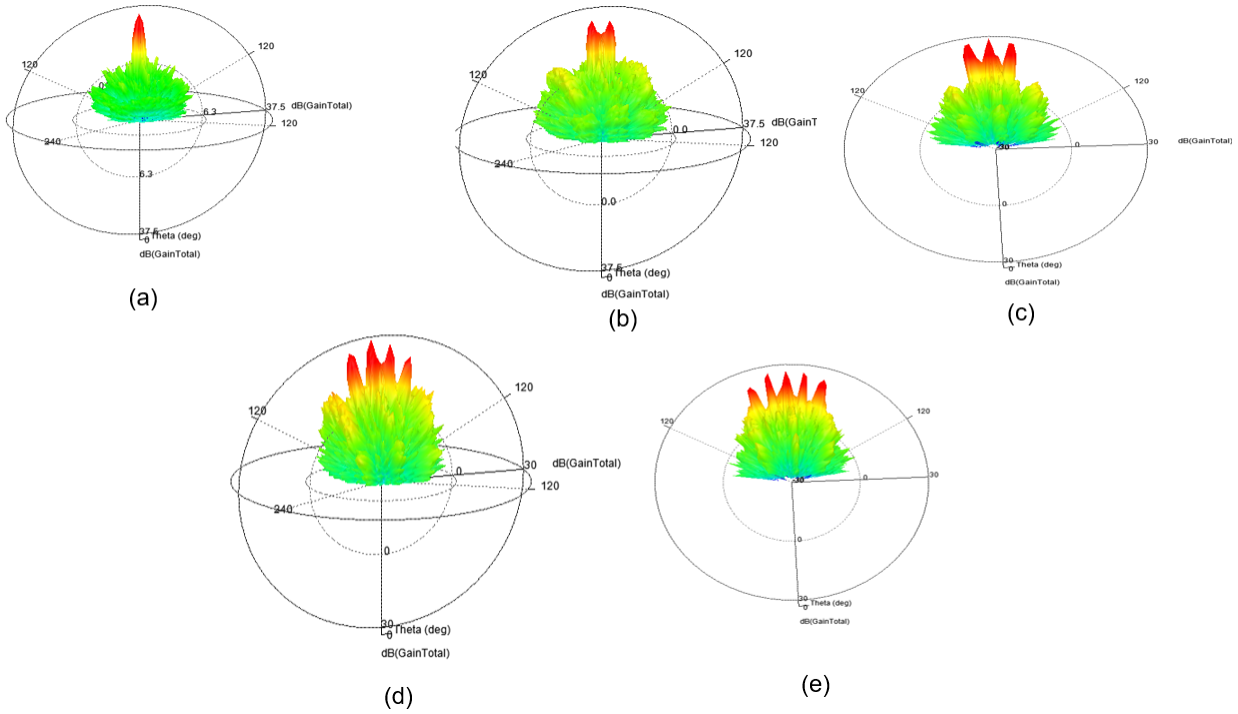

Figure 4.20: 3D radiation pattern for multiple simultaneous beams with peak gain of 35.5 dB. (a) single beam (b) dual beam (c) three independent beams, (d) four independent beams, and (e) five independent beams.

4.3 Fabricated Prototype and Measured Results

Simulated results for the linearly and circularly polarized transmitarray have been demonstrated in the previous section, we observed quite satisfactory results in the full wave analysis of designed transmit-array. This section will cover the fabricated model of transmitarray and measured results. The Rogers Duroid 5880 substrate provides good RF performance, has low outgassing and exhibits high strength which makes it suitable for harsh environment conditions. The copper pattern is etched on Rogers Duroid substrate. Bondply is used to bond the substrate layer. Fig. 4.21 shows the designed transmitarray. Fig. 4.21 shows the fabricated transmit-array mounted

in anechoic chamber for testing. The 3-dB measured gain bandwidth extends from 28.5 GHz to 32.2 GHz. The measured radiation patterns of metasurface from 27 GHz to 32 GHz are illustrated in Fig. 4.23. A good agreement is observed between theoretical, simulated and experimental gain responses. The measured maximum gain is equal to 34.2 dBi with a side-lobe level of 28.64 dB below the peak gain and co-pol below 35 dB from peak gain. Fig. 4.24 shows the antenna gain vs frequency plot. Fig. 4.25 depicts the measured total efficiency of antenna from 27 to 32 GHz. The total efficiency has been calculated by taking the ratio of measured realized gain and measured directivity.

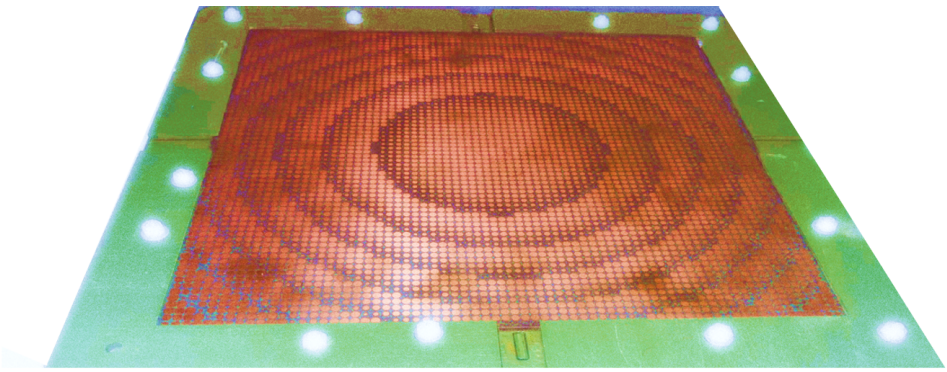

Figure 4.21: Fabricated transmitarray.

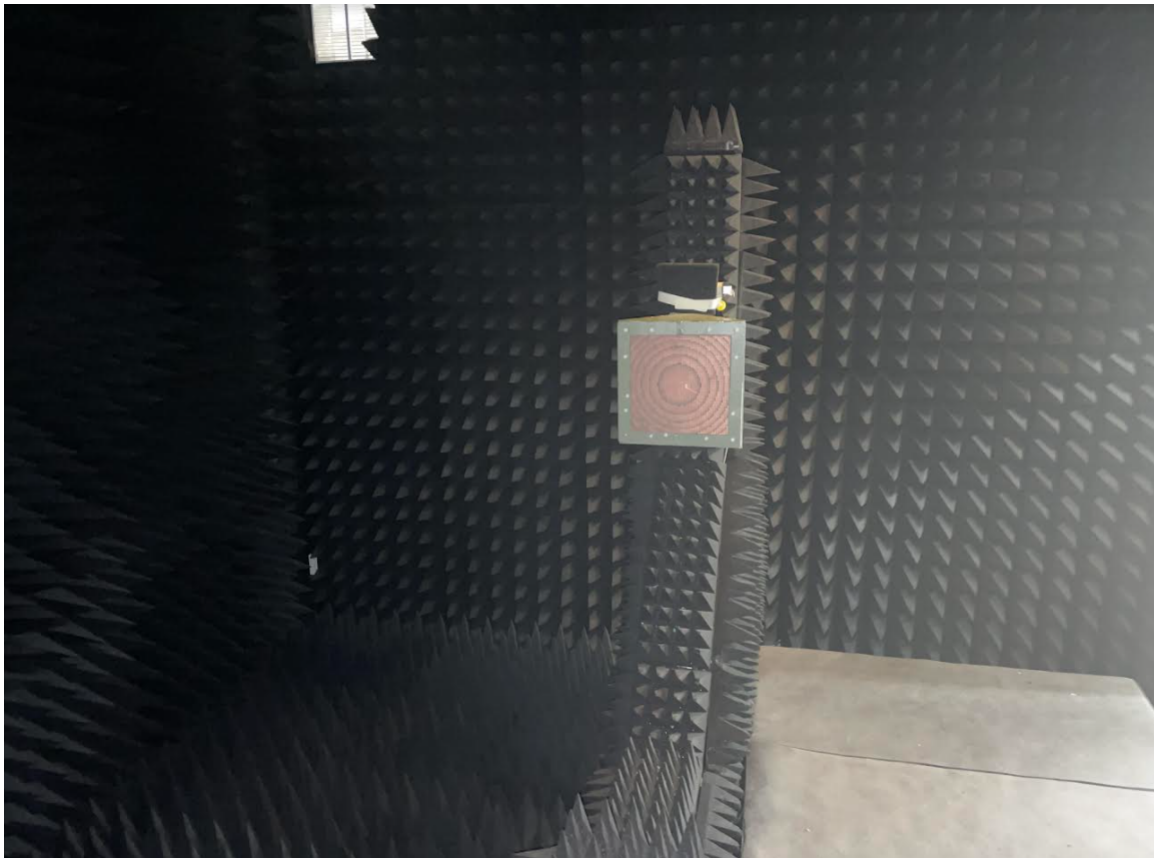

Figure 4.22: Measurement setup.

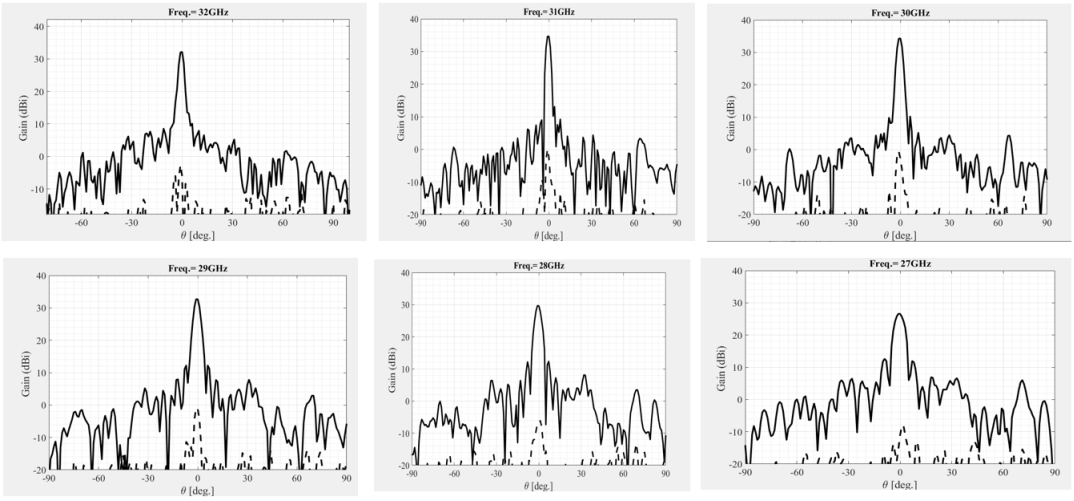

Figure 4.23: Measured bore-sight radiation patterns from 27 to 32 GHz.

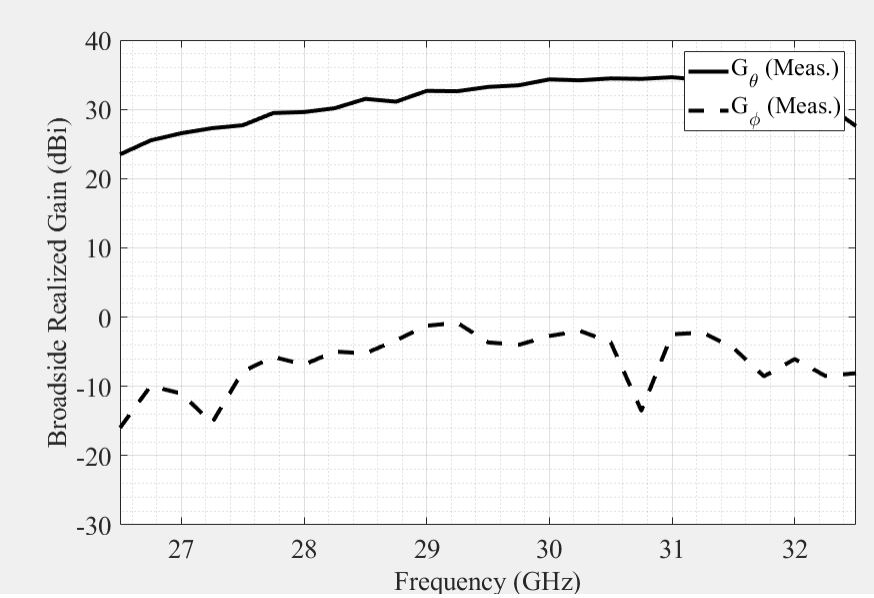

Figure 4.24: Bore-sight gain vs frequency plot.

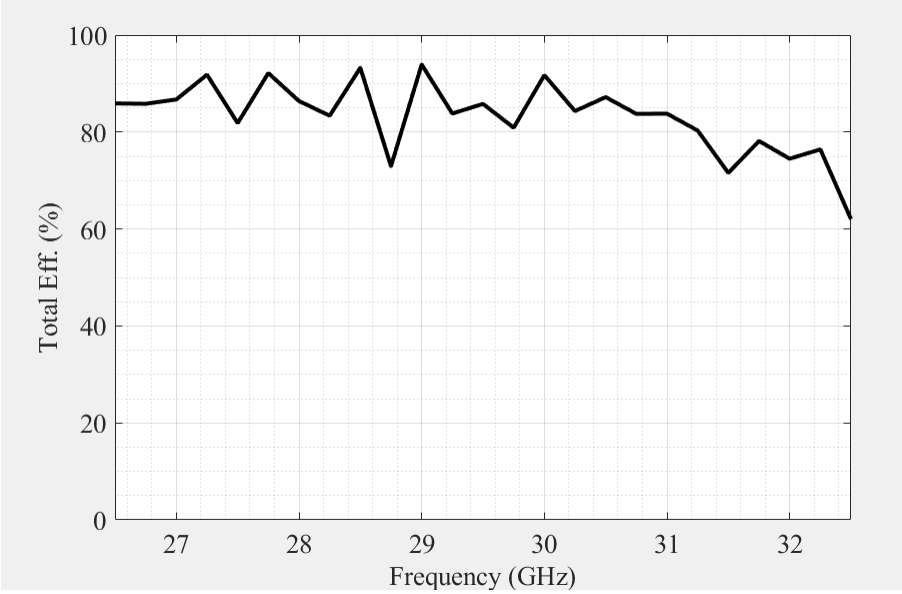

Figure 4.25: Total efficiency of antenna (boresight).

To validate the beam scanning by the designed surface the feed was moved to three different positions with the displacement of 30 mm, 60 mm and 78 mm from

the origin. Fig. 4.26 shows the radiation pattern plots for the feed displacement of 20 mm from the origin and Fig. 4.27 shows the variation of gain vs frequency, the 3dB bandwidth is 28.5 GHz to 32.2 GHz. The peak gain achieved is 32 dBi and the cross-pol is 34 dB below the peak gain.

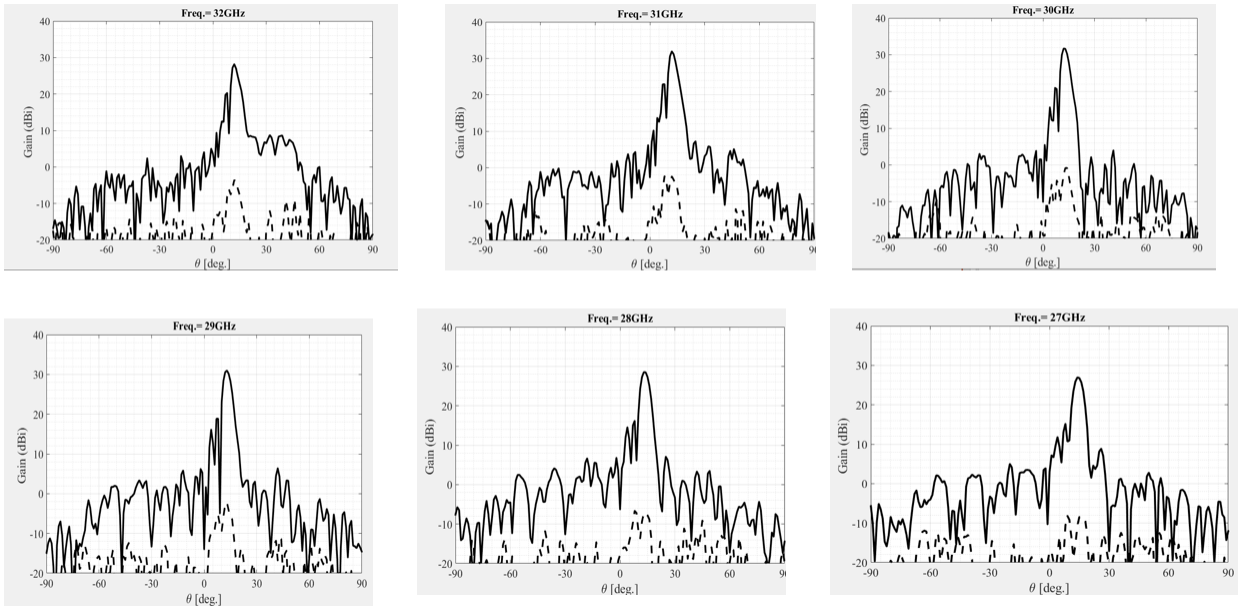

Figure 4.26: Measured radiation pattern from 27 to 32 GHz with the feed displacement of 30 mm from origin, beam steered at 13º .

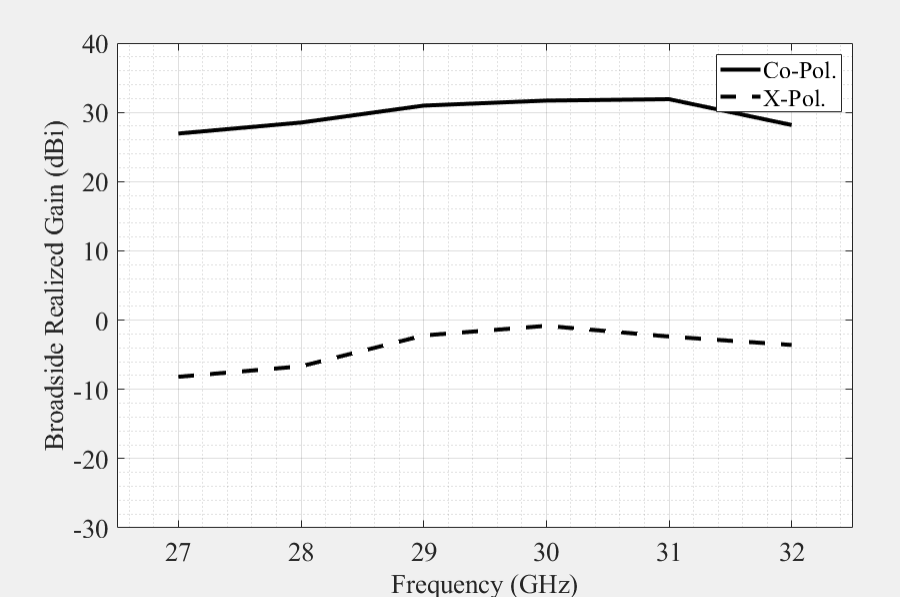

Figure 4.27: Antenna gain vs frequency plot for feed displacement of 30 mm.

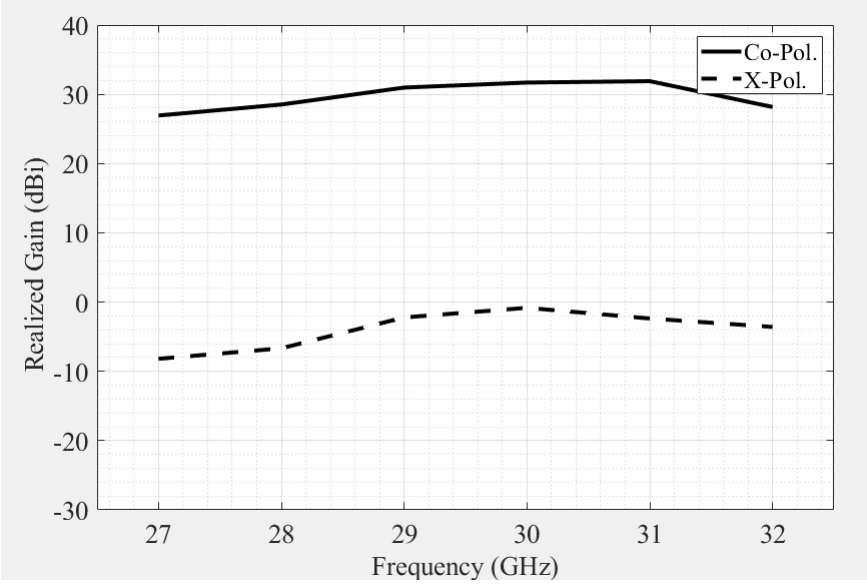

Figure 4.28: Peak gain vs frequency plot for 30 mm feed displacement

In the next step, the feed was displaced to position 2 i.e 60 mm from origin. Fig. 4.29 shows the corresponding radiation pattern, the main beam is scanned to 28^o by

feed displacement of 60 mm. Fig. 4.30 shows the gain deviation with frequency.

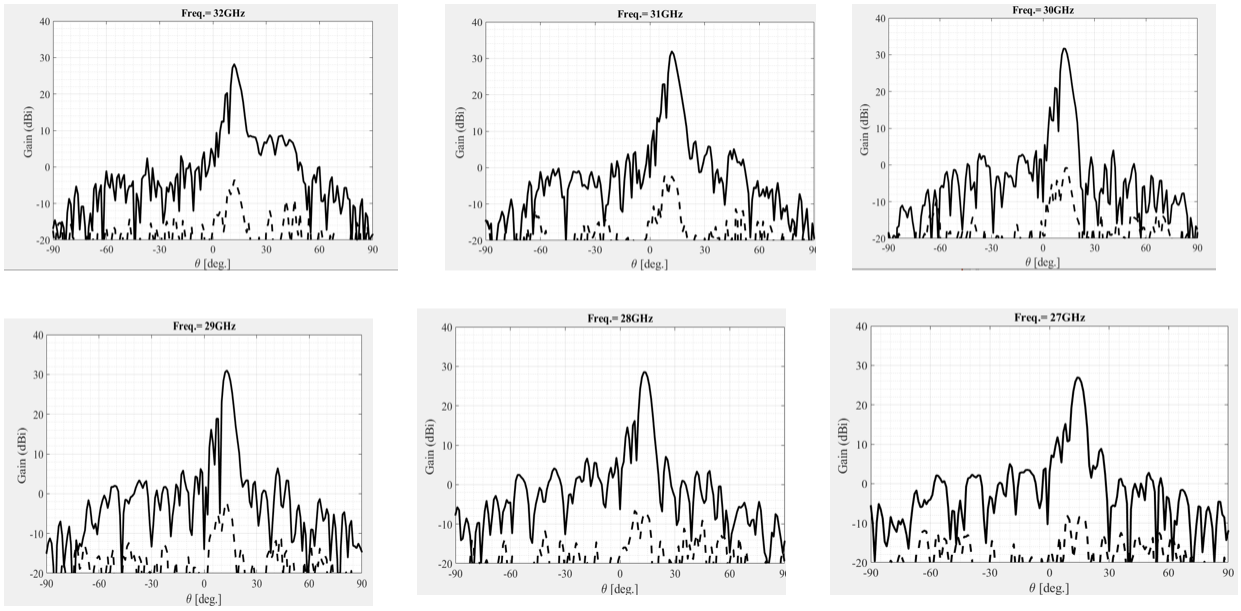

Figure 4.29: Measured radiation pattern from 27 GHz to 32 GHz with the feed displacement of 60 mm from origin, beam steered at 28 degrees.

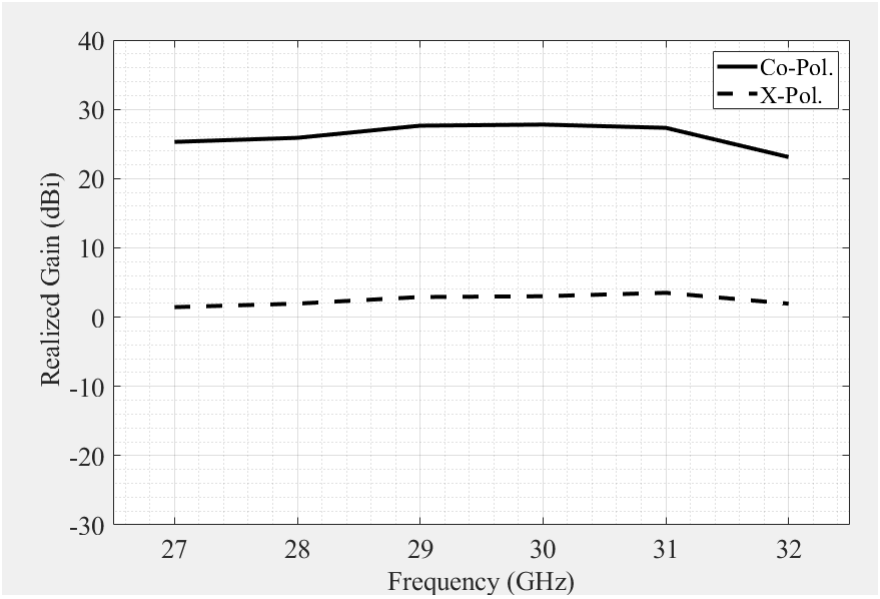

Figure 4.30: Peak gain vs frequency plot for 60 mm feed displacement.

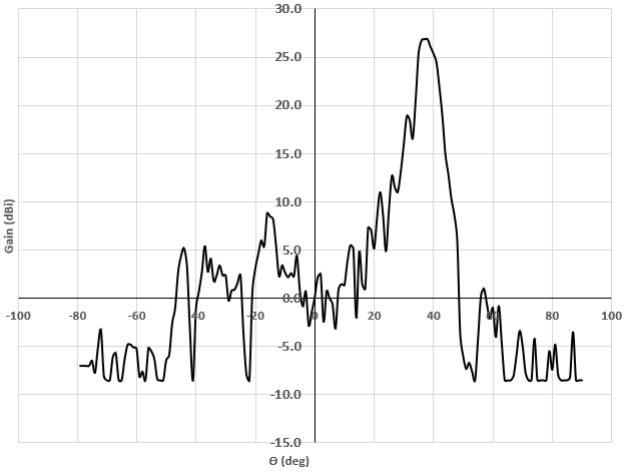

Figure 4.31: Beam steered at 40° at center frequency of 30 GHz (feed displacement of 78 mm from origin).

Fig. 4.31 shows the measured radiation pattern for displacement of 78 mm from origin. Beam was scanned to 40 degrees with peak gain of 26.5 dBi.

4.4 Phase Synthesis for Scan Loss Reduction

The previous section demonstrated the design and analysis of unifocal transmitarray. This section aims to address further advancements in designed transmitarray model to improve the scan performance. We observed that the designed transmitarray provides highly focused beam of 34.5 dBi with an excellent aperture efficiency. The designed antenna can be used in various applications where directive high gain steerable beam is required. The evolution of emerging LEO and MEO satellite constellations has massively increased the demand of beam scanning antennas as satellites revolve around Earth with high velocities and remain in the sight of ground terminal for a matter of minutes only. Therefore, the ground terminal has to track the satellites continuously with a wide scan angle. The level of aberrations caused by

feed displacement increases with an increase in transmit-array size. Therefore it is critical to optimize the scan loss for high gain transmitarray as phase error becomes prominent as array size increases. To minimize the scan loss, phase optimization has been done using bifocal phase distribution, the advantage of bifocal distribution against the unifocal distribution (expressed in 4.2) is the reduction in phase error as phase distribution is defined for two focal points instead of single focal point. By using the feed displacement technique this transmitarray system can be used for a 80° scan coverage (-40° to +40°) with the scan loss of below 3 dB. Fig. 4.32 shows the transmitarray performance after scan loss optimization. We can observe that in case of bifocal distribution the scan has been decreased from 8 dB to 3 dB and alternatively scan range can also be increased. This validates the effectivity of a metamaterial based array in adopting diverse optimization algorithms which otherwise can be complex for conventional lens antennas.

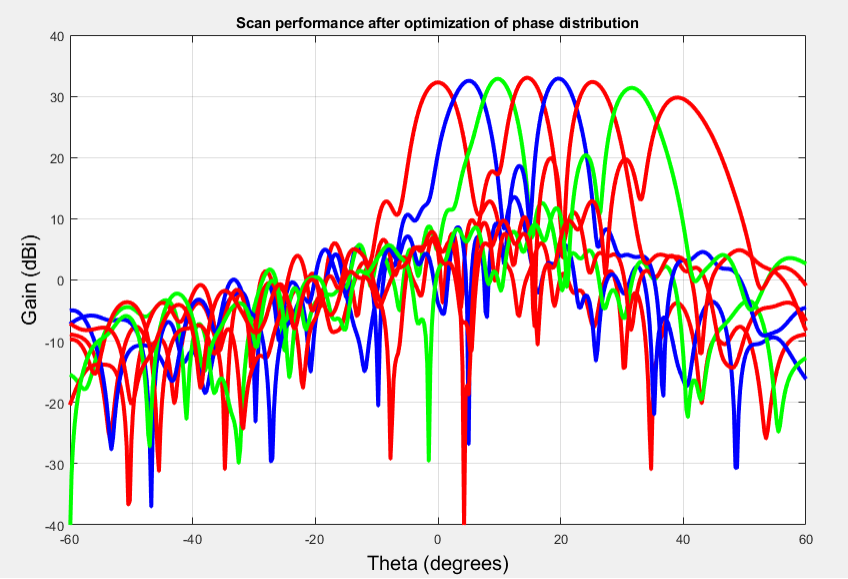

Figure 4.32: Beam scanning after scan loss optimization.

4.5 Folded Transmitarray for Deep Space Missions

In previous sections we have successfully designed and analyzed lens for beam scanning applications, this section will cover the design and analysis of fold-able transmitarray for small satellites like CubeSats. Small satellite launches for low Earth orbit (LEO) missions have increased radically in the last few years due to their fast development, low cost, low volume, and potential to support telecommunications, remote sensing, imaging and exploration missions. CubeSat design and deployment is a significant challenge for two key reasons, i.e transmit power and antenna gain. High gain antennas boost the capabilities of small spacecraft by providing the high data rates. However, high antenna gain is difficult to integrate in small satellites due to limited stowage volume and mass restrictions in the CubeSat. Since the launch volume of CubeSats are limited, the foldable antennas are a practical choice for CubeSats owing to their limited volume. We have designed the foldable version of the lens designed in section 4.2 for space deployment. Folded lens is composed of two flat panels that can be stowed for deployment, Fig. 4.34 shows the depiction of folded transmitarray on spacecraft. The folded lens antenna offers small stowed volume, low mass, and low cost. The folded version of the designed lens was realized by adding the air gap and hinges in the HFSS model of metasurface lens, Fig. 4.33 shows the final folded model consisting of two folded 111 mm x 111 mm panels attached by hinges. The figure also includes the location of the hinges and hinge fold line. The rectangular blocks illustrate the hinge part while the vertical black lines indicate hinge fold lines. We observed the gain loss of 0.3 dB due to hinges and air gap. However, we have successfully achieved the high gain and low stowed volume using the described methodology.

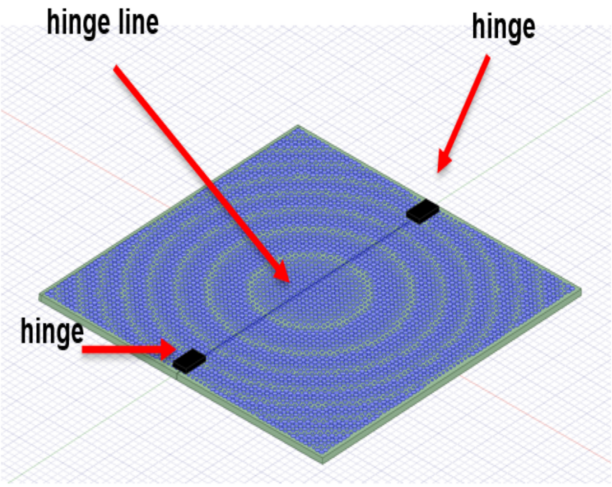

Figure 4.33: Simulated folded lens with hinges.

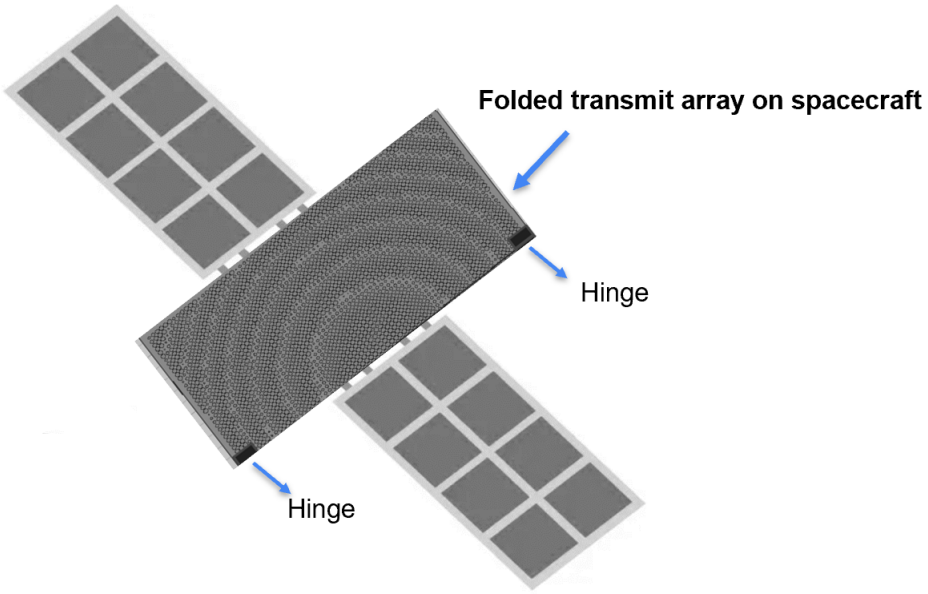

Figure 4.34: Depiction of folded transmitarray on spacecraft.

4.6 Multi-facet Transmitarray for Ultrawide Scan Angle

In this section we will discuss the multi-facet lens using the transmitarray designed in section 4.2. The purpose of a multifacet transmitarray is to design the ultra wide angle lens for applications requiring the ultra wide scanning. The novel multi-facet geometry consists of three transmitarray panels, these panels are joined such that the angle at the intersection of any two transmitarray panels is β.

Prominent advantage of this design is the strong control over side lobe level, the side lobe of beam scanning with feed displacement goes higher as the scan angle increases, the proposed approach limits the side lobe levels as the field of view of individual panel are +/-40 degrees, that poses a big advantage and this strategy overcomes the challenges of conventional transmit-array/lens antennas as high gain wide-angle beam scanning with low side lobe level can be realized. Sidelobes can cause severe problems in radars and Satcom applications and and their reduction is of high importance. To demonstrate the effectivity and working mechanism of the proposed approach, a curved transmitarray was designed using three individual sub-array panels. Each panel is rotated by bent angle β (+/-40 degree) with reference to the central planar panel, shown in Fig. 4.35. Each panel has its individual feed array. Dividing a big array into three panels reduces the phase error and scan loss which increases the scan range of the antenna, Fig. 4.36 depicts the beam steering performance of the proposed multi panel transmit array. The gain scan loss for multi-facet array can be reduced by using bifocal phase distribution covered in section 4.4

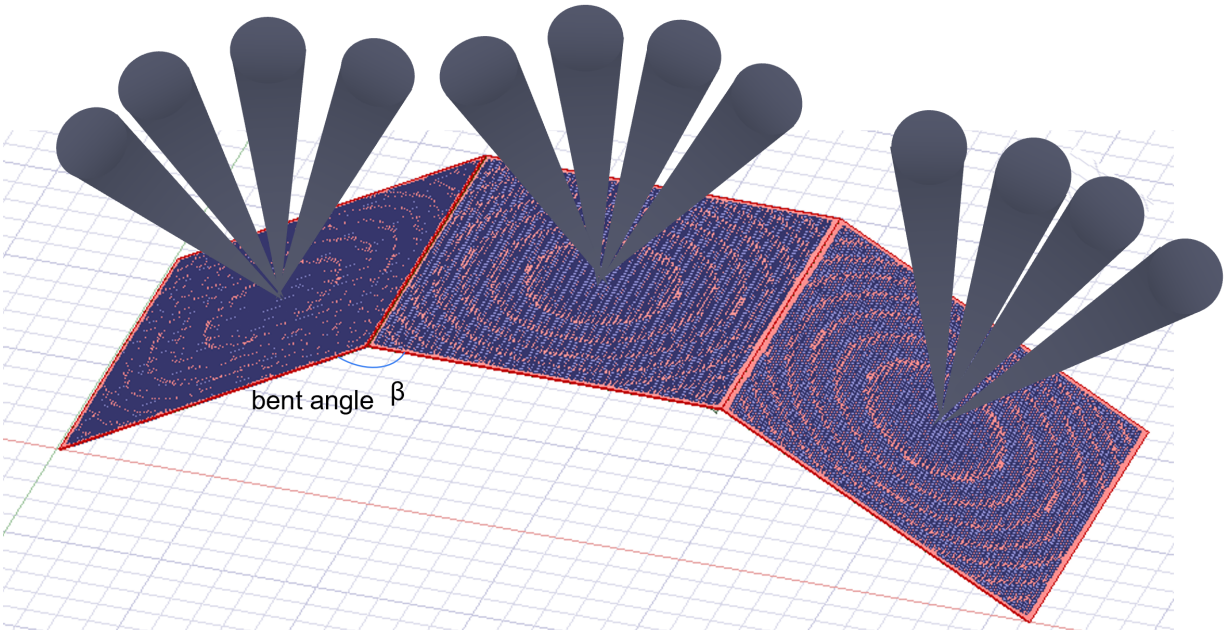

Figure 4.35: 3-Facet metasurface.

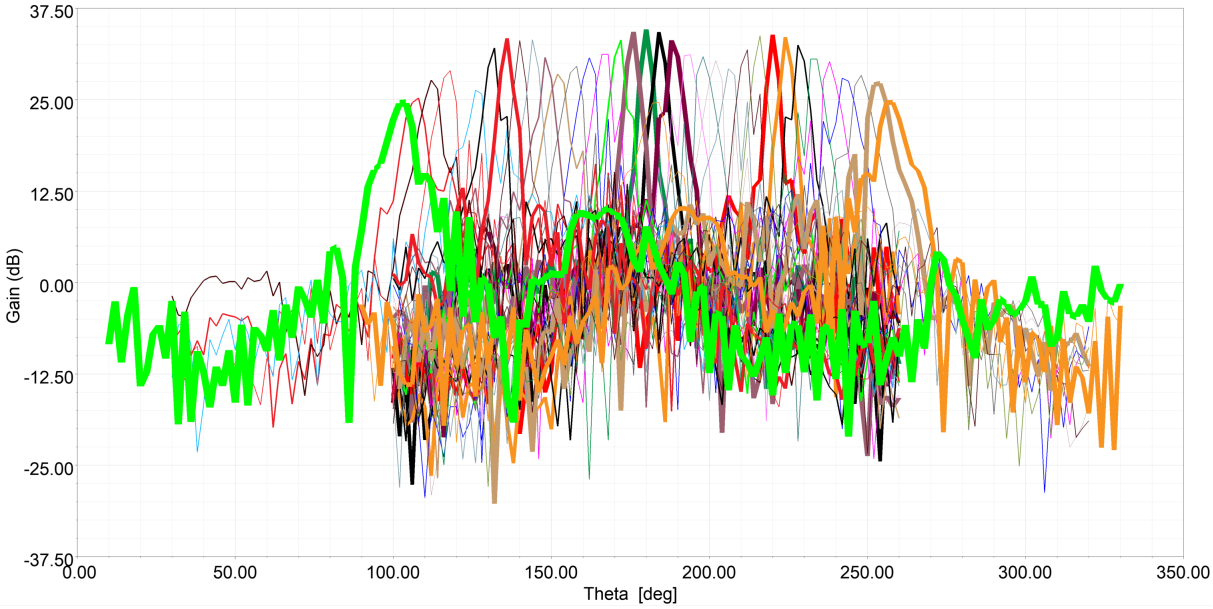

Figure 4.36: Radiation pattern of multifacet transmitarray.

4.7 Conclusion

The key contributions of our work can be summarized as the following:

- High gain wide angle beam steering is achieved by movement of feed radiator using robotic arm.
- Single/multiple beams can be formed using single antenna which provides spatial diversity and support MIMO implementation. Ultra wide scan angle of +/-80 degrees (with scan loss below 3 dB) is achieved using multi-facet transmit array.
- Capability to support both linear and circular polarization.
- Multiple users can be supported simultaneously.
- Simplified and robust setup that supports 1D and 2D steering to cater diverse users. Provides higher gain (with minimal gain scan loss) to counter high path losses at mmWave frequencies. Low cost and simple implementation.
- Compared to the existing mechanically steered antennas the designed antenna can generate multiple independently steerable beams simultaneously which increases the network capacity by multiple folds compared to the systems supporting only single beam.
- In comparison to current antennas for 5G communication system, the proposed antenna provides high gain and beam adaptability which can overcome propagation losses incurred at mm-Wave frequency bands.

CHAPTER 5

REFLECT-ARRAY SURFACE DESIGN AND ANALYSIS

This chapter will cover the reflectarray phasing element design and characterization, feed radiator design, phase aperture distribution and reflectarray surface design. As discussed in previous chapters, reflectarray antenna consists of a reflectarray surface and a feed radiator. The reflectarray surface consists of radiating elements (unit cells) and phasing circuit. The number of elements for a reflectarray surface may vary from hundreds to thousands of cells depending upon design specifications. As discussed in previous chapter unit cells typically have the same geometry but different phase distribution. The basis of reflectarray design is its unit cell design, characterization and analysis. In this chapter we shall first discuss the unit cell analysis, characterization and design. After unit cell design, we shall discuss the aperture phase distribution and design of the reflectarray aperture for electronic beam scanning.

5.1 Radiating Structure (Unit cell) Design

After investigating the optimum analysis method for reflectarray design, a radiating element was designed. The radiating structure consists of a varactor loaded conducing pattern printed on substrate over a ground plane, shown in Fig. 5.1. The conducting pattern of our designed unit cell consists of an inner square patch

and an outer hybrid square patch. The reason we are calling it hybrid square is that it is a hybrid of square and cross dipole. We have designed the unit cell by adding the versatility of multiple resonant elements. The designed unit cell combines the favorable features of crossed dipoles, square patches and square quads. Double square elements (quads) have increased bandwidth, that's why we have added an inner square patch. The hybrid outer square patch was designed by combining the geometries of cross dipoles and square patches. The designed unit cell has unique and novel conducting pattern which attributes to its excellent radiation characteristics. The conducting pattern was realized using 35 um thick copper etched on substrate. Substrate used is Rogers 5880 with thickness of 0.58 mm. For phase tuning, a varactor diode is loaded between the inner and outer square. The resonant frequency of patch changes with tuning the patch using the voltage controlled varactor. Fig. 5.2 shows the 3D view of the simulated unit cell (front plane and back plane). The dimensions of the unit cell are approximately $0.3\lambda_o \times 0.3\lambda_o$. The dielectric constant for substrate is $e_r = 2.2$ with loss tangent of 0.009. The behavior of the proposed unit cell configuration is studied using an infinite array analysis. This approach is pretty suitable for reflectarrays loaded with lumped components, which are typically large and made up of identical phasing elements. The unit cell is analyzed with commercial full-wave software HFSS. Floquet port excitation and periodic boundary conditions have been used to analyze the unit cell. Fig. 5.3 and Fig. 5.4 shows the unit cell excited by floquet modes and periodic boundary conditions.

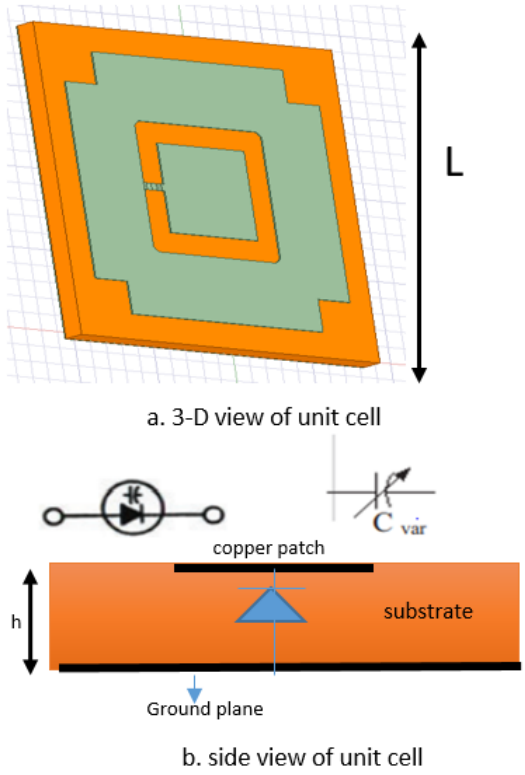

Figure 5.1: Designed reflectarray phasing element (unit cell).

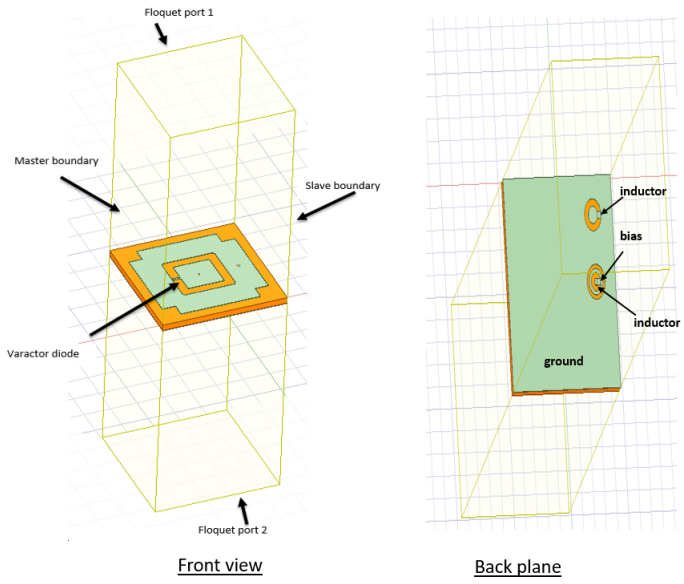

Figure 5.2: 3-D view of simulated unit cell.

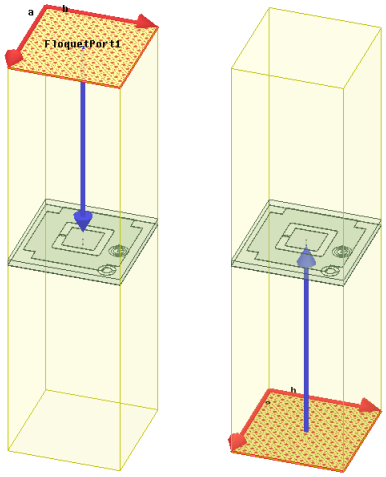

Figure 5.3: Floquet port analysis.

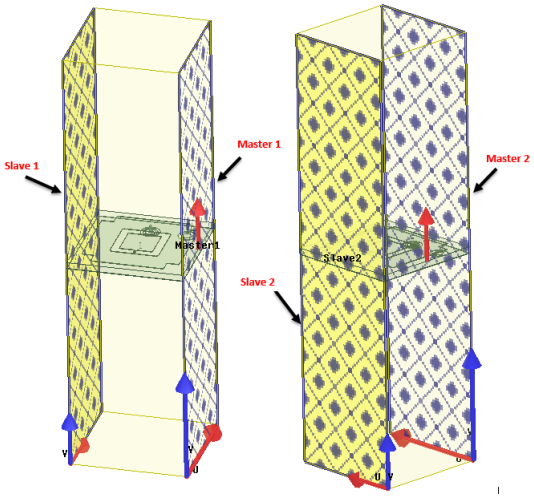

Figure 5.4: Unit cell with master slave boundaries.

5.2 Phase Shifting Mechanism

The previous section covered the unit cell geometry and approaches used to design the unit cell in electromagnetic simulation tools. Since unit cell should be able to produce phase shift of ideally 360 degrees therefore we need some tuning mechanism

to tune the unit cell. In the previous chapter we have discussed different phase tuning approaches. Different approaches can be realized to design the tunable reflectarrays which includes MEMs devices, liquid crystals, varactors and PIN diodes. PIN diodes have high power consumption and high losses at GHz frequencies. MEMs show good performance at high GHz frequencies but have complex structures, discrete tuning limitations and reliability issues. Reflectarrays based on tunable liquid crystals usually have limited phase range, low figure of merit, relatively slow switching speed, temperature sensitivity, and special facilities are needed to manufacture them. Varactors have continuous tuning ability, extremely low power consumption and offer faster switching speed compared to MEMs and tunable substrates. Hence, we have used varactor diodes to tune the unit cell of reflectarray. Characteristic impedance of element can be controlled by using variable capacitance which alters the reflection coefficient (phase and magnitude) of the element as indicated in the relationship below:

$$r = \frac{z_1 - z_2}{z_1 + z_2} \tag{5.1}$$

Where, r is the reflection coefficient, z_1 and z_2 are characteristic impedance of medium 1 and medium 2.

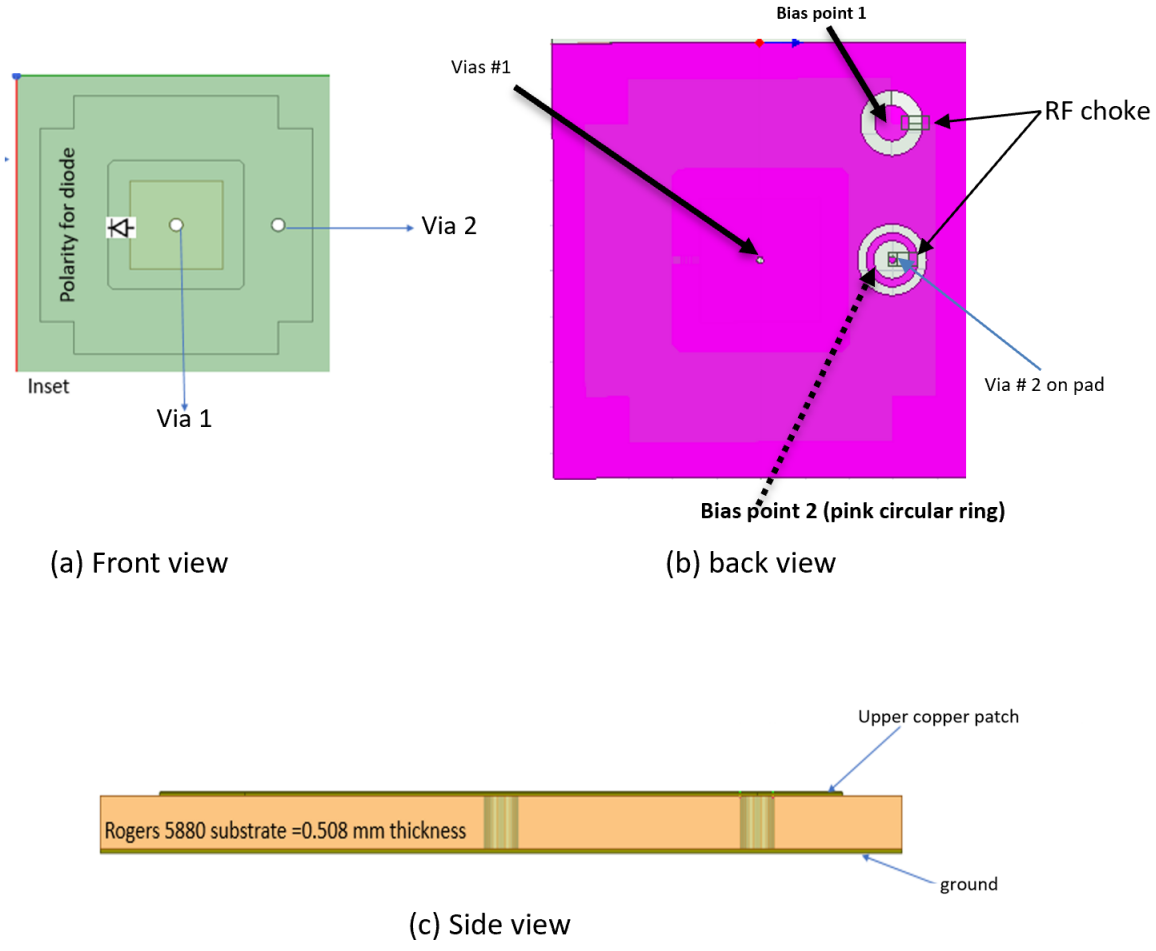

Figure 5.5: Schematics of varactor loaded unit cell.

5.3 Aperture Phase Distribution

Electronically controlled analog phase shifter provides voltage dependent capacitance. In our work a varactor based electronically controlled phase shifter that provides voltage controlled capacitance has been used. Fig. 5.5 shows conceptual interpretation of varactor loaded unit cell design. In the ground plane and core substrate holes (vias) are drilled to provide the biasing for the varactor diodes. Fig.

5.5b shows the bottom view of the unit cell, the holes show the vias that extends from ground plane to the copper patch and it provides the route for the biasing of the diode. The capacitance of the varactor ranges between 0.02 pF and 0.2 pF when it is reverse biased between 0-20 volts. In HFSS simulations, RLC boundaries are used to model the varactor diodes. For RF blocking an inductor is inserted at the bottom of a ground plane. Width of lumped element is set equal to diode diameter. As discussed, to realize the varactor tuning the value of capacitance of lumped component is varied from 0.02 pF to 0.2 pF. Since ideally the unit cell phase range should be 360°, the unit cell dimensions were optimized to design the optimum cell. For unit cell optimization, varactor tuning was characterized and cell dimensions were optimized by working around multiple parameters including unit cell length, width, inner and outer patch widths, diameter of vias, and substrate thickness. To evaluate the phase characteristics of a unit cell, a parametric study was carried out by varying the controlling parameter (varactor diode capacitance). The reflection coefficient vs diode capacitance has been studied to analyze the phase response of unit cell. By tuning varactor diodes between 0.02 pF – 0.2 pF we can achieve the phase agility of 360°, as shown in Fig. 5.6. Reflection coefficient amplitude for the designed unit cell remained below 1.9 dB in the complete range of 360 degrees, shown in Fig. 5.7.

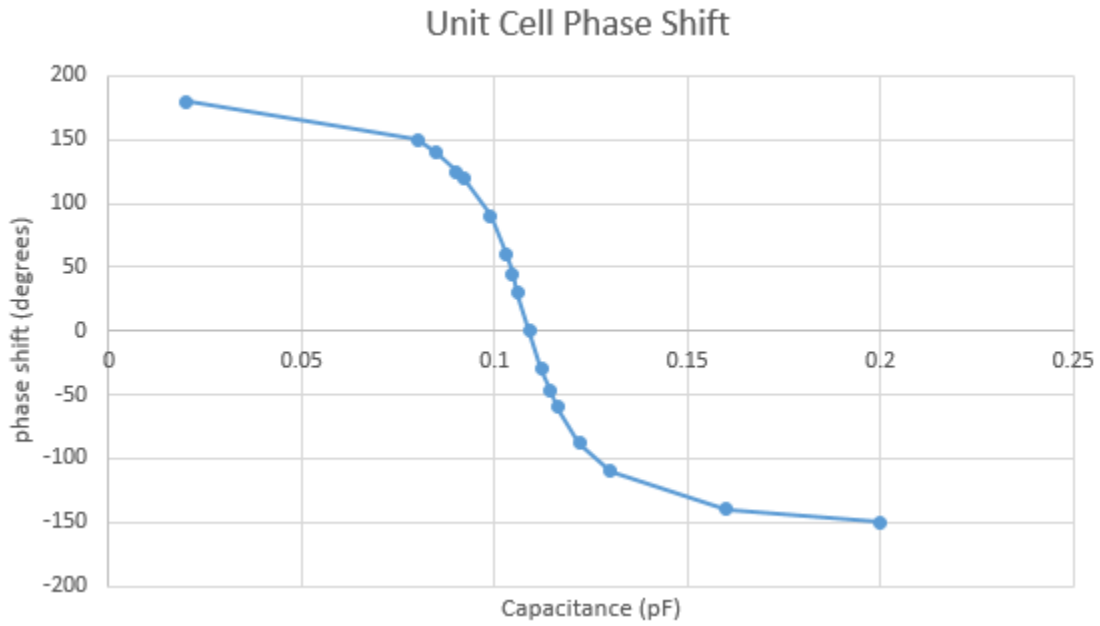

Figure 5.6: Phase range of unit cell.

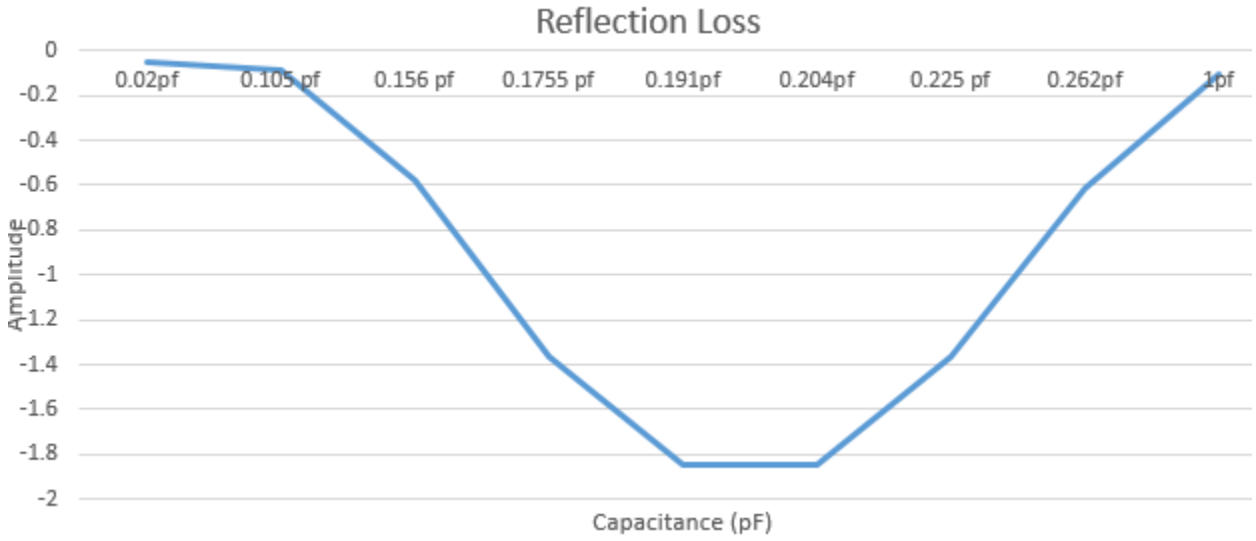

Figure 5.7: Reflection loss.

Our next step was aperture phase distribution. The database was created from the unit cell analysis which contains the reflection coefficents phase and corresponding

capacitance values. In our scenario the controlling parameter is bias voltage of varactor diode as by changing the bias voltage diode capacitance varies. Once unit cell phase variation of around 360 degrees was obtained and corresponding values were stored in the database, a reflectarray surface was designed taking into account the phase shift introduced by each element. First, we defined a grid having the coordinates of all the phasing elements. Phase delay at each element due to the path difference from the antenna feed is calculated by taking into account the respective position of each unit cell and distance from feed antenna. The phase required at i_{th} element to focus a beam in the direction (θ_o,ϕ_o) is given as:

$$\phi(a_i, b_i) = k_o sin\theta_o cos\phi_o a_i - k_o sin\theta_b sin\phi_o b_i \tag{5.2}$$

where k_o is the free space propagation constant and (a_i, b_i) are coordinates of i_{th} element.

The phase shift introduced on each reflectarray cell can be written as:

$$\psi_R(a_i, b_i) = k_o R_i - k_o a_i sin\theta_o cos\phi_o - k_o b_i sin\theta_o sin\phi_o \tag{5.3}$$

$$\psi_R(a_i, b_i) = 2\pi/\lambda R_i - 2\pi/\lambda a_i sin\theta_o cos\phi_o - 2\pi/\lambda b_i sin\theta_o sin\phi_o \tag{5.4}$$

$$R_i = \sqrt{(a_i - x_o)^2 + (b_i - y_o)^2 + (z_o)^2} \tag{5.5}$$

Where, R_i is the distance from the phase center of the feed to the i_{th} cell and (x_o, y_o, z_o) are coordinates of feed phase center.

According to the phase distribution expressed in the above equations the reflec-

tarray surface is designed such that each unit cell adds a linear phase shift. Since the array has a large number of cells therefore, to synthesize the aperture distribution efficiently we have designed a MATLAB algorithm to synthesize the phase distribution for each unit cell. The algorithm efficiently calculates the phase required on all the unit cells and corresponding capacitance values. The capacitance values are then assigned to individual array elements in HFSS for full wave EM simulation.

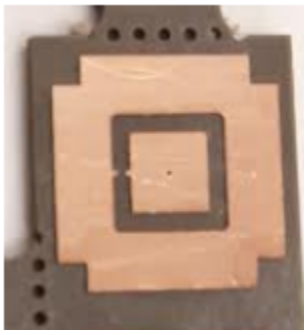

Figure 5.8: Fabricated unit cell (front view).

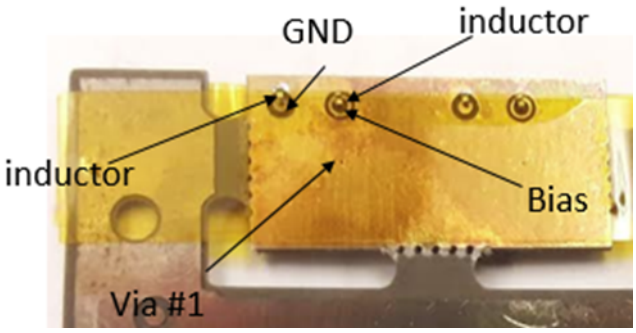

Figure 5.9: Fabricated unit cell (back plane).

5.4 Fabricated Prototype

The proposed varactor-loaded model was experimentally validated through the fabrication of reflectarray cell at the frequency of 11 GHz. Design parameters includ-

ing varacator position, patch length (inner and outer patch), vias length, thickness and positions were optimized to get the optimal results. The varactor-loaded reflectarray unit cell was then fabricated on top of the Rogers Duroid 5880 substrate. Conducting pattern was printed on 0.35 um thick copper. Fig. 5.8 shows the front view of fabricated unit cell. Fig. 5.9 shows the back plane of the fabricated unit cell, showing the via and inductors (39 nH) for RF chocking. Vias and RF chokes (39 nH) were used to make the biasing circuit for dynamic tuning. The waveguide (W75S001-3) was used for experimental validation of unit cell phase characteristics (reference Fig.5.10). The prototype was placed at one end of waveguide and the variable voltage (0-20 V) was applied across the varactor diode to tune the unit cell.

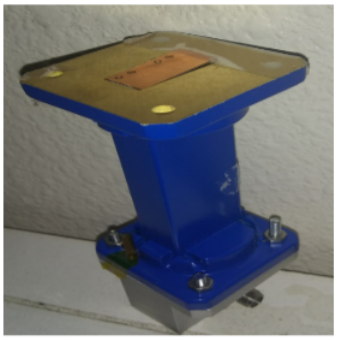

Figure 5.10: Unit cell placed at the end of waveguide (W75S001-3).

5.5 Reflectarray Surface Design Using the Novel Unit Cell

To validate the dynamic tuning capabilities of designed unit cell, a 14 x 14 element reflectarray has been designed. The 14 x 14 microstrip reflectarray antenna is designed at the operating frequency of 11 GHz. According to the aperture phase distribution in 5.4 the varactor diode is tuned to provide the required phase compensation to form the beam towards the intended direction. Aperture phase distribution was

designed using increments of 45°. MATLAB algorithm was written that calculated the desired phase distribution and generated the corresponding values of capacitance. The capacitance values were then loaded to the individual array elements. Fig 5.11 shows the simulated 14 x 14 reflectarray consisting of 196 elements. To validate the beam steering capability of the desired unit cell, reflectarray surface was tuned to steer the beam from 0 to 60° by adjusting the capacitive loading of unit cells using varactor diode. Fig. 5.12 shows the beam steered from 0 to 60° that validates the beam steering capability of proposed design. The peak gain of the reflectarray antenna at 11 GHz is 19 dBi. Linearly polarized pyramidal horn antennas was used to illuminate the reflectarray. The cross-pol remained below 15 dB and return loss remained below 10 dB from peak gain for the all the steering angles. In next phase we fabricated the scaled version of simulated reflectarray. Fabricated reflectarray consists of 22 x 22 element array shown in Fig. 5.13. Fig. 5.14 shows the measurement setup for designed reflectarray. Measured performance is in reasonable agreement with simulated performance.

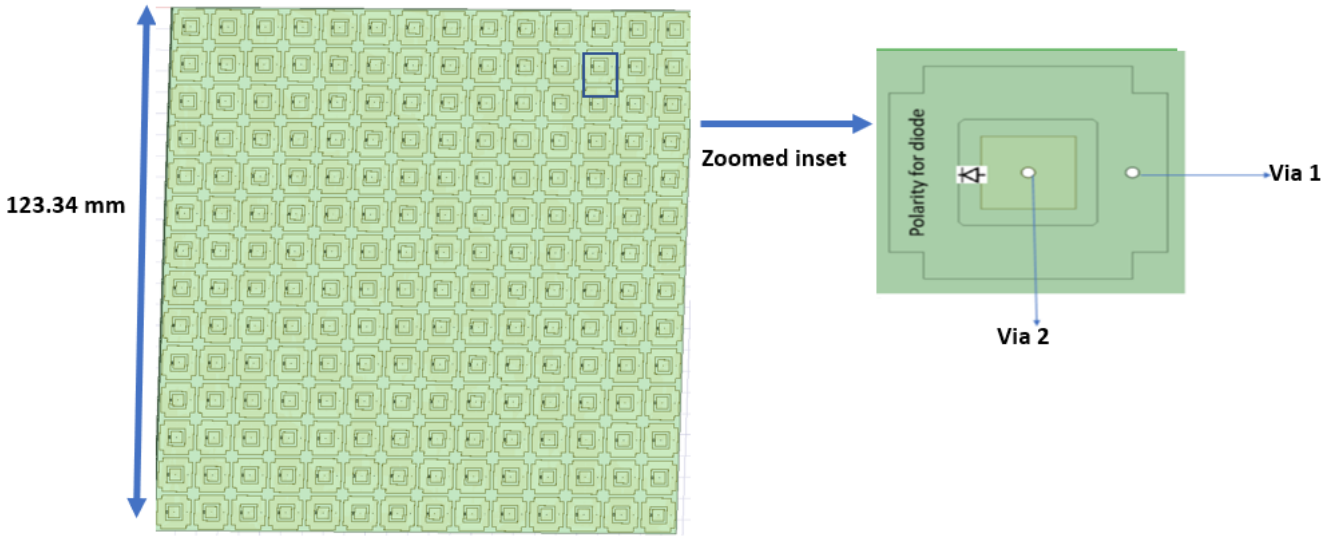

Figure 5.11: Array of unit cells (back plane).

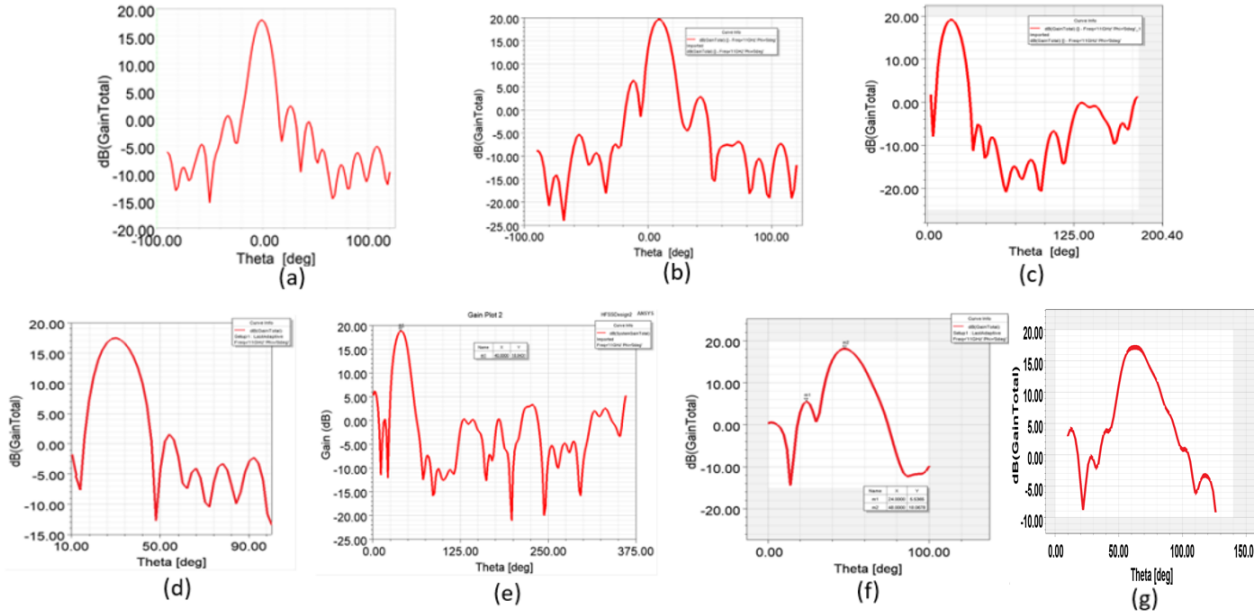

Figure 5.12: Radiation pattern of designed 14x14 element reflectarray. (a) Boresight pattern (b) steered at 10°(c) steered at 20° (d) steered at 30° (e) steered at 40° (f) steered at 50°, and (g) steered at 60°.

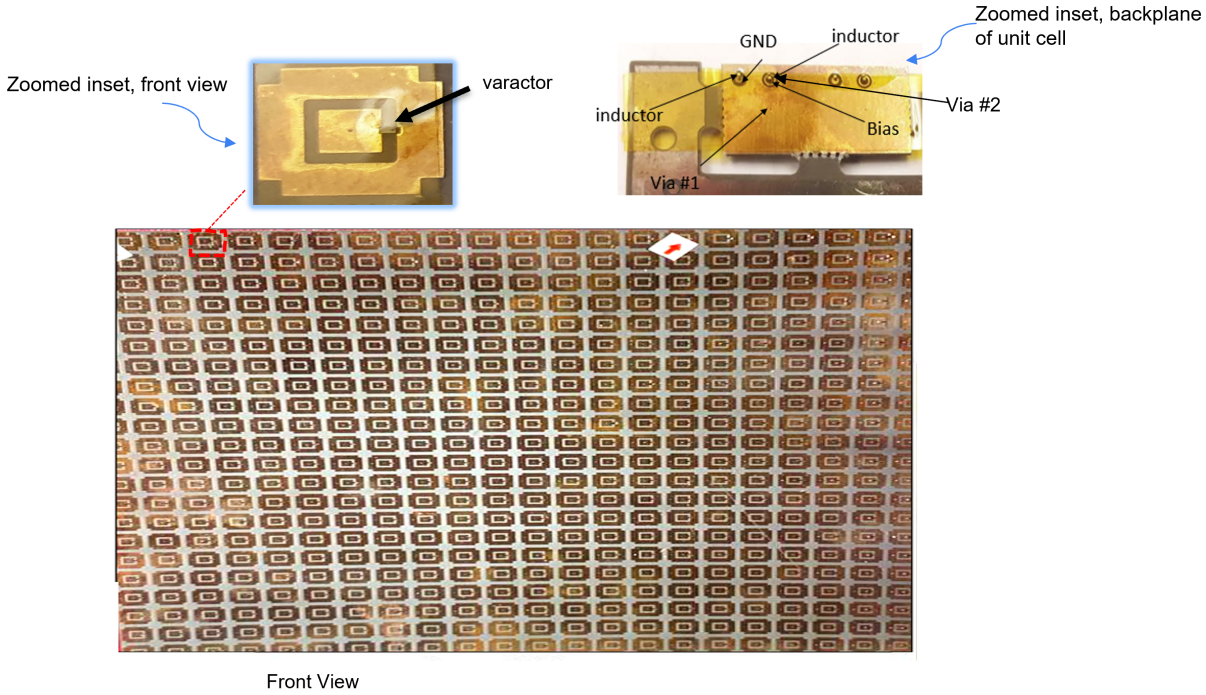

Figure 5.13: Fabricated reflectarray.

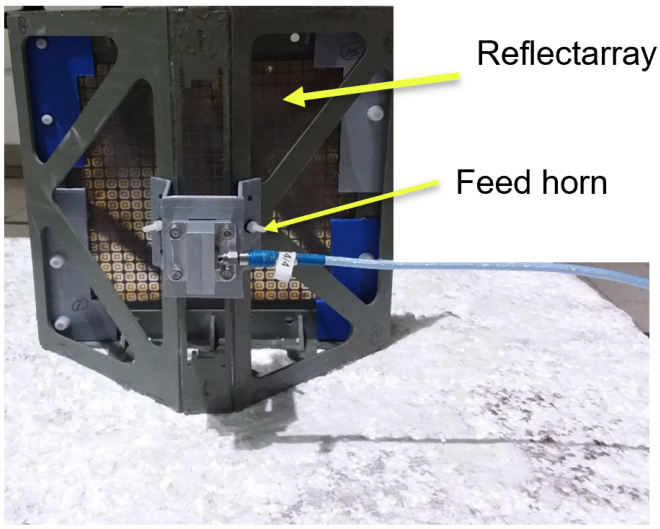

Figure 5.14: Reflectarray mounted on turn-table in test chamber.

5.6 Reflect-array design using passive unit cell

Another approach which we have used for reflectarray surface design is using variable sized phasing elements. In this design we are achieving variation in phase distribution by varying the dimension of the unit cell. To design the optimum unit cell, geometries of three different unit cell designs (shown in Fig. 5.15) were analyzed including; circular ring, double square and a combination of circular rings and double square ring. It was observed that the unit cells composed of a circular ring or a double square provide limited phase variation, Fig. 5.16 shows the phase variation comparison of all the three geometries, hence to achieve wider phase range we combined both geometries and selected a unit cell with the circular ring and a double square. Dimensions of a unit cell are 10 mm x 10 mm, which is equal to 0.6λ. To determine the phase characteristics of the unit cell, parametric study was carried out by varying the dimensions of the unit cell, and their corresponding reflection

coefficient phases were stored in the database. Dimensions of the circular ring, inner square and outer square are varied to create the database of the phase of the reflection coefficients. Fifty five different dimension sets have been used to get a linear phase range of 360°. The reflectarray surface is composed of 28 × 28 unit cells, these unit cells are symmetrically located in a 280 mm x 280 mm square grid. The designed reflectarray surface consists of 784 unit cells, unit cells have the same geometry but different sizes, 55 different dimension sets have been used to achieve a linear phase range of 360 degrees.

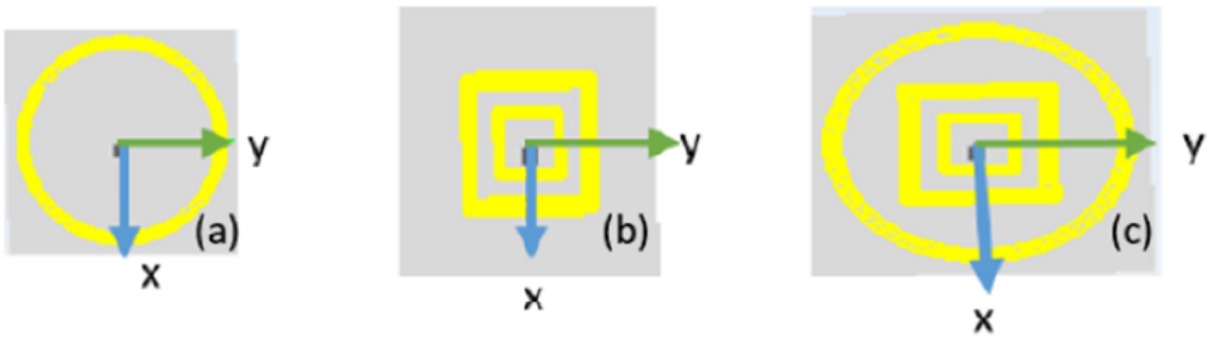

Figure 5.15: Unit cell geometries (a) Circular Ring (b) Double square (c) Circular ring and double square elements

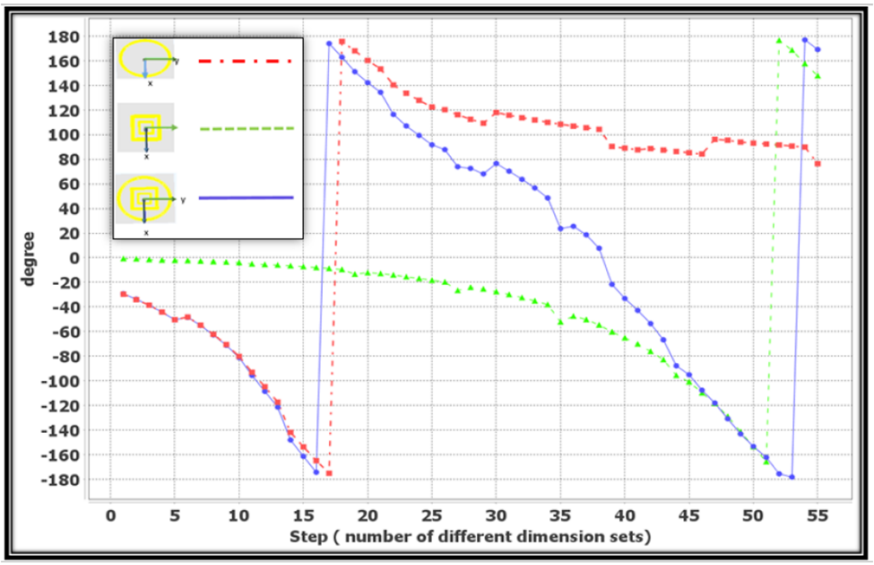

Figure 5.16: Phase range for different geometries.

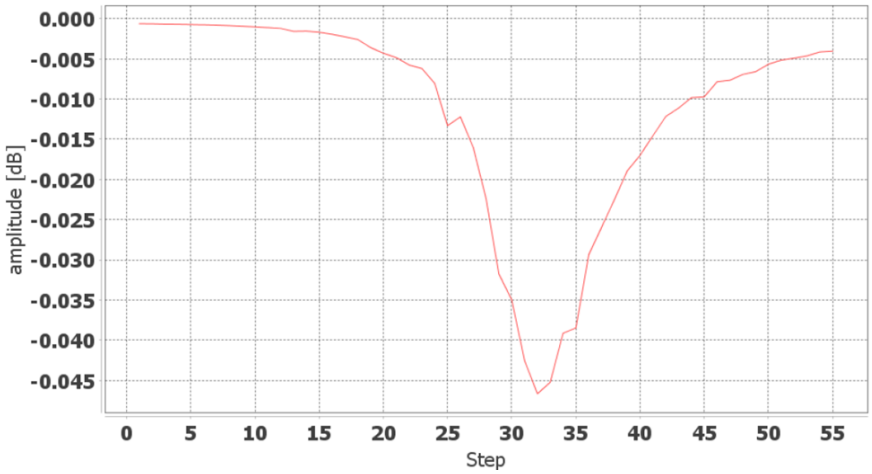

Figure 5.17: Reflection loss.

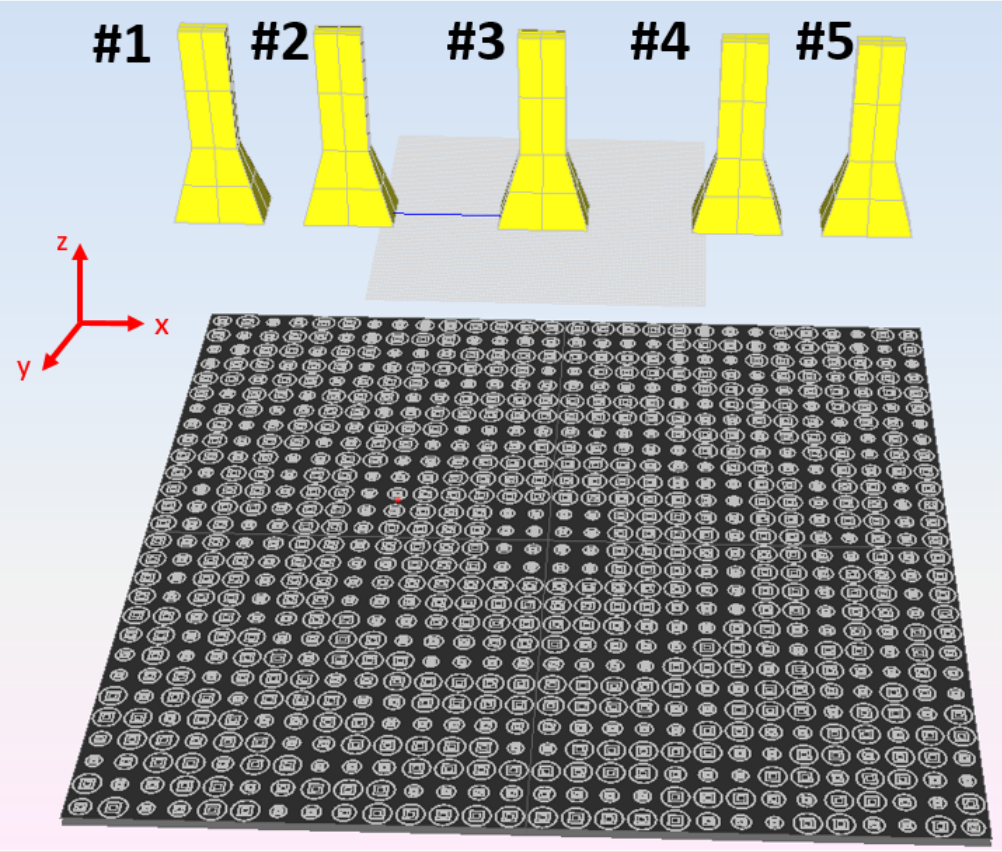

Figure 5.18: Reflect-array surface and beam steering configuration.

5.6.1 Beam Steering Configuration

Beam steering configuration in this design consists of multiple feed antennas placed in front of the reflectarray surface with F/D of 0.5 as shown in Fig. 5.18. Horn 1 is located at (x, y, z) = (-10, 0, 14) cm. Horn 2 is located at (x, y, z) = (-6, 0, 14) cm. Horn 3 is located at (x, y, z) = (0, 0, 14) cm. Horn 4 is located at (x, y, z) = (6, 0, 14) cm and horn 5 is located at (x, y, z) = (10, 0, 14) cm. Horn antennas are turned on individually and only one horn antenna is active at a time. By switching between feed horn antennas the main beam can be steered at angles between -40 and +40 in H-plane. Fig. 5.19 shows the simulated 3D radiation patterns at multiple angles with

a peak gain of 29.77 dBi. Radiation pattern is shown in Fig. 5.20.

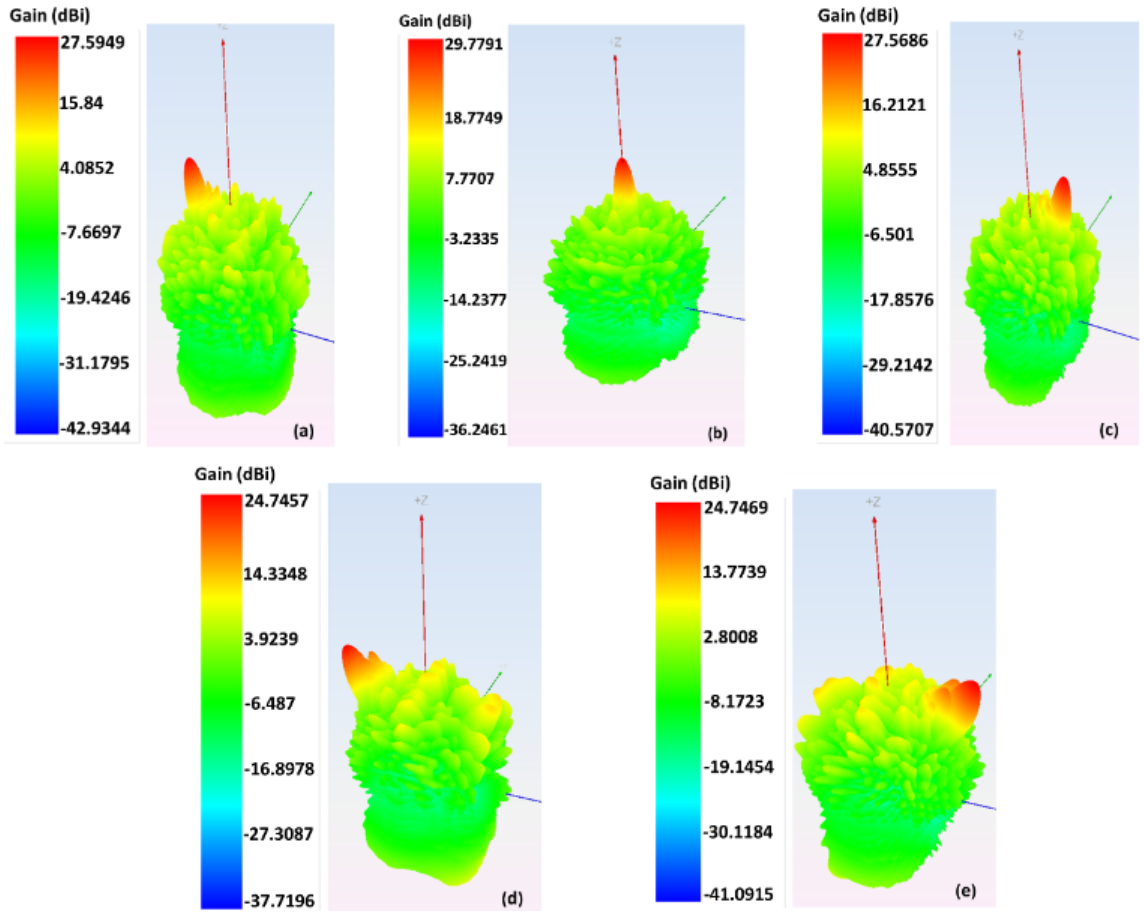

Figure 5.19: 3D radiation pattern showing beam steering: (a) - 20, (b) 0, (c) +20; (d) -40; (e) +40.

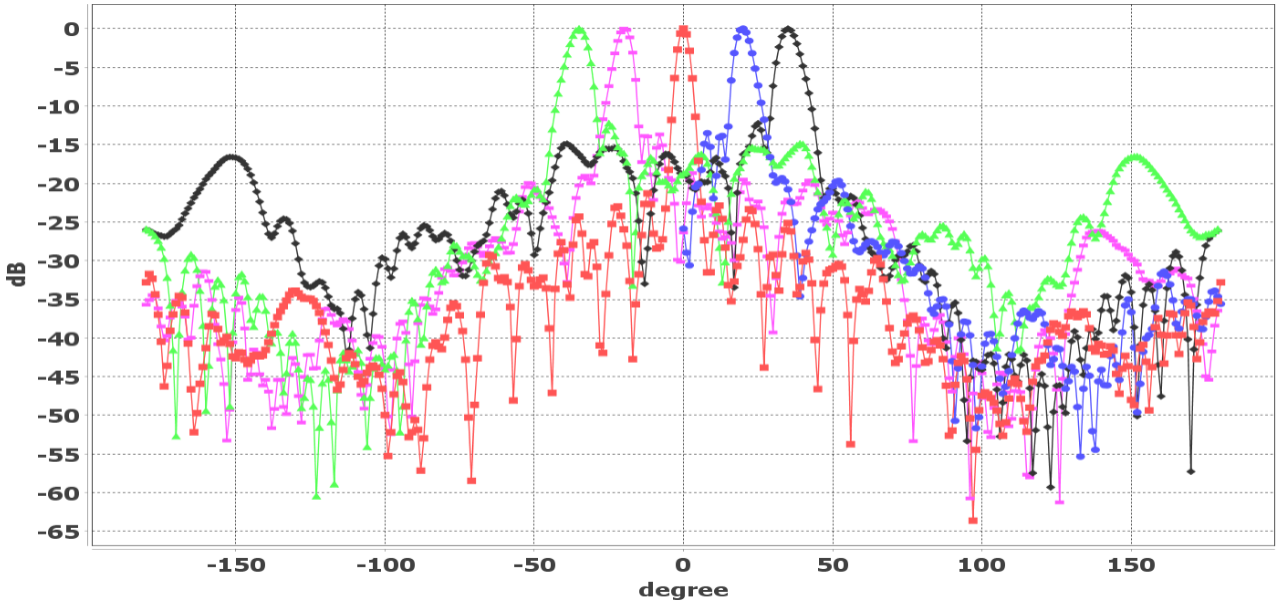

Figure 5.20: Far-field radiation pattern in the H-plane. Peaks at -40, -20, 0, +20 and +40.

Table 5.1: Beam steering mechanism.

Elevation Angle	Feed 1	Feed 2	Feed 3	Feed 4	Feed 5
-40°	On	Off	Off	Off	Off
-20°	Off	On	Off	Off	Off
0°	Off	Off	On	Off	Off
+40°	Off	Off	Off	On	Off
+20°	Off	Off	Off	Off	On

CHAPTER 6

CONCLUSION AND APPLICATIONS

6.1 5G Millimetric Wave (mm-Wave) Communication

Fifth generation (5G) wireless networks are the next step in the evolution of wireless communication. The next generation of wireless networks aim to deliver fast data rates with low latency [1, 2, 32]. Beam steerable antennas are an essential requirement for 5G millimetric wave networks; they mitigate interference by channeling and focusing the antenna signal towards the desired direction. This ability is significant for millimetric wave frequency applications such as cellular backhaul links where high path loss, diffraction, attenuation from obstacles, material penetrations and misalignment due to rain and wind storms are dominant. Fig. 6.1 shows an example of a back haul network using directional antennas. High gain directional antennas are a way forward to maintain the quality of wireless link for mmWave network. Furthermore, beam reconfigurability increases the network capacity by focusing antenna beam towards the high demand regions.

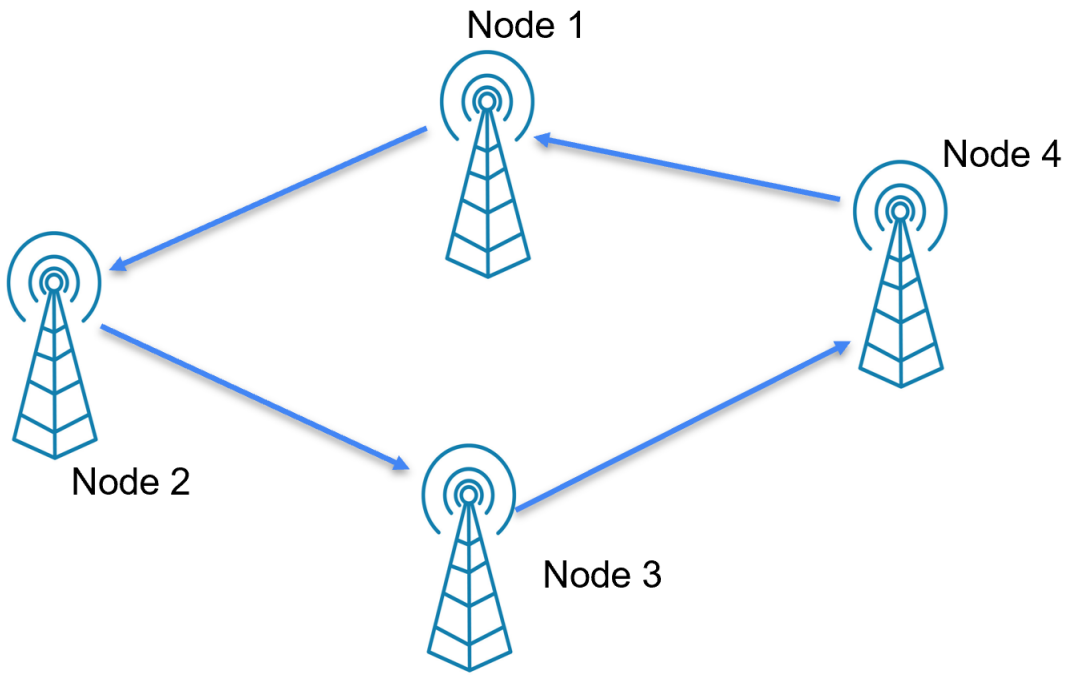

Figure 6.1: Back-haul networks using high gain antennas.

6.2 Satellite Communication (LEO & MEO)

Major SATCOM companies are working to launch the LEO (low Earth orbit) and MEO (middle Earth orbit satellites). Fig. 6.2 shows a comparison of GEO, MEO and LEO constellations. LEO & MEO satellites are much smaller in size (compared to GEO satellites) and their orbits are much closer to Earth therefore the cost to launch these satellites is much cheaper, they offer reduced latency compared to GEO satellites which makes them a great platform for next generation wireless systems. About four billion people in the world who do not have internet at present will be served by emerging LEO and MEO satellites. However, due to close proximity to Earth, unlike GEO satellites, these satellites will not be stationary and they will keep revolving around the Earth. Therefore, to communicate with LEO and MEO

satellites we need efficient beam steering antennas. Fig. 6.3 shows the conceptual representation of satellite communication using smart antennas. Satellite tracking antennas currently in the market are extremely expensive due to the presence of expensive phase shifting components (e.g., conventional phase arrays) or have limited number of beams (e.g., conventional mechanically steered parabolic dishes). Proposed multi-beam metamaterial based antenna provides a cost-effective solution for satellite communication with good figure of merit, high gain and multiple steerable beams.

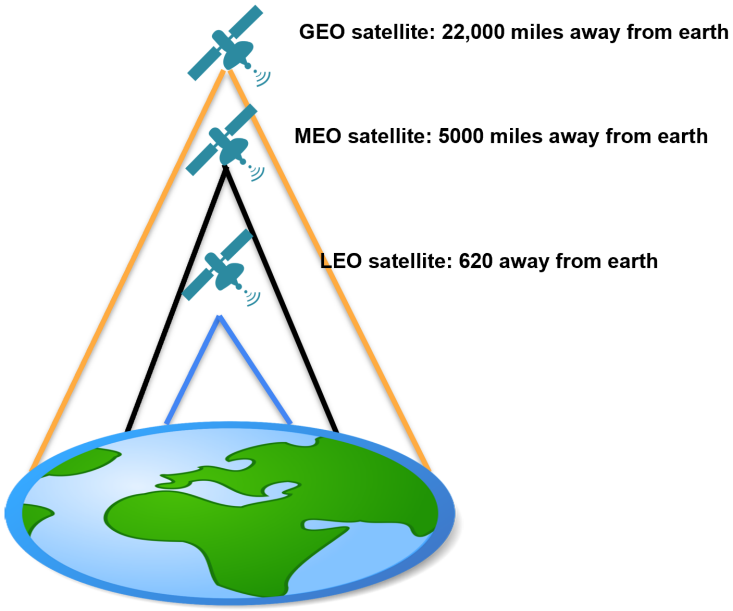

Figure 6.2: Satellite communication.

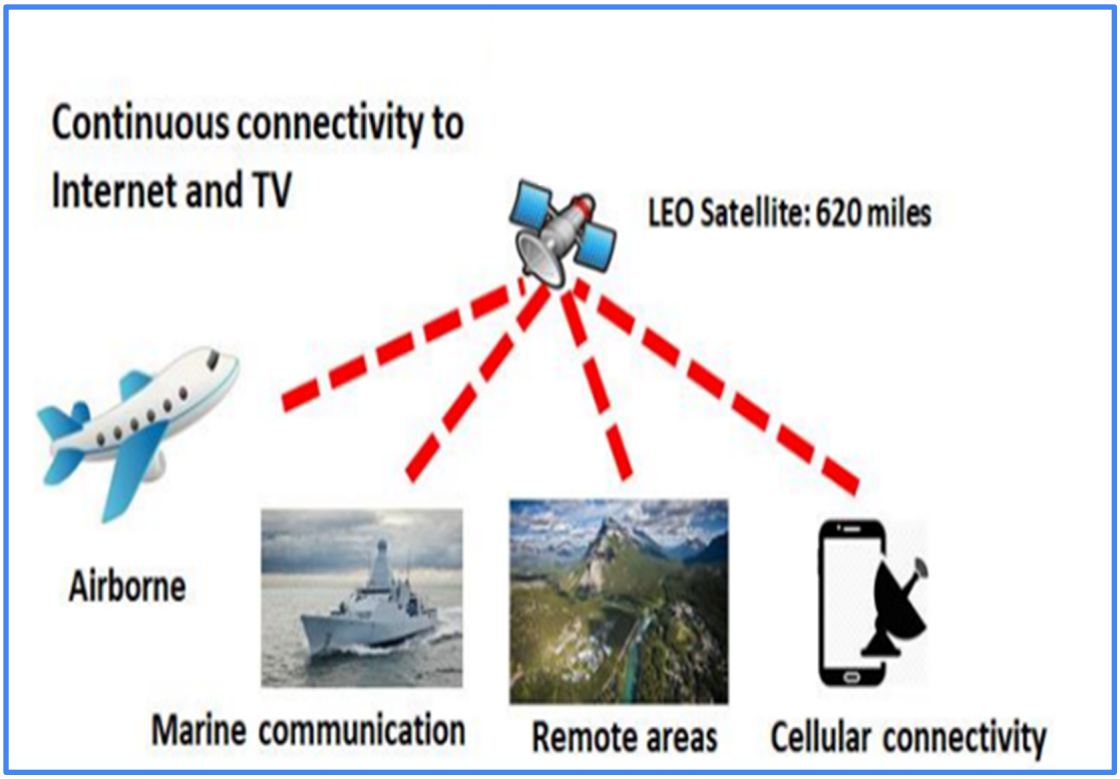

Figure 6.3: Satellite communication.

6.3 SATCOM On-the-move (Communication with GEO Satellite)

The demand of mobile broadband satellite communication has been increasing day by day. SATCOM on-the-move antennas provide reliable satellite communication link while on the move, enabling beyond-line-of-sight communication link with GEO satellite. Fig. 6.4 shows the conceptual interpretation of satellite communication on the move. Ground terminals are required to maintain the communication link hence beam steering antennas are required for SATCOM on-the-move. Beam steering antennas are key components of SOTM mobile terminals.

Figure 6.4: Satellite Communication-on-the-Move (SOTM).

Another advantage of multi beam antenna is the multi satellite communication (reference Fig. 6.5), in the traces where a GEO satellite is not available if antenna supports multiple beams it can switch to a MEO satellite, multi beam antennas can overcome the blockage due to line of sight issues.

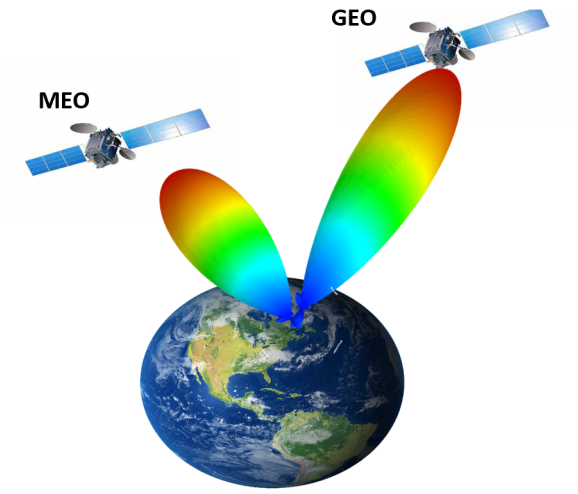

Figure 6.5: Multi-Satellite Connectivity.

6.4 Enabling the High Throughput with Spot Beams and Polarization Diversity

In satellite communication, the engineering problem is to pack more bits into the available spectrum and achieve high throughput in a power-efficient manner. Spectrum reuse is obtained by the use of tight spot beams. The ability to generate the tight spot beams enable beams to be focused on high-demand areas. It also helps to overcome the path losses at high frequencies allowing the use of high frequency bands. Using the multi beam lens antenna described in chapter 4, high gain spot beams can be produced which can be reconfigured as per need. By using such an antenna, a single satellite can produce multiple spot beams. Polarization diversity enables frequency reuse, as neighboring spots have opposite polarization hence beams do not interfere. Fig. 6.6 shows an example of a four-color coverage based on hexagonal cells.

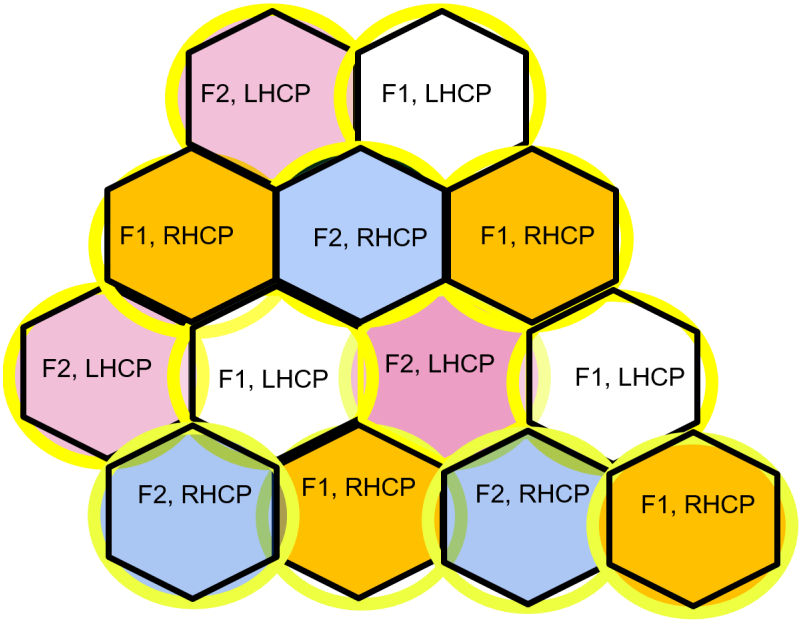

Figure 6.6: Example of four-color multi spot coverage.

REFERENCES

[1] Wonbin Hong, Kwang-Hyun Baek, and Seungtae Ko. Millimeter-wave 5g antennas for smartphones: Overview and experimental demonstration. *IEEE Transactions on Antennas and Propagation*, 65(12):6250–6261, 2017.

[2] Theodore S. Rappaport, Shu Sun, Rimma Mayzus, Hang Zhao, Yaniv Azar, Kevin Wang, George N. Wong, Jocelyn K. Schulz, Mathew Samimi, and Felix Gutierrez. Millimeter wave mobile communications for 5g cellular: It will work! *IEEE Access*, 1:335–349, 2013.

[3] Frederick W. Vook, Amitava Ghosh, and Timothy A. Thomas. Mimo and beamforming solutions for 5g technology. In *2014 IEEE MTT-S International Microwave Symposium (IMS2014)*, pages 1–4, 2014.

[4] M. U. Hadi. Extending the benefits of lte to unlicensed spectrum. In *2015 International Conference on Information and Communication Technologies (ICICT)*, pages 1–3, 2015.

[5] Randy L. Haupt and Michael Lanagan. Reconfigurable antennas. *IEEE Antennas and Propagation Magazine*, 55(1):49–61, 2013.

[6] Muhammad Usman Hadi. Sigma delta radio frequency transport system for 5g sub-6 ghz fronthauls. In *2020 IEEE 15th International Conference on Industrial and Information Systems (ICIIS)*, pages 596–600, 2020.

[7] Muhammad Usman Hadi, Shafaq Kausar, and Isha Mittal. Efficient pre-bpf based sigma delta radio over fiber system for 5g nr fronthauls. In *IEEE EUROCON 2021 - 19th International Conference on Smart Technologies*, pages 308–311, 2021.

[8] Ahmed Kausar, Shafaq Kausar, and Hani Mehrpouyan. Hybrid beam-forming smart antenna for 5g networks. In *2019 IEEE International Symposium on Antennas and Propagation and USNC-URSI Radio Science Meeting*, pages 1525–1526, 2019.

[9] Mathew K. Samimi, Theodore S. Rappaport, and George R. MacCartney. Probabilistic omnidirectional path loss models for millimeter-wave outdoor communications. *IEEE Wireless Communications Letters*, 4(4):357–360, 2015.

[10] Mahfuza Khatun, Changyu Guo, David Matolak, and Hani Mehrpouyan. Indoor and outdoor penetration loss measurements at 73 and 81 ghz. In *2019 IEEE Global Communications Conference (GLOBECOM)*, pages 1–5, 2019.

[11] Mahfuza Khatun, Hani Mehrpouyan, David Matolak, and Ismail Guvenc. Millimeter wave systems for airports and short-range aviation communications: A survey of the current channel models at mmwave frequencies. In *2017 IEEE/AIAA 36th Digital Avionics Systems Conference (DASC)*, pages 1–8, 2017.

[12] Shafaq Kausar, Ahmed Kausar, and Hani Mehrpouyan. Challenges for antenna design at mm-waves. In *2019 IEEE International Symposium on Antennas and Propagation and USNC-URSI Radio Science Meeting*, pages 1387–1388, 2019.

[13] Mikhail E. Sinitsyn, Alexey S. Podstrigaev, Andrey V. Smolyakov, and Vadim V. Davydov. Analysis of the sea surface influence on the shape of microwave

spiral antenna radiation pattern. In *2019 Antennas Design and Measurement International Conference (ADMInC)*, pages 72–74, 2019.

[14] Han Wang, Zhijun Zhang, Yue Li, and Magdy F. Iskander. A switched beam antenna with shaped radiation pattern and interleaving array architecture. *IEEE Transactions on Antennas and Propagation*, 63(7):2914–2921, 2015.

[15] Mohamad Kamal Abdul Rahim, Mohd Nazif Mat Salleh, Osman Ayop, and Thelaha Masri. Switched beam antenna system design. In *2008 IEEE International RF and Microwave Conference*, pages 302–305, 2008.

[16] Shafaq Kausar, Hamood ur Rahman, Ahmed Kausar, and Tayyab Hassan. Espar antenna system for dynamic tracking of active targets. In *2013 European Modelling Symposium*, pages 533–535, 2013.

[17] Shafaq Kausar, Ahmed Kausar, Hani Mehrpouyan, and Hamoud Rahman. Design of miniaturized espar antenna for next generation communication systems. In *2019 IEEE International Symposium on Antennas and Propagation and USNC-URSI Radio Science Meeting*, pages 1359–1360, 2019.

[18] Ahmed Kausar, Hamood ur Rahman, Shafaq Kausar, and Tayyab Hassan. Smart adaptive beam forming antenna for interference minimization. In *Second International Conference on Future Generation Communication Technologies (FGCT 2013)*, pages 6–9, 2013.

[19] Ahmed Kausar and Shafaq Kausar. Smart adaptive beam forming antenna for interference cancellation. In *2013 IFIP Wireless Days (WD)*, pages 1–3, 2013.

[20] Shafaq Kausar, Hamood Ur Rahman, Tayyab Hassan, and Ahmed Kausar. Miniaturization of espar antenna using folded monopoles and conical central element. In *2015 International Conference on Radar, Antenna, Microwave, Electronics and Telecommunications (ICRAMET)*, pages 87–91, 2015.

[21] Ahmed Kausar, Hani Mehrpouyan, Mathini Sellathurai, Rongrong Qian, and Shafaq Kausar. Energy efficient switched parasitic array antenna for 5g networks and iot. In *2016 Loughborough Antennas Propagation Conference (LAPC)*, pages 1–5, 2016.

[22] Muhammad Hashim Dahri, Mohd Haizal Jamaluddin, Muhammad Inam Abbasi, and Muhammad Ramlee Kamarudin. A review of wideband reflectarray antennas for 5g communication systems. *IEEE Access*, 5:17803–17815, 2017.

[23] Shafaq Kausar, Saeideh Shad, Ahmed Kausar, and Hani Mehrpouyan. Design of high gain low cost beam-steering reflectarray antenna. In *2019 IEEE International Symposium on Antennas and Propagation and USNC-URSI Radio Science Meeting*, pages 315–316, 2019.

[24] D. Berry, R. Malech, and W. Kennedy. The reflectarray antenna. *IEEE Transactions on Antennas and Propagation*, 11(6):645–651, 1963.

[25] J. Huang and JA. Encina. *Reflectarray Antennas*. IEEE Press, John Wiley and Sons, Hoboken, 2008.

[26] Constantine A. Balanis. *Antenna Theory: Analysis and Design*. Wiley, 2016.

[27] Ahmed H. Abdelrahman, Fan Yang, Atef Z. Elsherbeni, Payam Nayeri, and Constantine A. Balanis. 2017.

[28] J. Huang and R.J. Pogorzelski. A ka-band microstrip reflectarray with elements having variable rotation angles. *IEEE Transactions on Antennas and Propagation*, 46(5):650–656, 1998.

[29] G. Perez-Palomino, J. A. Encinar, R. Dickie, and R. Cahill. Preliminary design of a liquid crystal-based reflectarray antenna for beam-scanning in thz. In *2013 IEEE Antennas and Propagation Society International Symposium (APSURSI)*, pages 2277–2278, 2013.

[30] Mojtaba Ahmadi Almasi, Roohollah Amiri, Mojtaba Vaezi, and Hani Mehrpouyan. Lens-based millimeter wave reconfigurable antenna noma. In *2019 IEEE International Conference on Communications Workshops (ICC Workshops)*, pages 1–5, 2019.

[31] Muhammad Usman Hadi, Abdul Basit, and Kiran Khurshid. Mimo enabled multiband 5g nr fiberwireless using sigma delta over fibertechnology. In *2021 International Bhurban Conference on Applied Sciences and Technologies (IBCAST)*, pages 1007–1010, 2021.

[32] Muhammad Usman Hadi, Abdul Basit, and Kiran Khurshid. Mimo enabled multiband 5g nr fiberwireless using sigma delta over fibertechnology. In *2021 International Bhurban Conference on Applied Sciences and Technologies (IBCAST)*, pages 1007–1010, 2021.